



# LUND UNIVERSITY

## Understanding and Optimization of III-V nanowire growth in Aerotaxy

Sivakumar, Sudhakar

2021

*Document Version:*

Publisher's PDF, also known as Version of record

[Link to publication](#)

*Citation for published version (APA):*

Sivakumar, S. (2021). *Understanding and Optimization of III-V nanowire growth in Aerotaxy*. Lund University.

*Total number of authors:*

1

**General rights**

Unless other specific re-use rights are stated the following general rights apply:

Copyright and moral rights for the publications made accessible in the public portal are retained by the authors and/or other copyright owners and it is a condition of accessing publications that users recognise and abide by the legal requirements associated with these rights.

- Users may download and print one copy of any publication from the public portal for the purpose of private study or research.
- You may not further distribute the material or use it for any profit-making activity or commercial gain
- You may freely distribute the URL identifying the publication in the public portal

Read more about Creative commons licenses: <https://creativecommons.org/licenses/>

**Take down policy**

If you believe that this document breaches copyright please contact us providing details, and we will remove access to the work immediately and investigate your claim.

LUND UNIVERSITY

PO Box 117  
221 00 Lund  
+46 46-222 00 00

Scanning electron micrograph (SEM) showing a dense forest of vertically oriented III-V nanowires. The nanowires are thin, cylindrical structures that grow from a substrate, creating a complex, interconnected network. The background is dark, highlighting the bright, metallic appearance of the nanowires.

# Understanding and Optimization of III-V nanowire growth in Aerotaxy

SUDHAKAR SIVAKUMAR

DIVISION OF SOLID STATE PHYSICS | DEPARTMENT OF PHYSICS | LUND UNIVERSITY





## Understanding and Optimization of III-V nanowire growth in Aerotaxy



# Understanding and Optimization of III-V nanowire growth in Aerotaxy

Sudhakar Sivakumar



**LUND**  
UNIVERSITY

DOCTORAL DISSERTATION

which, by due permission of the Faculty of Engineering at Lund University,  
Sweden, will be publicly defended on Friday June 18<sup>th</sup> 2021 at 09.15 in  
Rydbergsalen, Sölvegatan 14, Lund, for the degree of Doctor of Philosophy in  
Engineering

*Faculty opponent*

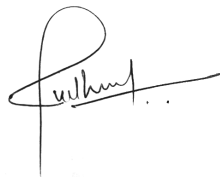
Prof. Albert Nasibulin

Skolkovo Institute of Science and Technology, Russia

<b>Organization</b> LUND UNIVERSITY Division of Solid State Physics Department of Physics P.O. Box 118, SE-221 00 Lund, Sweden Author: Sudhakar Sivakumar		<b>Document name</b> <b>DOCTORAL DISSERTATION</b>	
		<b>Date of issue</b>	
		Sponsoring organization	
<b>Title and subtitle</b> <b>Understanding and Optimization of III-V nanowire growth in Aerotaxy</b>			
<b>Abstract</b> <p>III-V semiconductor nanowires are high aspect ratio nanostructures with superior properties that can potentially enhance the functionality of next-generation opto-electronic devices. At present, the most reliable method for fabricating III-V semiconductor nanowires is the particle-assisted vapor-liquid-solid growth using a substrate-based growth process. However, a substrate based process limits the amount of nanowires that can be produced per cycle and is an obstacle to the industrial production of III-V nanowires. A viable alternative technology for the high-throughput synthesis of III-V nanowires is vital to exploit the true potential of III-V semiconductor nanowires. Aerotaxy is a gas-phase vapor-liquid-solid growth technology that can mass-produce III-V semiconductor nanowires without a substrate. It reduces the cost of production by eliminating the need for a crystalline substrate and can produce nanowires at a phenomenal rate.</p> <p>This thesis explores the fundamental limits of the Aerotaxy technology in producing III-V nanowires. GaAs and GaAsP material systems were adopted to explore the fundamentals of Aerotaxy nanowire growth. Growth experiments were designed to probe the growth parameter dependence of nanowire properties like morphology, crystal structure and composition. In addition to that, the efficiency of in situ doping (<i>p</i>- and <i>n</i>- type) in Aerotaxy was evaluated using optical and electrical characterization techniques. The growth parameter space was explored to demonstrate the reproducibility and efficiency of Aerotaxy nanowire growth. To better understand the growth, a pseudo-particle continuum model for Aerotaxy growth was developed. The results from the model shows good agreement with experimental quantitative and qualitative observations.</p> <p>The studies presented in the thesis also explores the fabrication of complex nanostructures like branched GaAsP nanowires. By tuning the diameter of the initial catalytic particle, we were able to induce branching in GaAsP nanowires. Apart from that, GaAs nanowires grown from alternative metal particles like Ga, AuAg and Ag in Aerotaxy shows promising initial results. Mass-producing III-V nanowires using alternative seed metals that are compatible with Si could bring novel functionalities while reducing production costs. The importance nano-safety is also highlighted in the context of a high-throughput production environment.</p>			
<b>Key words</b> III-V semiconductor materials, nanowires, Aerotaxy, mass-production			
Classification system and/or index terms (if any)			
Supplementary bibliographical information		<b>Language</b> English	
<b>ISSN and key title</b>		<b>ISBN</b> 978-91-7895-908-2	
Recipient's notes	<b>Number of pages</b> 102		Price
	Security classification		

I, the undersigned, being the copyright owner of the abstract of the above-mentioned dissertation, hereby grant to all reference sources permission to publish and disseminate the abstract of the above-mentioned dissertation.

Signature



Date 2021-05-07

# Understanding and Optimization of III-V nanowire growth in Aerotaxy

Sudhakar Sivakumar



**LUND**  
UNIVERSITY



Cover photo: Scanning electron micrograph showing an ensemble of GaAs nanowires collected on a Si substrate. The micrograph demonstrates the ability of Aerotaxy to mass-produce semiconductor nanowires. © Sudhakar Sivakumar

Copyright pp 1-102 Sudhakar Sivakumar

Paper 1 © 2020 IOP Publishing

Paper 2 © 2018 IOP Publishing

Paper 3 © by the Authors

Paper 4 © 2020 Multidisciplinary Digital Publishing Institute (MDPI)

Paper 5 © by the Authors

Paper 6 © 2019 Oxford University Press

Paper 7 © 2018 Wiley-VCH

Division of Solid State Physics  
Department of Physics  
Lund University  
SE-221 00 Lund  
Sweden

ISBN 978-91-7895-908-2 (print)

ISBN 978-91-7895-907-5 (digital)

Printed in Sweden by Media-Tryck, Lund University  
Lund 2021



Media-Tryck is a Nordic Swan Ecolabel certified provider of printed material. Read more about our environmental work at [www.mediatryck.lu.se](http://www.mediatryck.lu.se)

**MADE IN SWEDEN** 

*If we can really understand the problem,  
the answer will come out of it,  
because the answer is not separate from the problem.*

*-Jiddu Krishnamurti.*

# Table of Contents

<b>Acknowledgements</b> .....	<b>10</b>
<b>Abstract</b> .....	<b>13</b>
<b>List of Papers</b> .....	<b>14</b>
<b>Popular science summary</b> .....	<b>17</b>
<b>1 Introduction</b> .....	<b>19</b>
Nanowires .....	20
Scope .....	22
<b>2 Semiconductor Crystal growth</b> .....	<b>23</b>
2.1 Concepts in Crystal growth.....	24
2.1.1 Thermodynamics and kinetics of crystal growth.....	24
2.2 Nanowire growth.....	30
2.3 Metal Organic Vapor Phase Epitaxy .....	31
2.3.1 Vapor–liquid–solid nanowire growth.....	31
2.3.2 Interfacial Kinetics and Nucleation .....	33
2.4 Aerotaxy .....	36
2.4.1 Gas-phase nucleation.....	37
2.4.2 Rate-limiting steps.....	39
<b>3 Nanowire Characterization</b> .....	<b>41</b>
3.1 Electron microscopy.....	41
3.1.1 Scanning Electron Microscopy.....	42
3.1.2 Transmission Electron Microscope .....	44
3.2 X-ray Energy Dispersive Spectroscopy .....	45
3.3 Photoluminescence spectroscopy .....	46
3.3.1 $\mu$ -PL Spectroscopy .....	46
3.4 Electrical Characterization .....	47

<b>4 Aerotaxy III-V nanowires</b> .....	<b>51</b>
4.1 Material system .....	51
4.2 Morphology .....	52
4.3 Crystal Structure.....	56
4.5 Composition .....	57
4.6 Nanowire doping .....	59
4.6.1 Doping evaluation .....	60
4.7 Branched nanostructures .....	65
4.8 Alternative metal seed particles .....	69
4.9 Pseudo-particle continuum model.....	71
<b>5 Aerotaxy instrumentation and Safety</b> .....	<b>75</b>
5.1 The Aerotaxy Instrument .....	75
5.1.1 Aerosol Particle Generator .....	75
5.1.2 Aerotaxy Reactor and Precursor Supply System.....	77
5.2 Aerotaxy Challenges .....	80
5.2.1 Reactor Memory Effect .....	81
5.2.2 Reactor lifetime and conditioning .....	81
5.2.3 Software issues .....	82
5.3 Nano Safety .....	82
5.3.1 Exposure in the workplace .....	83
<b>6 Concluding remarks</b> .....	<b>85</b>
<b>References</b> .....	<b>89</b>

# Acknowledgements

The journey through doctoral education is often a lonely one. I spent so much time inside the lab that at some point, I was convinced that the Aerotaxy machine has become sentient and was capable of perceiving time (just sarcasm, in case someone is worried about me). Still..within a short span of five years, I had the opportunity to come across some truly inspiring and helpful personalities at FTF. I will forever carry those experiences, cherish those interactions and remember their kindness. I am indebted to everyone at FTF for creating such an encouraging and inclusive atmosphere. You made me feel comfortable, helped me with perfecting my purpose and made me confident. To some special people, I would like to express my gratitude here.

First, I would like to thank my supervisor Martin Magnusson, for providing me this opportunity. It is very rare for me to work on something that I like, and you made that possible. I appreciate all the guidance and support that you provided me in the past five years. I am a fan of your ‘jokes’ and the entertaining and informative tangents that you go on during our meetings. I am grateful that your door was always open to me, even during your time as the Deputy Prefect of the Department. You are a great mentor and your enthusiasm is highly contagious. You have no idea about the impact of your support, and my gratitude cannot be expressed in words. If I am given a choice to work on something I like or to work under your mentorship, I would choose working with you without hesitance.

Knut, you always go above and beyond your role as a co-supervisor. You may not remember this, but you were the first person to offer me a home-made *kanelbulle* in Sweden during my time as a ‘Lab-buddy’. Your kindness and humility towards your colleagues have taught me some very important life lessons. Your funny and witty remarks always light up the room. Your support and kindness towards me even when I disappoint you is something that I will never forget. You instilled a great deal of confidence in me, and I have a deep sense of respect for you. I am thankful for the part you have played in my life.

Lars, I am grateful for having you as a co-supervisor. I enjoyed the chats we had during our meetings. You have been warm and kind to me, your enthusiasm to talk about Aerotaxy has always inspired me. My first interaction with you and your cheerful demeanour is something that beset me on my current path. Thank you for everything.

Dan Hessman, you have been a mentor and a pillar of support since I started my post graduate education at FTF in 2013. I am thankful for all the opportunities you have given me. I like that you always wear a smile and that you can find a solution for almost any problem.

Wondwosen, you taught me how to operate the Aerotaxy tool and I am thankful for that. I learnt a great deal about nanowire growth from you. Thank you for driving me around Lund and helping with everything. Bengt, I am not sure where to begin. You always came up with a solution for hardware and software issues that were beyond my capability. You played a major role in my research and taught me a lot about hardware maintenance. I enjoyed our lunch time conversations when it was still allowed at FTF. Thank you for being the *handyman* and a mentor. Olof Hultin, you taught me how to perform electrical characterization. I really appreciate your enthusiasm and patience while teaching. Although you knew more, you were kind enough to listen to my suggestions and I am thankful for that. Irene Geijselaers, I appreciate your help with PL measurements and your attempts to teach me PL along with Neimantas. I enjoyed our conversations during lunch breaks, summer schools and the Wednesday nights at Rydberg's pub. You always sparkle whenever you talk about something you like. Axel Persson—thanks for helping me with TEM characterization. Reine and Crispin—thanks for your patience while teaching electron microscopy to me and I really appreciate your help with the TEM. Both of you were kind and always helpful to me and I am grateful for that.

Sara. F, you have been a dear friend, a colleague and my office mate since 2016. I would like to thank you for your support. I will always remember how you drove me around Arizona, and I promise to bring a better playlist for the road next time. Mohammad. K, you have been a good friend and an office mate. I enjoyed our office conversations and like that you always smile. Thanks. Calle. P, you are my office mate on the other side. You have inspired me many times with your perseverance and positive attitude. Robert. H, I enjoyed the time spent working with you in the Aerotaxy lab. Thank you for sharing your books with me. Maria. M—I am always inspired by your management skills and energy during our weekly meetings. I am fascinated by your ability to identify and appreciate hard work. Thanks for trying to arrange meetings outside work, I enjoy those little meetings outside the lab. Markus. S—I will always remember your enthusiasm and involvement in everything you do. Namsoon, I enjoyed your presentations about molecular simulations. Pau, Marie and Mehran, you joined the group very recently, but I am happy about all the interactions we had.

Magnus. H and Sungyoun—I appreciate that you shared your knowledge about Aerotaxy with me. Thank you and I enjoyed our discussions. Sven, Anette, Asmita, Kristi, Antti and Jonathan—thank you for the nice conversations during courses and teaching, I enjoyed it. Pradheebha, thank you for tolerating me as your house mate for more than a year. In no particular order, Lukas, David. A, David. B, Erik. M, Martin. J, Artis, Florinda, Xulu, Gaute, Luna, Reza, Yang. C, Ali. N, Regina, Frida,

Alexander, Vilgaile, Markus. T, Damiano, Mercy and Rong—all of you have helped me to feel comfortable in one way or the other. I am thankful for all the good times.

I would like to extend my heartfelt thanks to the technical and administrative staff of FTF and LNL: (in no particular order) Luke, Ivan, Peter. B, Anders. K, Anneli, Carina, Claes. T, Heiner, Magnus. B, Mats-Erik, Ville, Christelle, Adam. B, Alfons. E, Anastasiia, Dmitry, Gerda, Marica, Natalia, Mariusz, Sara. A, Therese and Anders. G. Without you, FTF would literally fall apart. Thank you for creating a warm and nice atmosphere. Håkan. L, I enjoyed every single interaction I had with you. You are—to put it lightly—*cool*. George, you have always been helpful and kind towards me. Jonas. J, you have been extremely understanding and kind to me. Thank you for teaching me crystal growth and thermodynamics. Sören, I am grateful for the technical help and the wisdom that you were kind enough to share with me over lunch breaks. Janne, I enjoyed working with you. Every time we pass each other on the corridor, you ask me if I started speaking Swedish. I promise you that I will, someday. Neimantas, thanks for the innebandy and badminton sessions, the hikes and teaching me to hunt for mushrooms in the Swedish wilderness.

Markus. H—thank you for being a beacon amidst the storm. You have introduced me to countless European traditions and some great German phrases. If I have to do it all again, I will probably change many things but not your friendship. Ali. H, I am really glad that we became friends. Thank you for sharing your unique perspectives with me during our weekly lunch. Kush, you have truly inspired me by your resilience both in your personal and professional life. Thanks for just being there. Abhinaya, you have been there for me as a friend during some bad times, thanks. I am happy for the way that your life has evolved over the years.

Although my family was miles away, I could always feel their love and support. Thanks for your support Amma, I know how much you wanted me to stay right next to you in India, but you still supported me in every way you knew. Appa—you say a lot with a few words. Thanks for teaching me the importance of resilience. Thanks to my sister and grandma for their unconditional love and support.

# Abstract

III-V semiconductor nanowires are high aspect ratio nanostructures with superior properties that can potentially enhance the functionality of next-generation optoelectronic devices. At present, the most reliable method for fabricating III-V semiconductor nanowires is the particle-assisted vapor-liquid-solid growth using a substrate-based growth process. However, a substrate-based process limits the number of nanowires that can be produced per cycle and is an obstacle to the industrial production of III-V nanowires. A viable alternative technology for the high-throughput synthesis of III-V nanowires is vital to exploit the true potential of III-V semiconductor nanowires. Aerotaxy is a gas-phase vapor-liquid-solid growth technology that can mass-produce III-V semiconductor nanowires without a substrate. It reduces the cost of production by eliminating the need for a crystalline substrate and can produce nanowires at a phenomenal rate.

This thesis explores the fundamental limits of the Aerotaxy technology in producing III-V nanowires. GaAs and GaAsP material systems were adopted to explore the fundamentals of Aerotaxy nanowire growth. Growth experiments were designed to probe the growth parameter dependence of nanowire properties like morphology, crystal structure and composition. In addition to that, the efficiency of in situ doping (*p*- and *n*- type) in Aerotaxy was evaluated using optical and electrical characterization techniques. The growth parameter space was explored to demonstrate the reproducibility and efficiency of Aerotaxy nanowire growth. To better understand the growth, a pseudo-particle continuum model for Aerotaxy growth was developed. The results from the model shows good agreement with experimental quantitative and qualitative observations.

The studies presented in the thesis also explores the fabrication of complex nanostructures like branched GaAsP nanowires. By tuning the diameter of the initial catalytic particle, we were able to induce branching in GaAsP nanowires. Apart from that, GaAs nanowires grown from alternative metal particles like Ga, AuAg and Ag in Aerotaxy shows promising initial results. Mass-producing III-V nanowires using alternative seed metals that are compatible with Si could bring novel functionalities while reducing production costs. The importance nano-safety is also highlighted in the context of a high-throughput production environment.



# List of Papers

Results discussed in this thesis are based on the following articles, they are referred in the text by their roman numerals

## **I. Aerotaxy: gas-phase epitaxy of quasi 1D nanostructures**

Sudhakar Sivakumar, Axel R Persson, Wondwosen Metaferia, Magnus Heurlin, Reine Wallenberg, Lars Samuelson, Knut Deppert, Jonas Johansson and Martin H Magnusson

*Nanotechnology*, **2020**, 32 025605

I formulated the project with M.H.M and K.D. I performed all the experimental work and data analysis except the CFD wire growth simulation. I authored the article, the CFD simulation part of the article was authored by M.H.M and J.J.

## **II. *n*-type doping and morphology of GaAs nanowire in Aerotaxy**

Wondwosen Metaferia, Sudhakar Sivakumar, Axel R Persson, Irene Geijselaers, L Reine Wallenberg, Knut Deppert, Lars Samuelson and Martin H Magnusson

*Nanotechnology*, **2018**, 29 285601

I planned and performed the nanowire growth along with W.M. I fabricated the devices, performed SEM, electrical characterization and participated in photoluminescence measurements and data analysis. I co-authored the paper with W.M and all the co-authors.

## **III. Diameter-dependent branching in Aerotaxy growth GaAsP nanostructures**

Sudhakar Sivakumar, Reine Wallenberg, Jonas Johansson, Magnus T. Borgström, Lars Samuelson, Knut Deppert and Martin H. Magnusson

*Manuscript submitted to Journal of Nanomaterials.*

I formulated the project and optimized the nanowire growth for the ternary system. I performed SEM characterization and was responsible for writing the paper and data analysis.

**IV. Calculation of hole concentrations in Zn doped GaAs nanowires**

Jonas Johansson, Masoomeh Ghasemi, Sudhakar Sivakumar, Kilian Mergenthaler, Axel R. Persson, Wondwosen Metaferia and Martin H. Magnusson

*Nanomaterials*, **2020**, 10(12), 2524

I participated in planning and grew the nanowires. I fabricated the devices and performed electrical characterization. I authored the parts related to electrical characterization.

**V. Ga-seeded growth of GaAs nanowires using Aerotaxy**

Sudhakar Sivakumar, Eric Ceccarelli, Lars Samuelson, Knut Deppert and Martin H. Magnusson

*Manuscript to be submitted*

I formulated the project with M.H.M, K.D and E.C. I participated in discussions and data analysis. I wrote the paper with E.C.

**VI. Workplace Emissions and Exposures During Semiconductor Nanowire Production, Post-production, and Maintenance Work**

Christina Isaxon, Karin Lovén, Linus Ludvigsson, Sudhakar Sivakumar, Anders Gudmundsson, Maria E Messing, Joakim Pagels, Maria Hedmer

*Annals of Work Exposures and Health*, **2020**, 64, 1, 38–54

I performed SEM and XEDS characterization and analysed the data.

**VII. Electron Tomography Reveals the Droplet Covered Surface Structure of Nanowires Grown by Aerotaxy**

Axel R. Persson, Wondwosen Metaferia, Sudhakar Sivakumar, Lars Samuelson, Martin H. Magnusson and Reine Wallenberg

*Small*, **2018**, 14, 33, 8

I grew the nanowires with W.M and participated in discussions.

The following articles are relevant to the field, but not included as they fall outside the scope of this thesis.

**VIII. Dual topography of laminin corona on gallium arsenide nanowires**

Stefán Bragi Gunnarsson, Cesare Mellace<sup>1</sup>, Katja Bernfur, Sudhakar Sivakumar, Martin H. Magnusson and Tommy Cedervall

*Biointerphases*, **2020**,15, 051007

**IX. Optical far-field extinction of a single GaAs nanowire towards *in situ* size control of nanowire growth**

Yang Chen, Nicklas Anttu, Sudhakar Sivakumar, Eleni Gompou and Martin H Magnusson

*Nanotechnology*, **2020**, 31 134001

# Popular science summary

The famous physicist and Noble Laureate Richard Feynman once delivered a speech entitled '*There is Plenty of Room at the bottom*'. He was referring to the tremendous potential of *Nanotechnology* and the ramifications of the ability to manipulate material at the atomic-scale. Now, decades after his talk, we are surrounded by nanoscale devices. Probably—right now—you are carrying billions of nanoscale semiconductor devices in your pocket in the form a smart phone, wearing one on your wrist or reading this very text on a smart device. These nanoscale devices are at the heart of all the smart electronics that continually improve the quality our lives. Interestingly, these devices are fabricated in a similar fashion to how one builds a Lego structure by arranging Lego bricks; but instead of Lego bricks, material scientists use nanoscale building blocks made from semiconducting materials.

Semiconducting nanowires belong to a class of nanomaterials that can be used as building blocks, where several billion of them can be arranged together to fabricate functional devices. Nanowires are rod-like structures that can be several micrometres long, but only a few hundred nanometres wide. If they are made from elements that belong to Group III and V of the periodic table, they are rightly referred as III-V semiconducting nanowires. Researchers around the world hope that nanowires can change our lives in the future by playing an active role in next generation LEDs, solar cells, etc. In order for this to become a reality, an inexpensive and precise method is required to mass-produce nanowires with perfect crystallinity, uniform size distribution and composition. If one plants a seed, the seed collects material and nourishment from its immediate environment to grow into a tree according to the seed's genetic blueprint. The common way to make semiconductor nanowires is very similar to growing a tree; where gold seed particles placed on a substrate is supplied with the necessary material and a nurturing environment that encourages nanowire growth. But this method is time consuming, has low production rate and needs an expensive substrate.

To manufacture the billions of nanowires that are needed to make functional devices, novel synthetic techniques must be developed. The manufacturing technique must be able to produce nanowires at a large scale with uniform properties. In this thesis, I have investigated the synthetic Aerotaxy technology and its potential to grow large quantities of III-V semiconductor nanowires in a controllable fashion.

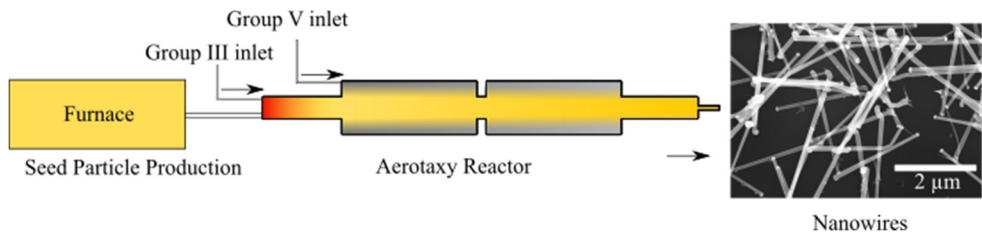


**Figure 1.** Illustration of the Aerotaxy growth system. The growth process begins by evaporating gold and size selecting the nanoparticles. The size-selected gold nanoparticles are sent through the heated Aerotaxy reactor, where III-V material is mixed with the gold nanoparticles, and the wires grow on the nanoparticles. Afterwards, the nanowires can be deposited on a substrate.

With Aerotaxy technique, nanowires can be manufactured without a substrate at phenomenal rates (see Figure 1). Gold is evaporated in a furnace to form nanoparticles in a gas similar to how clouds form. The gas containing the gold nanoparticles is then sent through a growth reactor, where the gas temperature is raised and mixed with growth material (III-V precursor material). Crystalline nanowires grow on the gold particle at a phenomenal rate which is  $\sim 1,000$  times faster than when they are produced on a substrate. The nanowires can be collected on any substrate and later incorporated into a suitable device. The whole process from start to finish lasts for about 6s.

In this thesis, I have used the Aerotaxy technique to produce GaAs and GaAsP semiconductor nanowires and investigated their opto-electronic properties. I used these material systems to understand the fundamental processes that makes Aerotaxy synthesis possible. Understanding and optimizing Aerotaxy growth is crucial for incorporating nanowires into functional devices of the future. And the insights obtained here will ultimately contribute towards building a sustainable and technologically advanced future.

# 1 Introduction

The machines of early 19<sup>th</sup> century powered by abundant fossil fuel hurled the human society into an era of rapid development which continues to this day. Titans like Michael Faraday and Walter Schottky laid a comprehensive foundation during the 19<sup>th</sup> and 20<sup>th</sup> centuries for contemporary semiconductor physics. The *point contact transistor* developed in 1947 heralded the arrival of the semiconductor era<sup>1</sup> and fast-tracked the progress of our civilization. As we begin to realize the lasting repercussions of ongoing and relentless consumption, the world is currently facing some of the greatest challenges of the 21<sup>st</sup> century. Out the many challenges, the transcendence to sustainable and renewable energy sources should be our battle of choice.

As of 2020, the estimated global share of electricity produced from renewable sources like solar, wind, etc, in total electricity production is around 27.8%.<sup>2,3</sup> More than 115 GW of additional solar photovoltaic (PV) power generation capacity was added in 2019. This additional PV capacity increased the electricity production by 57% from the previous year, thus making PV the leading renewable electricity producer.<sup>4</sup> Major cities and countries around the globe have adopted policies to phase-out coal and to reduce emissions in the past few years. Crystalline Si solar cells still dominate the PV market with average cell efficiency reaching 22.8% for *p*-type monocrystalline solar cells.<sup>5</sup> Continuous developments has reduced PV module costs, which dropped by 10% in 2020<sup>5</sup> compared to 2018. By increasing the conversion efficiency and power capacity, the price of PV modules can be further reduced. This emphasises the need for the development of next-generation, high-efficiency PV technologies. Though crystalline Si solar cells still dominate the PV market, in recent years the overall conversion efficiency of Si solar cells has barely improved. Alternative PV technologies like III-V multi-junction solar cells, perovskites and nanowire ensemble devices have shown promising development i.e., their efficiencies have surpassed the efficiency of commercially available Si solar cells. But, the raw materials and manufacturing processes used in these alternative technologies are expensive and the manufacturing cost limits their use to areas like space applications, where high production costs can be accommodated.

Nanoscale materials exhibit properties that are very different from their bulk counterparts. Interesting properties emerge at this scale since the dimensions of the functional components are on the same order as the charge carrier wavelength.<sup>6</sup> Furthermore, the large surface-to-volume ratio of nanostructures give rise to

interesting optical, electronic, magnetic and catalytic properties. By engineering the shape and size of these nanostructures, their properties can be exploited to fabricate opto-electronic and mechanical devices with novel functionalities. These engineered nanostructures due to their small size, inherently utilize less material compared to their bulk counterparts, thereby reducing the overall production cost.

## Nanowires

The semiconductor industry faces challenges that are complex and multifarious, but most of these challenges can be combated by using a nanowire-like architecture. Nanowires are rod-like, high aspect ratio structures that are few tens of nanometres in diameter and several micrometres long. Being dimensionally close to the wavelength of visible light, nanowires have interesting light-matter interactions, providing a suitable geometry for the photoconversion process in nanowire solar cells.<sup>7</sup> The small footprint of nanowire architecture and the possibility for efficient strain relaxation enables the fabrication of heterostructures using lattice mismatched materials with relative ease. Nanowires—in particular the ones produced by combining elements from groups III and V of the periodic table—manufactured using a gas-phase fabrication technique called Aerotaxy<sup>8</sup> and their characterization will be the primal focus of this thesis. Nanowires can act as basic building blocks and by assembling billions of nanowires together we can fabricate devices with complex and novel functionalities. A variety of useful devices already utilize the nanowire architecture for e.g. nanowire LEDs,<sup>9</sup> solar cells,<sup>10</sup> field effect transistors (FET)<sup>11</sup> and nanoscale lasers,<sup>12</sup> etc.

Semiconductor nanowires can be synthesized either by ‘Top-Down’ or ‘Bottom-Up’ approach. In top-down approach, the manufacturing process involves selective etching of the nanowires from a bulk crystalline material using lithographically defined masks in combination with chemical or physical etching techniques. In this case, the composition of the nanowire is determined by the composition of the bulk material. This approach is widely used in the semiconductor industry for manufacturing Si-based opto-electronic devices. Silicon is well suited for top-down nanowire synthesis as Si can be etched precisely into well-defined arrays with high homogeneity.<sup>13</sup> However, for III-V semiconductor nanowires, the etching process always introduces surface roughness and other unintended effects which degrades the useful electronic properties of the nanowire geometry.<sup>14</sup> The ability to obtain high-quality nanowire heterostructures like core-shell and superlattice heterostructures makes the bottom-up approach preferable for III-V nanowire synthesis.

In the bottom-up approach, a metal nanocluster/nanoparticle placed on a crystalline substrate is heated above the eutectic temperature of the metal–semiconductor

system in the presence of gas-phase semiconductor material-source. The gas-phase semiconductor material mixes with the metal nanoparticle and forms a liquid metal–semiconductor alloy. A continuous supply of semiconductor material from the gas-phase creates a supersaturated liquid alloy. This supersaturation disrupts the equilibrium of the system and results in nucleation of the solid semiconductor, returning the system closer to equilibrium. The newly formed liquid–solid (L-S) interface is the growth front and further nanowire growth will proceed at the L-S interface. A constant supply of semiconductor material ensures that the liquid alloy retains the supersaturation necessary for precipitation at the L-S interface. The crystalline substrate also forms a vapor–solid interface (V-S) with the gas-phase in addition to the existing vapor–liquid (V-L) interface. Nanowire growth will proceed if nucleation at the vapor–liquid (V-L) interface is preferred over the V-S interface. This kind of self-assembling manufacturing process gives precise control over the electronic properties and the composition of the nanowire. The fascinating and novel properties observed in the nanowire geometry present enough motivation to develop a scalable synthetic method to produce III-V semiconductor nanowires.

Metal Organic Vapor-Phase Epitaxy (MOVPE) is a bottom-up approach and has been used for manufacturing semiconductor nanowires since the early 90's.<sup>15</sup> MOVPE can fabricate high-quality nanostructures on par with Chemical Beam Epitaxy (CBE) and is an industrial standard for semiconductor thin film manufacturing.<sup>16</sup> The technology has evolved tremendously to keep up with market requirements since the late 90's. Current *state-of-the-art* MOVPE tools have multi-wafer production capacity with *in situ* monitoring capabilities for process tuning and can produce high-quality semiconductor thin films.<sup>17</sup> However, for nanowire growth, the technology is still in its early stage of development due to the inherent complexity and the lack of a unified theory to explain nanowire growth. MOVPE nanowire growth generally involves expensive crystalline substrates that require some level of pre-processing to achieve nanowire growth. Using an expensive substrate with limited space effectively limits the number of nanowires that can be grown while increasing the cost of production.<sup>18</sup>

In order for the semiconductor industry to consider nanowires as a viable alternative to planar devices, a cost-efficient and high-throughput nanowire production method is essential. Aerotaxy is a patented<sup>19</sup> growth technology that serves this exact purpose by producing nanowires continuously without a substrate. Aerotaxy provides a platform to produce III-V semiconductor nanowires with tunable properties. While Aerotaxy is still in its early stages of development, it exploits the high-volume production capability of continuous gas-phase production techniques.<sup>8</sup> In this thesis, the Aerotaxy growth technology is described and its unique capabilities are emphasized. Results obtained from various experiments performed with the Aerotaxy tool are discussed in detail. Nanowire properties like



composition, doping, length, bandgap, carrier concentration and their relation to the controllable Aerotaxy growth parameters are summarised.

## Scope

The topic of this dissertation is fabrication of III-V semiconductor nanowires using the gas-phase Aerotaxy technique and their characterization. Production of doped and undoped GaAs and GaAsP nanowires and their characterization is the main premise of this thesis.

In Chapter 2, theoretical framework for both VLS growth techniques namely MOVPE and Aerotaxy are discussed. The two methods are compared and their differences are highlighted.

In Chapter 3, an overview of different techniques used to characterize the Aerotaxy grown III-V semiconductor nanowires is provided.

The qualitative and quantitative findings common for Aerotaxy grown III-V nanowires are discussed in Chapter 4. Results from Paper II, III, V, VI and VII are highlighted in this chapter.

Chapter 5 discusses in detail about the importance of Nano-safety in a gas-phase nanomaterial production environment. Details about the custom built Aerotaxy tool is presented in this chapter along with highlights from Paper I and IV.

The final chapter presents the concluding remarks.

## 2 Semiconductor Crystal growth

This chapter introduces the fundamental concepts of semiconductor crystal growth like nucleation, supersaturation and the thermodynamic driving force. An overview of the two closely related nanowire growth methods, (i) MOVPE and (ii) Aerotaxy is presented. Description of Aerotaxy nanowire growth builds on the concepts of crystal growth and MOVPE.

The III-V semiconductor nanowires discussed in this thesis were fabricated using the gas-phase Aerotaxy technique. In Aerotaxy, gaseous hydride and metal-organic (MO) precursors precipitate into a crystalline phase in the presence of a liquid alloy droplet, which occurs through the so-called vapor–liquid–solid (VLS) growth mode as first described by Wagner and Ellis.<sup>20</sup> The alloy droplet acts as a collector to concentrate the precursor species from the vapor phase. This process is mainly controlled by temperature, pressure, precursor partial pressures, precursor flux ratios and gas flow rates. The VLS crystal growth can be tailored by varying any of the previously mentioned parameters. The growth temperature for instance governs precursor decomposition and interfacial kinetics. As the name suggests, components of a VLS system may exist in one of the three phases and their chemical potentials are determined by the thermodynamic properties of the growth system. If the growth conditions are tailored such that the crystal (solid) phase has the lowest chemical potential, the system favors crystal growth. This favorable chemical potential gradient, which is influenced by the growth temperature, is called the *thermodynamic driving force*. Various other processes that are vital for VLS crystal growth like Brownian diffusion, thermal evaporation and condensation has an obvious dependence on the temperature. Decomposition of metal-organic precursors like trimethylgallium (TMG) is enhanced at high growth temperatures.<sup>21</sup> Apart from that, growth temperature governs many aspects of VLS growth due to its influence on phase transitions, interface kinetics and precursor flux density.

The growth rate and crystal structure of GaP nanowires were found to be influenced by the precursor flux ratio,<sup>22</sup> which reflects the relative proportions of precursors present in the gas-phase. Engineering the alloy droplet by tuning its shape, size and composition has been reported to improve the thermal stability of GaAs<sup>23</sup> nanowires i.e., it reduced the probability of particle-assisted thermal decomposition of GaAs nanowires during growth. It is also possible to grow complex nanostructures like nanotrees,<sup>24</sup> tetrapods,<sup>25</sup> horizontal nanowires,<sup>26</sup> branches<sup>27,28</sup> and other 3D nanostructures through droplet engineering (Paper III).

## 2.1 Concepts in Crystal growth

Naturally occurring crystals usually start out as a liquid and as the liquid cools, the atoms, ions or molecules in the liquid come together to form an ordered crystalline solid. This crystallization/solidification usually nucleates from a single nucleus or crystallites from multiple nuclei meet each other to form a unified growth front. Crystal growth is in principle a transformation from one phase to another resulting in a crystalline solid (most crystals are solid). If we consider a simple III-V semiconductor like GaAs, the vapor phase ( $v$ ) consisting group III (TMG) and group V ( $\text{AsH}_3$ ) precursors transforms into a crystalline solid phase ( $s$ ) in a controlled environment. The overall reaction can be written as:



### 2.1.1 Thermodynamics and kinetics of crystal growth

Thermodynamic studies of phase transitions by J. Willard Gibbs (1839–1903)<sup>29</sup> in a heterogenous system laid the foundation for our understanding of contemporary crystal growth. In a typical solid material, inter-atomic and intermolecular cohesive forces determine the structural dynamics and phase of the solid. Phase transitions in a system can thus be studied using the intermolecular chemical potentials or particle–particle interactions. As mentioned earlier, semiconductor crystal growth deals with phase transitions which can be readily described using classical thermodynamics. And by combining the kinetics of processes at the nanoscale with the thermodynamic description, a clear understanding of crystal growth can be achieved.

#### *Chemical Potential*

From a thermodynamic perspective, phase transition occurs in the direction of declining chemical potential, which is defined as the rate of change of Gibbs free energy ( $G$ )<sup>30,31</sup> with respect to the change in number of atoms or molecules of reactive species. Chemical potential quantifies the inherent capacity of a material for change or phase transformation.<sup>32</sup> The individual reactions in a system are driven to minimize the free energy of the system so that the different phases eventually attain equilibrium in terms of chemical potential. Chemical potential can be defined in terms of change in Gibbs free energy as:

$$\mu_x = \left( \frac{\partial G}{\partial N_x} \right)_{P,T,N_{j \neq x}}, \quad 2.2$$

where  $\mu_x$  is the chemical potential of species  $x$  with a small change in the number of moles  $N_x$  at a given pressure  $P$  and temperature  $T$ . Thermodynamic equilibrium can

only be achieved in a closed system,<sup>33</sup> which is not possible during crystal growth due to a constant influx of precursor material. This constant influx of precursor species ensures the presence of a chemical potential gradient that favors crystal growth. If we consider a vapor-phase epitaxy system like MOVPE with three phases (vapor, liquid, solid) and their respective chemical potentials ( $\mu_v, \mu_l, \mu_s$ ), then crystal growth is favored when the chemical potential of the solid phase is the lowest:

$$\mu_v \gg \mu_l \gg \mu_s. \quad 2.3$$

For example, if the difference in chemical potential between the vapor and solid phases ( $\Delta\mu_{v-s}$ ) is positive, the thermodynamic driving force favors crystal growth and if the difference is negative, material is removed from the crystal phase and is called reverse growth or melting. This potential gradient also determines the rate at which material is added to or removed from the crystal phase.

#### *Thermodynamic Supersaturation*

In this section, the term supersaturation is used to denote the driving force of crystallization. A single component system with two infinitely large phases  $\alpha$  and  $\beta$  with their respective chemical potentials  $\mu_\alpha$  and  $\mu_\beta$ , is said to be in equilibrium if it satisfies eq-2.4:

$$\mu_\alpha(T, P) = \mu_\beta(T, P), \quad 2.4$$

where  $T$  is the temperature and  $P$  is the pressure that are equal for both phases. The boundary lines in the phase diagram<sup>34</sup> (Figure 2.1) separating two phases of a typical one component system must satisfy eq-2.4.

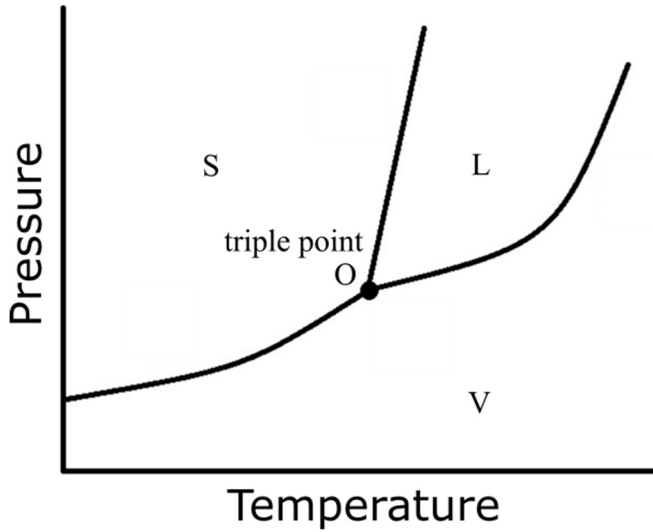


**Figure 2.1.** Phase diagram of a one component system. The lines represent equilibrium/equipotential boundaries between different phases S, L and V. The point at which two lines intersect is the triple point (O) that represents the pressure and temperature at which all three physical states can co-exist.

If the pressure and temperature are varied along the boundary lines in Figure 2.1, the corresponding phases satisfies eq-2.4 and are said to be in equilibrium. If the conditions are changed so that we deviate from the boundary line, the chemical potential of one of the phases becomes smaller than the chemical potentials in all the other regions leading to phase transition. Phase transition also occurs if the temperature is fixed while changing the pressure and vice versa. If phase S is solid and phase V is vapor (similar to phase diagram of ice), increasing the pressure  $P$  beyond the equilibrium pressure  $P_0$  or reducing temperature  $T$  beyond the boundary lines will lead to crystallization or sublimation (if  $P < P_0$ ). If  $P > P_0$ , the vapor phase should readily crystallize and the difference in chemical potential between vapor and crystal phases ( $\Delta\mu_{v-s}$ ) is called the supersaturation. Supersaturation is a pre-requisite for a solid crystal-phase to appear in a saturated solution (not the case for single-component system). So, by varying the vapor pressure under constant temperature or vice versa, a potential gradient that favors crystallization can be established. Without great detail, the supersaturation of a single-component ideal gas system can be expressed as:

$$\Delta\mu = kT \ln \frac{P}{P_0}, \quad 2.5$$

where  $k$  is the Boltzmann constant. The potential gradient which is established through careful manipulation of vapor pressure and temperature represents the *thermodynamic driving force* of crystallization.<sup>20,35,36</sup>

## Nucleation

Nucleation is a ubiquitous phenomenon in nature that occurs as part of formation of rock, rain, fog, ice, etc. Classical nucleation theory suggests that, in order to ensure thermodynamic stability, phase transition occurs in infinitesimally small steps infinitely close to the boundary between the two phases.<sup>37</sup> This is referred as the *first-order phase transition*. For atoms or molecules to nucleate into clusters, (i) the system must gain energy by displacing matter from the vapor to crystal phase or reduce its free energy and (ii) the cost of forming new surfaces/phase-boundaries (nucleation barrier) must be low. The thermodynamic supersaturation ( $\Delta\mu_{v-s}$ ) given by eq-2.5, directly relates to the amount of energy the system will gain by favoring crystallization and is measured in eV/atom-pair incorporated into the crystal. So, the number of atom-pairs that constitute the nucleus determines the amount of energy gained from crystallization, which is expressed in normalized volume ( $V/\Omega$ ) of the nucleus.<sup>36-38</sup>

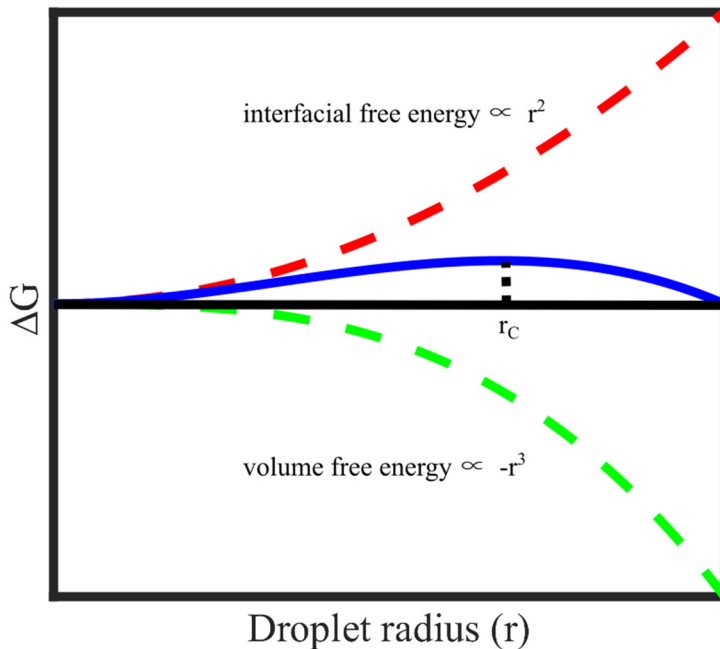


**Figure 2.2** Change in Gibbs free energy as a function of nucleus radius for the case of homogenous nucleation of a spherical nucleus.

The surface atoms of an emerging nucleus must interact with the mother phase, which poses an energy barrier that must be overcome. The surface energy  $\gamma$  expressed in eV/Å, for formation and maintenance of new surfaces depend on the

thermodynamic properties of the system, the type of material and the atomic arrangement at the surface of the mother phase. Therefore, the energy barrier for formation and maintenance of new surfaces depends on the areas ( $A$ ) of the different sides of a nucleus. The change in Gibbs free energy for nucleation ( $\Delta G_N$ ) is a sum of thermodynamic supersaturation ( $\Delta\mu_{v-s}$ ) and energy barrier for formation and maintenance ( $\gamma * A$ ). The change in  $\Delta G_N$  for a nucleus that has  $i$  surfaces with area  $A$  can be expressed as:

$$\Delta G_N = (\mu_v - \mu_s) \frac{V}{\Omega} + \sum_i \gamma_i A_i. \quad 2.6$$

Figure 2.2 plots the relationship between  $\Delta G_N$  and the size of an emerging nucleus. If we consider nucleation in vapor-phase, the emerging nucleus is assumed to be spherical, then the supersaturation term in eq-2.6 is proportional to  $r^3$  (where  $r$  is the radius of the emerging nucleus) and the surface term is proportional to  $r^2$ . While eq-2.6 is true for a single-component system, the supersaturation term must also account for the shape of the nucleus in a multicomponent heterogenous system. In a multicomponent crystal growth process like VLS GaAs nanowire growth, the shape of the initial nucleus also depends on the wettability of the growth surface (i.e. wettability of the crystalline substrate) and the supersaturation term in eq-2.6 must reflect that. The term  $r_c$  in Figure 2.2 refers to the critical radius of the nucleus and for any emerging cluster with size below the critical radius the surface energy term dominates eq-2.6 and leads to decay of the cluster. Beyond  $r_c$ , the nucleus is likely to grow in size and form a stable crystal phase the growth is now limited by kinetics or mass transport into the crystal phase rather than the rate of nucleation. If nucleation occurs spontaneously and with a uniform probability throughout the system then it is called homogenous nucleation. The rate of homogenous nucleation ( $J_n$ ) is found to have an Arrhenius dependence on the rate of change of Gibbs free energy i.e. the number of nuclei that appear in a unit volume per unit time, which was approximated by Volmer<sup>37,39,40</sup> using statistical thermodynamics as:

$$J_n = A e^{-\Delta G_N(r_c)/k_B T}, \quad 2.7$$

where  $k_B$  and  $T$  represents the Boltzmann constant and the temperature respectively and  $A$  is the exponential pre-factor.

### *Role of Kinetic barriers*

Previous sections presented a description of crystal growth based on the thermodynamic state and phase transition. But there are kinetic barriers involved in mass transport, gas-phase subprocesses and the associated chemical reactions. The kinetic barriers represent the energy spent in processes like adatom migration, surface diffusion and nucleation and is dependent on the direction of the reaction.

In a typical vapor phase crystal growth process, the incoming atoms can get *adsorbed* on the growth surface through weak van der Waals forces (physisorption) or become incorporated to the crystal phase through *chemisorption*.<sup>41,42</sup> The chemisorbed atom can get desorbed through chemical decomposition. A detailed treatment of kinetic barriers from the perspective of nanowire growth is presented in section 2.3.2. The crystal growth rate has a dependence on all these kinetic processes.

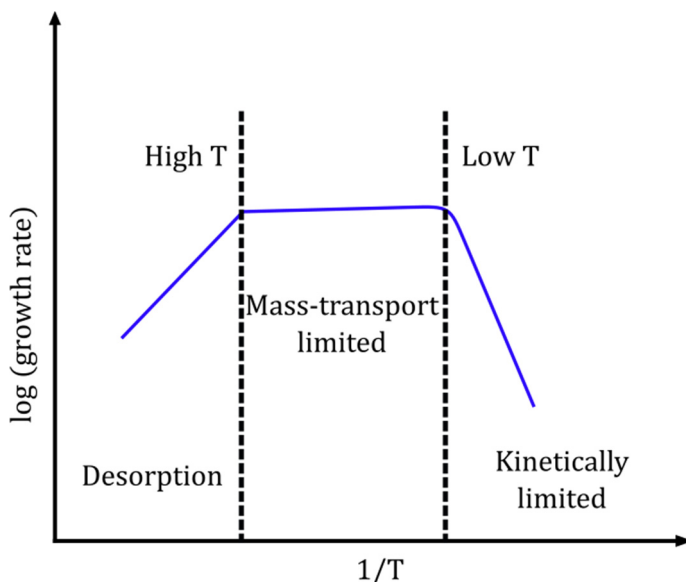


**Figure 2.3.** A typical log (growth rate) vs inverse temperature plot of an epitaxial process. At low temperature, the growth rate increases exponentially with temperature due to thermally activated processes. At intermediate temperatures, the growth is transport limited and only has a weak dependence on the temperature. At high enough temperature, the growth rate is reversed due to decomposition and deposition on the reactor walls.

Figure 2.3 shows the growth rate dependence on inverse growth temperature due to the expected Arrhenius relationships among the rate constants. It maps the various crystal growth regimes and their temperature range in a typical epitaxial process. For low temperatures, the growth rate increases exponentially with the temperature. This is because at low temperatures, the gas phase supplies precursors at a higher rate and the growth is kinetically limited. For moderate growth temperatures, the growth rate is independent of the temperature and depends mostly on mass-transport to the crystal phase. At high temperatures, the growth rate becomes kinetically limited once again. Nanowire growth is usually achieved in the low to moderate temperature regimes. At this range, the thermally activated reactions like precursor pyrolysis and diffusion occur with an exponential dependence on growth temperature as seen in Figure 2.3.



## Diffusion

Surface diffusion of adatoms/molecules is a vital kinetic process in VLS nanowire growth.<sup>43,44</sup> In a typical epitaxial VLS growth, the vapor phase contains a constant flux of precursor species, a small proportion of which may be partially pyrolyzed. This incoming flux of adatoms can either physisorb on the surface or chemisorb if they find a suitable site for incorporation. An adsorbed adatom might diffuse along the surface if suitable adsorption sites are available. For successful surface diffusion, the adatom must overcome the kinetic barrier of diffusion expressed in terms of activation energy ( $E_D$ ). The extent to which an adsorbed adatom can diffuse depends on the mean-free path ( $\lambda$ ) of the adsorbed species, which has a temperature dependence. This means that surface diffusion between suitable sites also has a temperature dependence. The coefficient of diffusion  $D$  has an Arrhenius dependence on  $E_D$  and can be expressed as:

$$D = D_o e^{-E_D/k_B T}, \quad 2.8$$

where  $D_o$  is the exponential pre-factor.

## 2.2 Nanowire growth

Previous sections introduced the basic concepts necessary to understand crystal growth and phase transition. While they are generally applicable for semiconductor nanowire growth, certain concepts that are unique to nanowire growth are considered in the following sections. Additive bottom-up techniques used for manufacturing semiconductor nanowires can be categorized based on whether a catalytic particle or a mask is used to assist crystal growth. For particle-assisted processes, depending on the physical state of the particle, the growth can take either a VLS or a VSS<sup>45,46</sup> (vapor–solid–solid for solid catalyst particles) route to initiate crystal growth. The nanowire growth can also proceed as a self-catalysed reaction without the need for a foreign catalytic particle.<sup>47</sup> A type of template assisted growth referred to as *Selective Area Growth* employs an oxide mask with well-defined windows created by lithography and selective etching. The growth of crystalline nanowires occurs only within the pre-defined windows on the oxide mask.<sup>48–50</sup> In particle-assisted growth, gold nanoparticles are the usual choice for seed material. But alternative seed materials<sup>51,52</sup> have gained much attention due to the incompatibility of gold with Si-technology. VLS growth mechanism is the dominant path for gold-seeded nanowire growth, but literature also suggests that it can either proceed through VLS or VSS path depending on the reaction thermodynamics.<sup>53</sup> This thesis deals primarily with Au and Ga seeded VLS nanowire growth using the Aerotaxy growth platform.

## 2.3 Metal Organic Vapor Phase Epitaxy

The process of crystal growth by assembling atoms or molecules in a piece-by-piece additive fashion is called *epitaxy*, a Greek term which means *epi*-upon; *taxis*-arrangement. While the nanowires in this thesis are fabricated using Aerotaxy, both MOVPE and Aerotaxy processes overlap substantially. Both processes use MO precursors and the VLS growth route to fabricate semiconductor nanowires. The fundamentals of III-V nanowire growth in substrate based MOVPE are discussed here so that it can be used to describe Aerotaxy nanowire growth in the subsequent section. MOVPE is the most widely used epitaxial technique for the growth of device-quality, crystalline semiconductor thin-films and nanowires. As the name suggests, MOVPE is a vapor phase process, where material from the vapor phase is condensed into a solid crystal phase. The growth process is controlled by thermodynamics, interfacial kinetics and hydrodynamics. MOVPE usually employs a crystalline substrate that serves as an atomic template for the incoming precursor species to crystallize upon. Apart from MO precursors, hydrides like AsH<sub>3</sub> and PH<sub>3</sub> are used to source group V elements for III-V nanowire growth. MOVPE is usually operated in the moderate temperature regime (Figure 2.3), where the growth is mass-transport limited and hardly exhibits any temperature dependence. MO and hydride precursors are transported to the reaction environment in a carrier gas (H<sub>2</sub> or N<sub>2</sub>). The temperature and pressure controlled reaction environment is usually a quartz tube within which, a crystalline substrate is placed on a susceptor. The precursors can decompose through various pyrolytic mechanisms, but most commonly through homolysis, i.e., where the atomic bond breaks and each atom departs with one electron from the bond. The precursors can pyrolyse (homogenous pyrolysis) in the gas-phase if the temperature is high enough. However, usually, most of the pyrolysis happens in the presence of a surface (heterogenous pyrolysis). This decomposition typically occurs very close to the substrate thus establishing a precursor concentration gradient in the vapor-phase.<sup>54</sup> MOVPE typically involve numerous vapor-phase and interface or surface reactions, a detailed description of which is beyond the scope of this thesis. Therefore, only a general account of MOVPE which is essential for the description of Aerotaxy growth is provided here.

### 2.3.1 Vapor–liquid–solid nanowire growth

As mentioned earlier, MOVPE can either take a VLS or VSS route for nanowire growth.<sup>55</sup> But, in gold seeded nanowire growth; the VLS mechanism is found to dominate the growth process. As the name suggests, VLS growth deals with the phase transition of semiconductor material from vapor to liquid (precursors to Au droplet) and then from liquid to the solid phase (liquid alloy droplet to nanowire). Wagner and Ellis<sup>20</sup> were the pioneers who described the VLS growth of Si microwires (the Si wires were in the sub-mm range). In a typical VLS GaAs

nanowire growth process, a liquid gold droplet alloys with Ga and assists in further unidirectional growth of GaAs nanowires when exposed to As precursor. The nanowires typically grow perpendicular (for [111] B substrates) to the crystalline substrate and the initial location and size of the alloy droplet determines the location and diameter of the nanowire. MO precursors are reported to undergo efficient decomposition in the presence of a liquid alloy droplet.<sup>56</sup>

A typical VLS process consists of the following steps,

1. Surface preparation by deposition of the metal catalyst particles through lithography or by aerosol deposition.
2. Surface treatment by annealing above the eutectic melting point to produce liquid metal–semiconductor alloy droplets. This is referred as the pattern pre-annealing; the pattern fidelity is reported to be improved by annealing the deposited Au pattern in the presence of group III precursor.<sup>57</sup>
3. Then, controlled nanowire growth is initiated by modulating growth conditions such as the growth temperature, group III and V precursor fluxes in a closed reaction environment.

For III-V nanowire growth in MOVPE, a crystalline substrate of suitable material is patterned or deposited with metal nanoparticles. The substrate is then supplied with gaseous group III precursor to form an alloyed nanoparticle. To facilitate alloying, the temperature of the system is increased above the eutectic melting point of the metal–semiconductor mixture. Above the eutectic temperature, the alloy should exist as a liquid. It is obvious by now that nanowire growth is a non-equilibrium process involving numerous kinetic and thermodynamic processes. Similar to any epitaxial process, VLS nanowire growth occurs at positive thermodynamic supersaturation gradient ( $\Delta\mu_{v-s} = \mu_v - \mu_s$ ). But, VLS nanowire growth employs an intermediate liquid alloy droplet with a chemical potential  $\mu_l$  to mediate growth. In order to drive the phase transition, chemical potential of the liquid phase must satisfy eq-2.3. Once the driving force is established, nucleation of the crystal phase initiates and the nanowire growth is sustained by a continuous supply of group III and V precursors. The supply of precursors is based on a pre-determined V/III injection ratio and can be adjusted to precisely control the crystal structure and morphology of the nanowire.<sup>58,59</sup> According to eq-2.3, if  $\Delta\mu_{v-s} > \Delta\mu_{l-s}$ , then the system will favor direct crystallization from the vapor phase and does not follow the droplet-mediated VLS growth mode. Thus, the importance of an intermediate liquid phase cannot be established with a simple thermodynamic description.

### 2.3.2 Interfacial Kinetics and Nucleation

Wacaser *et al.*<sup>60</sup>, has studied the role of liquid alloy droplet in nanowire growth in detail. Preferential nucleation at the triple phase boundary (TPB) or liquid–crystal interface and the associated interfacial kinetics were reported to be important for nanowire growth. In addition to that, direct growth from vapor to crystal phase is suppressed, leading to highly anisotropic/preferential nanowire growth under the liquid alloy droplet. As mentioned earlier, the energy penalty involved in creation of new surfaces directly affects the nucleation barrier  $\Delta G_N$  according to eq-2.6. A liquid alloy droplet introduces additional interfaces, which complicates our simple assumption.

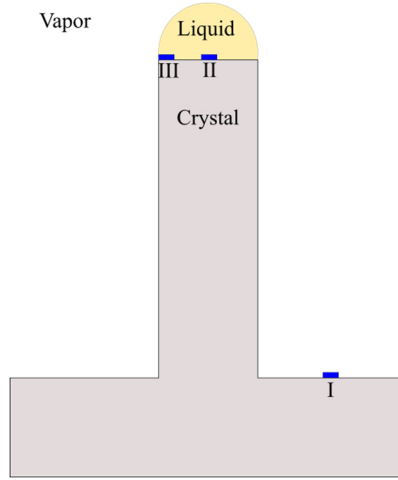


**Figure 2.4.** Schematic illustration of various nucleation sites for a droplet assisted VLS nanowire growth: (I) crystal–vapor interface, (II) liquid–crystal interface, (III) triple-phase boundary (TPB).

If we consider a typical particle-assisted VLS growth process, the possible sites for nucleation are the crystal–vapor interface (I), the liquid–crystal interface (II), and the TPB (III) as illustrated in Figure 2.4. Wacaser *et al.*<sup>60</sup> assumed a flat and smooth liquid–crystal interface and the change in Gibbs free energy  $\Delta G$  for nucleation events at sites I, II and III is given by:

$$\Delta G_I = -\Delta\mu_{v-c}n + Ph\gamma_{v-c}, \quad 2.9$$

$$\Delta G_{II} = -\Delta\mu_{l-c}n + Ph\gamma_{l-c}, \quad 2.10$$

$$\Delta G_{III} = -\Delta\mu_{v-c}n + P_{l-c}h\gamma_{l-c} + P_{v-c}h\gamma_{v-c}, \quad 2.11$$

where  $\Delta\mu$  is the chemical potential difference per mole of atoms added to the nucleus, the phases are denoted by subscripts  $v$  for vapor,  $l$  for liquid and  $c$  for solid,

$n$  is the number of moles added to the nucleus,  $\gamma$  is the surface energy at the respective interface,  $P$  is the nucleus perimeter and  $h$  is the height of the nanowire (nanowire is assumed to be a 2D cylinder). A simple thermodynamic treatment based on chemical potential energies reveals that site I is preferred for nucleation as  $\Delta\mu_{v-c} > \Delta\mu_{l-c}$ . But, if we consider the surface energies,  $\gamma_{l-c}$  must be smaller than  $\gamma_{v-c}$ . As a collective effect, the nucleation barrier is lowest at site III/TPB as the nucleus can modify its shape to minimize the surface energy contributions.<sup>60</sup> It is important to note that the actual process is more complicated and our assumption of a planar, smooth interface between the crystal and liquid droplet is an over simplification.<sup>61</sup>

Recent studies on Ge, Si and GaP nanowires revealed that the TPB is truncated, and its morphology undergoes a periodical change.<sup>62</sup> As a result of this periodic change in morphology, the main liquid–crystal interface does not lie at the TBP. In this case, the nucleation starts at the TBP, which modifies the morphology of the truncated corner and the addition of new material proceeds with a lower nucleation barrier. *In situ* TEM studies have shown that the volume of the truncated corner oscillates between a minimum and a maximum with the maximum volume being reached at supersaturation followed by a non-linear decline towards the minimum with addition of a new layer.<sup>63</sup>

### *Precursor delivery*

In a MOVPE growth process, the building blocks of crystal phase are supplied as gaseous MO precursors. For incorporation into the crystal phase, the precursors must decompose into reactive species, so they can be incorporated through chemisorption. One way to achieve this is to pyrolyze the MO precursors by heating them either before or during crystal growth. Precursor decomposition is enhanced in the presence of a foreign phase like a liquid alloy droplet<sup>64</sup> or a growth interface. Most of the MO precursors are liquids and are stored inside a bubbler cylinder. A carrier gas like  $N_2$  or  $H_2$  at a set flow rate  $Q_{carr}$  is passed through the bubbler. At a given temperature the MO liquid has an equilibrium vapor pressure  $P_{oMO}$ . The bubbler pressure  $P_B$  is decoupled from the equilibrium vapor pressure by an outlet pressure regulator. The total pressure of the system  $P_{tot}$  is controlled independently. The carrier gas is bubbled through the liquid precursor which kept at a user-defined temperature and pressure. After passing through the precursor, the carrier gas is saturated with MO species. The partial pressure of a MO precursor  $P_{MO}$  can be expressed as:

$$P_{MO} = \frac{Q_{carr}}{Q_{tot}} \frac{P_{tot}}{P_B} P_{oMO}, \quad 2.13$$

where  $Q_{tot}$  is the total flow in the system which is the sum of all the flows. The hydride sources are available in gas-phase, and the partial pressure of a hydride source  $P_H$  with a flow  $Q_H$  is given as:

$$P_H = \frac{Q_H}{Q_{tot}} P_{tot}. \quad 2.14$$

### *Surface Diffusion*

VLS growth of III-V nanowires cannot be explained without considering the surface diffusion processes that are partly driven by the thermodynamic potential gradient. Group V hydrides like  $AsH_3$  and  $PH_3$  have a high vapor pressure and negligible surface diffusivity and are incorporated into the droplet by direct impingement.<sup>65,66</sup> Group III species like Ga and In typically have a low vapor pressure and long diffusion lengths that are several micrometres long; surface diffusion of group III species is reported to enhance nanowire growth rate by many orders of magnitude.<sup>67</sup> Studies have shown that more than 80% of In contribution in CBE grown InAs nanowires is through surface diffusion of In adatoms.<sup>68</sup> So, in addition to direct impingement to the liquid droplet, group III species can also diffuse along the substrate and nanowire surface (sidewalls) towards the growth interface. This disparity in surface diffusion lengths between group III and V precursors can lead to the axial growth rate being limited by the kinetics of group III adatoms.<sup>69</sup> The area around the nanowire within one diffusion length  $\lambda$ , is referred to as the collection area.<sup>64,65</sup> The collection areas may differ between nanowires of different dimensions, where a thinner wire grows faster than a thicker wire if the growth is surface diffusion limited.<sup>70</sup> During the initial stages of growth, surface diffusion from the substrate and nanowire sidewalls contribute to the axial growth rate. As the nanowire continues to grow, the collection area on the substrate surface reduces with its boundary (a sharp boundary is assumed for simplicity) still one  $\lambda$  away from the growth interface. Although additional collection area appears on the nanowire sidewalls, this additional area gain is smaller when compared to what it used to be on the substrate. This leads to a reduced axial growth rate with increasing growth time and if the nanowire length exceeds  $\lambda$ , the growth rate remains almost constant.

If the nanowire pitch is assumed to be larger than the surface diffusion lengths, axial wire growth can be described by mass transport through diffusion.<sup>70</sup> The nanowire pitch of an ordered array is defined by the pitch of initial catalytic particle pattern. In case of ordered arrays with a pitch smaller than the surface diffusion length, the nanowires compete for resources, which leads to an overall reduced growth rate.<sup>68</sup> For GaP nanowires, the axial growth rate was found to increase with decreasing pitch and the growth was said to be in a synergetic regime.<sup>64</sup> The synergetic growth regime for GaP nanowires stems from the partial pyrolysis of TMG at the surface of the Au droplet. Such a localized decomposition creates a local precursor concentration gradient around the Au particle accounting for the increased axial growth rate.

## 2.4 Aerotaxy

Bottom-up nanowire growth techniques, in general, require the use of an expensive crystalline substrate. Although successful growth of crystalline nanowires on amorphous glass substrates<sup>71,72</sup> have been reported; an amorphous substrate greatly modifies the wetting properties of the liquid droplet thus, directly affecting the nucleation energy barrier.<sup>73</sup> Surface features of the substrate (similar to the features on an amorphous substrate) are reported to direct the diffusion of the liquid alloy droplet<sup>73-75</sup> which leads to horizontal wire growth on top the substrate. Substrate-based growth techniques come with an inherent limitation as the number of nanowires that can be grown on a fixed area per unit time is finite.

Aerotaxy is a gas-phase VLS growth technique that can overcome the limitations of a substrate-based process. The term Aerotaxy is a combination of *Aerosol* and *epitaxy* which provides a brief description of the growth mechanism. Early work by Knut Deppert and Lars Samuelson<sup>76</sup> on the gas-phase conversion of Ga nanoparticles to GaAs nanocrystals in a heated H<sub>2</sub> environment in the presence of AsH<sub>3</sub> marks the inception of Aerotaxy. Paper I and Chapter 5 provides a detailed description of the custom-built third generation Aerotaxy tool. The additional concepts that are necessary to understand nanowire growth in gas-phase are introduced in this section.

In Aerotaxy nanowire growth, an aerosol of size-controlled gold nanoparticles is mixed with gaseous Group III and V precursors in a tube furnace. The Aerotaxy process shares many similarities with a typical MOVPE process and they are listed below,

- Both MOVPE and Aerotaxy uses MO and hydride precursors like trimethyl gallium (TMG), diethyl zinc (DEZn), tetraethyl tin (TESn), Arsine (AsH<sub>3</sub>) and phosphine (PH<sub>3</sub>) as III-V sources.
- The shape of the nanowire has a temperature dependence in both MOVPE<sup>77</sup> and Aerotaxy.<sup>8</sup>
- The dependence of nanowire growth rate on temperature under various growth temperature regimes (Figure 2.3) is similar for both processes, and growth is kinetically limited at low growth temperatures in both cases.

Major commonalities like these enable the application of MOVPE nanowire growth theory to explain Aerotaxy growth. In order to better explain Aerotaxy nanowire growth, some fundamental qualities of Aerotaxy growth are presented below.

- Aerotaxy is a substrate-free VLS growth process.
- It is a high throughput, low-cost, continuous process.

- Aerotaxy is a high-pressure epitaxial process and the reactor is operated at or near atmospheric pressure in contrast to the low and ultralow-pressure epitaxial processes like MOVPE, MBE and CBE.
- Group III and V precursors in Aerotaxy have relatively high vapor pressures ( $\sim 1$  mbar)<sup>8</sup> compared to MOVPE.
- Nucleation and nanowire growth occur simultaneously, under same growth conditions and on a very short timescale.
- The growth rate is  $\sim 1,000$  times higher<sup>8</sup> than MOVPE.
- Due to the continuous and flow-through design of the Aerotaxy reaction environment, the emergent nanowires are subjected to spatiotemporal variation of vital growth parameters that control nanowire growth.
- *In situ* characterization of growth in gas phase is beyond the tool's current capability.

### 2.4.1 Gas-phase nucleation

Similar to a typical VLS process, the thermodynamic supersaturation drives nanowire growth in Aerotaxy. The process of nucleation in Aerotaxy occurs rapidly and can be considered crudely similar to how water vapor in the atmosphere nucleates on a tiny dust particle.<sup>78</sup>

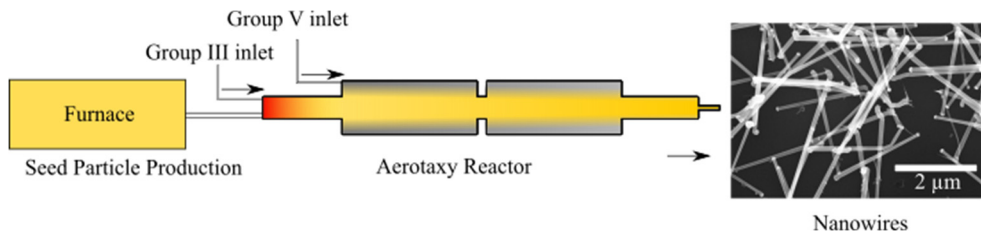


**Figure 2.5.** Schematic of the Aerotaxy reactor. Group III (red), Group V (grey) and the Au aerosol (yellow) flows are color coded for reference.

For Aerotaxy growth of GaAs nanowires, size-selected Au seeds are mixed with TMG in the first stage of the reactor. This stage is maintained at a temperature above the eutectic melting point of Au–Ga mixture ( $\sim 430$  °C) to encourage the formation of a liquid alloyed droplet. This is similar to the substrate pre-annealing<sup>79</sup> process employed in MOVPE. Decomposition rate of TMG is enhanced at the Au droplet's surface. The Au droplet spends only a fraction of the growth time in the alloying stage of the reactor, but this duration is enough to form an alloyed droplet due to the high Ga precursor pressure (typically few hundred Pa). The alloyed liquid Au–Ga droplet along with the excess TMG flows into the next stage of the reactor. This is



the growth stage and is maintained at a temperature tailored for the material being grown ( $\sim 530$  °C for GaAs nanowires). The alloy droplet is exposed to  $\text{AsH}_3$  in the growth stage where the Group V adatoms directly impinge on the liquid droplet, and most of the incoming precursor may get adsorbed onto the alloyed droplet. High precursor pressures again play an important role as it ensures rapid saturation of the droplet with Ga and As (schematized in Figure 2.6).

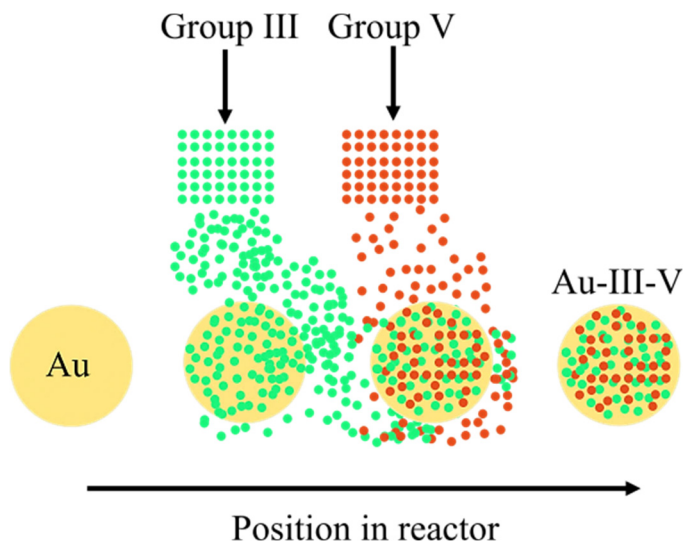


**Figure 2.6.** Schematic illustration of liquid droplet supersaturation with group III and V precursor species. The Au droplet (yellow) is mixed with group III precursor species (green) in the alloying stage at a suitable temperature. The alloyed droplet is exposed to group V precursor species (red) in the subsequent growth stage of the Aerotaxy reactor. The particle becomes supersaturated with group III and V species.

Initially, the excess Ga and As would homogeneously nucleate/precipitate somewhere on the Au droplet surface due to lack of a definite droplet–crystal interface. Homogeneous nucleation can be directly controlled by the degree of supersaturation (non-thermodynamic) in the vapor phase.<sup>80</sup> The high degree of supersaturation in the vapor phase ensures the precipitation of GaAs crystallites—barely larger than a few monolayers—on the surface of the liquid droplet. Continuous supply of precursors at high partial pressure quickly replenishes the liquid droplet with Ga- and As- species that are consumed during the phase transition. This drives the supersaturated liquid droplet towards the next nucleation event. It is possible that the next nucleation event might occur adjacent to or far away from the previous crystallite; multiple nucleation events may also occur simultaneously. The crystallographic orientation of the crystallites is determined by a delicate balance between surface and interface energies.<sup>73</sup> Thus, it is likely the case that multiple nucleation events yield GaAs crystallite clusters that are not aligned with each other (as seen in Figure 2.7).

These crystallite clusters soon grow in size forcing the liquid droplet to one side of the cluster as seen in Figure 2.7. Initially, the nucleation events might establish numerous crystallographic orientations and the fast-growing facets among them may taper into a point or extend towards the droplet edge, where further growth of such a facet will halt. The fast-growing, high-energy facets will eventually disappear leaving only the slow-growing facet.<sup>81–84</sup> In case of Aerotaxy, this is the (111) B surface which forms an interface with the liquid droplet. Once a stable direction is established, further nanowire growth proceeds by adding more layers until eventually the nanowire exits the growth stage.

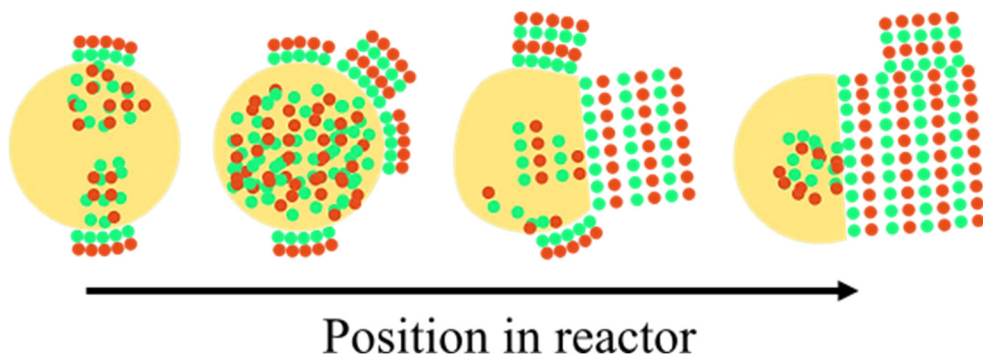


**Figure 2.7.** Schematic illustration of Aerotaxy nanowire growth. The Au droplet (yellow) precipitates III-V crystallites followed by rapid supersaturation of the Au particle with group III (green) and group V precursor species (red). Eventually, a stable growth facet permeates the growth interface leading to VLS nanowire growth.

An important aspect of Aerotaxy growth that must be elaborated on is the spatiotemporal variation in growth conditions. Since the Aerotaxy reactor is literally a long tube without any physical boundaries between the different zones, it is difficult to ensure a uniform and controlled growth environment over large volumes. Despite our best efforts, the emergent nanowires will encounter a temporal variation in growth condition. And as time passes, the hot walls of the reactor will suffer from material deposition which further complicates our control over the growth process. As a result, the nanowires grown in our system have considerable spread in their physical and opto-electronic properties.

## 2.4.2 Rate-limiting steps

VLS nanowire growth at its core is a sequential chemical reaction whose rate is determined by the slowest step. Based on the pioneering work by Givargizov<sup>85</sup> the rate-limiting steps in III-V nanowire growth can be (i) mass-transport through the phase boundary; (ii) chemical reactions or precursor pyrolysis; (iii) surface and bulk diffusion; (iv) nucleation. Steps i–iii have been discussed already from a VLS growth perspective in sections 2.1–2.3. For nucleation to be the rate limiting step, the surface diffusion and direct impingement of growth species at the boundary layer

must be faster than the nucleation rate. Johansson *et.al*<sup>86</sup> investigated the high-pressure growth rate limit that is applicable for Aerotaxy nanowire growth. The growth rate was reported to be limited by the incorporation rate  $I$ , independent of the operating pressure and nanowire radius. Since the incorporation rate is an activated process, it has an Arrhenius dependence on temperature and can be expressed as:

$$I = k_a e^{-\frac{E_a}{k_B T}}, \quad 2.15$$

where  $k_a$  is the exponential pre-factor and  $T$  is the growth temperature. As mentioned earlier, Aerotaxy nanowire growth occur in conditions under which both group III and V precursor pressures are sufficiently high. Under this condition, the nanowire is reported to have the maximum axial growth rate and is only limited by the incorporation kinetics of the growth species.

# 3 Nanowire Characterization

Proper control over any fabrication technique can only be realized when there are provisions for feedback on the quality of fabricated material. The relevant optoelectronic properties of nanowires can be optimized by engineering their shape, size, composition, etc. It is imperative to understand how such properties can be controlled so that the nanowires can be fabricated in a predictable manner. Ideally, *in situ* monitoring and characterization techniques using absorption, reflectance<sup>87</sup> and resonance<sup>88</sup> phenomena can provide rapid feedback about the effectiveness of control over the fabrication process. Modification of the *in situ* characterization techniques and tools intended for substrate-based growth processes to suit the Aerotaxy hardware was tedious and ineffective. Existing aerosol particle characterization techniques cannot provide accurate information about nanowires due to their anisotropic dimensions. *In situ*, on-the-fly size measurements of aerosolised carbon nanotubes (CNTs)<sup>89,90</sup> based on gas-phase electrophoresis is claimed to be a generic method suitable for measuring the size of any fibre like material. However, the high production volume of Aerotaxy may either impede such measurements or provide inaccurate readings. If *in situ* process monitoring were to be developed for the Aerotaxy platform, it may dramatically reduce the complexity and the time involved in parameter tuning and growth optimization. On the other hand, *ex situ* characterization techniques like electron microscopy and photoluminescence spectroscopy usually requires some level of sample preparation, but are widely used as nanowire characterization tools. The rapid growth, high production volume and the flow-through Aerotaxy production environment restricts us to just *ex situ* characterization tools.

This chapter provides an overview of the characterization techniques used in this thesis to investigate nanowire morphology, composition, crystal structure and doping.

## 3.1 Electron microscopy

A timeless approach to study an unknown object is to shoot a well-understood probe at the unknown and recreate the unknown based on how it interacts with the probe. Light microscopes, just like a human eye, use the photons that get reflected from an object to analyse the microscopic characteristics of that object. The smallest

resolvable distance in a visible light microscope is limited by the diffraction of light to  $\sim(\lambda/2) \cdot NA$ , known as the Abbe diffraction limit, where  $\lambda$  is the optical wavelength and  $NA$  is the numerical aperture of the microscope. This limit can be circumvented, for instance, by using an immersed objective lens (as it increases the  $NA$ ). But in general, imaging features below one-half the wavelength of the shortest visible light ( $\sim 200$  nm) is difficult for a conventional light microscope. The wave–particle duality of electrons is well documented i.e., electrons may be described either as a particle or a wave. The wavelength of electrons in motion is given by *L de Broglie's* equation as:

$$\lambda = \frac{h}{\sqrt{(2m_0eU)}}, \quad 3.1$$

where  $U$  is the acceleration voltage in an electron microscope,  $e$  is the elementary charge,  $m_0$  is the electron rest mass and  $h$  is Planck's constant. Since electrons interact strongly with matter, if they are used as a probe, only a few microns of a given material is enough to stop a high-energy electron. This means an enormous amount of information about the material can be extracted when a suitable detector is used to analyse the electron-matter interaction.<sup>91</sup> Since the accelerated electrons carry a much higher energy than a photon, they have shorter wavelengths and the spatial resolution limit can be improved by at least five orders of magnitude.<sup>91</sup> This high spatial resolution makes Electron Microscopy an indispensable method for characterization of nanostructures.

The two most commonly used electron microscopes are the Scanning Electron Microscope (SEM) and Transmission Electron Microscope (TEM) and are briefly described in the following sections. Both techniques use a well-defined electron probe as an illumination source, but differ in their resolution, electron-matter interaction and sample preparation methods.

### 3.1.1 Scanning Electron Microscopy

A standard SEM operates at a lower acceleration voltage (0.1–40 kV) in comparison to a TEM. SEM typically have a resolution on the order of 1–10 nm and the resolution is limited by the width of the electron probe and the interaction volume of electrons in the sample. SEM samples typically do not require any special preparation, making SEM a quick and essential *ex situ* characterization tool.

SEM is operated under high vacuum, without which the electron beam cannot be generated nor controlled. All microscopes require three important parts to work: an illumination source, a lens to focus the beam into a fine probe and a detector. Electrons in motion only react to an electrostatic or a magnetic field. The illuminating electron beam in a SEM can be produced by either thermionic or field emission from a suitable filament. In the former, thermally extracted electrons are

focused into a fine beam, while in the latter, a huge potential difference pulls the electrons out of a filament tip.<sup>92</sup> Field emission guns are preferred over thermionic guns as they provide better spatial resolution and a monochromatic (coherent) electron beam. The filaments in field emission guns also have a longer life.<sup>92</sup> In a SEM the electrons are successively focused into a fine probe using a series of electromagnetic lenses and scanned across the sample. This series of electromagnetic lenses collectively form the focusing optics and is called the *condenser lens* system. Magnification depends on the ratio of the scanned area to the area displayed on the screen. The number of electrons collected from a particular position on the specimen determines the brightness of a spatially equivalent pixel(s) in the displayed image i.e. contrast.

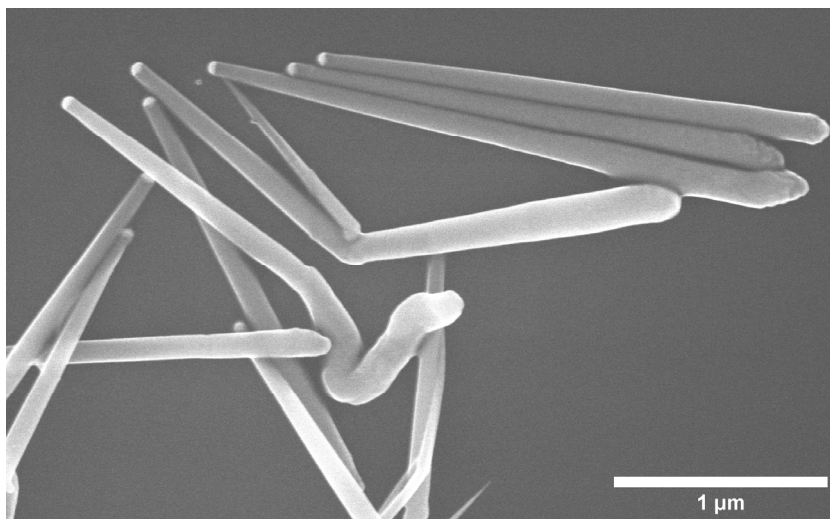


**Figure 3.1.** SEM image of Aerotaxy grown GaAsP nanowires. The nanowires have a 80 nm gold seed particle at the tip and display various morphological features like kinks and branches.

The incident electron beam can interact with the specimen either elastically or inelastically and results in the generation of a multitude of signals including secondary electrons (SE), back-scattered electrons (BSE), Auger electrons, characteristic X-rays, photons, etc. The incident electron beam affects a larger volume compared to the electron probe-width, known as the interaction volume. Size of this interaction volume depends on the sample density, acceleration voltage and the beam current.<sup>93</sup> BSEs are elastically scattered through large angles and used to be a part of the incident beam. They carry energies close to that of the incident beam and can originate from deep within the interaction volume. Once they exit the sample surface, they can be collected to form an electron image where the compositional variation in the specimen translates to contrast in the acquired image (depth and width of the BSE emission volume of the specimen decreases with

increasing atomic number). Since BSEs can be generated anywhere within the interaction volume, the resulting image has a poor resolution. SEs typically carry low energy (few tens of eVs) and belong to the target specimen, originating very close to the specimen's surface. The incident electron beam inelastically knocks out some of the loosely bound outer-shell electrons close to the specimen surface. If this process imparts adequate kinetic energy to the electrons, they may eventually escape the sample and be detected. As they are generated very close to the specimen surface, they carry surface information and exhibit topography contrast.

Most Aerotaxy nanowire samples collected during my thesis work were inspected in an SEM to check their morphology, distribution, texture, dimensions (diameter, length) and kinking (Paper III). SEM provides a quick feedback on whether the fabricated nanowires meet the desired morphology and dimensions.

### 3.1.2 Transmission Electron Microscope

TEM operates at a higher acceleration voltage (up to 400 kV for the majority of specimens) and can provide much better resolution (down to the scale of an atom). TEM detects the elastically scattered electrons after they pass *through* a thin sample. As it requires ultra-thin samples, TEM investigation usually starts with sample preparation where the samples are thinned down by mechanical grinding or ion-milling.

The electron gun and the electromagnetic condenser lens system together form the illumination system of a typical TEM. The type of electron gun used in a TEM depends on the nature of the task at hand, but field emission guns are usually preferred.<sup>94</sup> The illumination system extracts the electrons from the gun to focus them either into a fine spot (for scanning-TEM imaging mode and compositional analysis) or a parallel beam (traditional TEM mode) to illuminate the sample. The sample is placed on a specimen stage, which together with an *objective lens system* is the heart of a TEM.<sup>94</sup> The electron beam after passing through the sample is focused by the objective lens system located below the stage, onto to a set of *projector lenses* through an aperture(s) that limits the beam width around the optical axis. The projector lens system magnifies the incident image from the objective lens onto a phosphor screen/CCD camera.

Crystalline nanowires, when illuminated with a parallel beam can produce a diffraction pattern due to the ordered arrangement of atoms within the crystal. This is achieved by careful manipulation of the various lens systems and inserting a selective area aperture, that selects a particular area on the image to form a diffraction pattern. Since diffraction patterns are related to the crystallinity of a sample, one can also construct the diffraction pattern by applying fast Fourier transform on a high-resolution TEM (HR-TEM) image. Contrast in a TEM image is due to scattering of the incident electron beam by the specimen, which modifies

its amplitude and phase. Variation in mass or thickness of the specimen can give rise to amplitude contrast as the electrons either travel through different materials or simply more material. Phase contrast imaging is achieved by removing the objective apertures altogether and collecting both the diffracted and deflected electron beams to form an image. The beams exhibit a difference in phase simply due to the fact that they cover different distances in the specimen. This imaging mode can be used to produce HR-TEM images. For a more detailed description of the TEM and its various imaging capabilities, refer to the book on TEM by D.B Williams and C.B Carter.<sup>94</sup>

TEM samples must have an ultrathin cross-section and nanowires have a thin cross section by design, so Aerotaxy nanowires can be directly collected on to a TEM sample grid and imaged without extra preparation. TEM investigations on Aerotaxy nanowires were performed to extract information like crystallographic orientation, lattice spacing, defect density, etc.

## 3.2 X-ray Energy Dispersive Spectroscopy

X-ray Energy Dispersive Spectroscopy (XEDS) is used to analyse the chemical composition of a specimen using the inelastic beam–specimen interactions in a TEM (or a SEM). The electron beam is focussed to a fine spot (Scanning TEM mode) to perform XEDS characterization; the beam can be moved around the specimen to analyse the elemental makeup of different features. Most of the electrons in the incident electron beam interacts elastically with the specimen, but a fraction of them undergo inelastic scattering. The incident electron beam can penetrate through the outer shells of an atom in the specimen and interact inelastically by knocking off a core-electron. This leaves a hole/vacancy in the inner shell and the atom is in an excited state. The ionized atom can return to the ground state by refilling the vacancy with a high-energy electron from one of its outer shell. Such a transition will produce either a characteristic X-Ray photon or an Auger electron.<sup>94</sup> The energy of the emitted X-Ray photon depends on the difference in energy between the two shells that participate in the transition. Each element in the periodic table has a distinct set of energy levels and therefore will emit X-Ray photons unique to that element. There can be many such characteristic X-Rays emitted from an excited atom and the collective spectrum can be used to identify different elements present in a specimen. Computer controlled semiconductor detectors are used for signal collection and processing. The emitted X-Ray signal is collected by a reversed biased *p-i-n* detector, the signal is digitized and stored to a dedicated channel based on the energy of the X-Ray signal.

Peak intensities of the collective spectrum depend on specimen properties like size, density and ionization cross-section in addition to detector sensitivity and collection



angle.<sup>94</sup> By comparing relative peak intensities, it is possible to quantify the different elements present in the specimen relative to each other. XEDS is a powerful analytical tool with both qualitative and quantitative capabilities. However, prior knowledge about the specimen is important to be able to extract any useful information.

XEDS was used to characterise the composition of Aerotaxy nanowires, qualitatively understand nanowire doping (Paper II) and to analyse special surface features like branches (Paper III).

### 3.3 Photoluminescence spectroscopy

Semiconductors are, to a large extent, characterized by their band structure. They have a very small energy gap (bandgap) in their electronic band structure, spanning a range of 0–6 eV.<sup>95</sup> The valence electrons in an intrinsic semiconductor material must always gain energy larger than this energy gap in order to become free electrons. If external excitation is applied to a semiconductor, the electrons in the valence band move across the bandgap to the vacant conduction band. The excited electron first relaxes to the conduction band edge (lowest vacant energy level within the conduction band) through non-radiative processes. The vacancy left behind by the electron (hole) in the valence band undergoes a similar non-radiative process and ends up at the valence band edge. The electron–hole pair then recombines by emitting a photon with energy that’s equivalent to the energy released in the recombination process. And if the excitation is achieved with light, then this process is called photoluminescence (PL). Ideally, the energy of the emitted photon must be equivalent to the bandgap of the semiconductor material under investigation. The energy of the emitted photon depends only on the properties of the semiconductor material and not on the source of illumination. However, at high illumination power or in degenerately doped semiconductors, the electron concentration exceeds the conduction band edge density of states (DOS) pushing the Fermi level well into the conduction band; thus, increasing the effective bandgap energy. This increases the energy of the emitted photon and such a shift in peak emission energy is known as Moss–Burstein shift.<sup>96</sup>

#### 3.3.1 $\mu$ -PL Spectroscopy

$\mu$ -PL spectroscopy is a powerful, non-destructive technique used to study the optical response of nanowires at low temperature (to reduce thermal noise). In  $\mu$ -PL spectroscopy, the emission spectra are typically obtained from areas that are on the order of a micrometre, making it suitable technique for nanowire characterization. By analysing the emission spectrum of a nanowire ensemble, information like

electronic band structure, carrier concentration and crystal quality can be extracted. As a result,  $\mu$ -PL spectroscopy has become a routine characterization technique for semiconductor nanowires. A typical PL spectrum of a semiconductor material can have many distinct electron–hole recombination and corresponding emission peaks. Therefore, prior knowledge of the material under investigation is important to extract useful information from a  $\mu$ -PL spectrum.

In Paper II, low temperature (7 K)  $\mu$ -PL spectroscopy was used to evaluate the doping concentration of Sn doped GaAs nanowires. The Si substrate carrying randomly oriented Sn doped GaAs nanowires was bonded to a cryostat using conductive Ag paste. Then the sample was cooled by pumping liquid helium through the cryostat. A frequency doubled solid-state laser emitting at 532 nm was focused on the sample to excite the sample with an excitation power density of  $\sim 200 \text{ W cm}^{-2}$ . The full width at half maximum (FWHM) of the PL emission peak obtained is related to  $(E_F - E_C)$ , where  $E_F$  and  $E_C$  are the Fermi level and conduction-band edge respectively. The carrier concentration was extracted from the Burstein–Moss shifted spectrum by fitting the high-energy tail of the emission spectrum to the estimated conduction band-edge DOS as described by Lindgren *et al.*<sup>97,98</sup> The estimated doping concentration was then compared with data from electrical doping characterization (section 2.4).

In Paper IV, Zn doped GaAs nanowires were characterized using 4 K  $\mu$ -PL spectroscopy to evaluate the doping concentration. The carrier concentration, in this case, was estimated using a similar method as explained above.

### 3.4 Electrical Characterization

The concentration of free charge carriers in a semiconductor can be modulated by doping the semiconductor with atomic impurities that have excess or fewer valence electrons. Doping adds free electrons or holes to the semiconductor material. Controlled doping is crucial for high-performance semiconductor devices as doping modulates the conductivity, charge carrier lifetime, electronic band structure, current density and carrier mobility. Although doping of bulk semiconductors is a mature technology, doping of nanostructures is still a nascent technology that was first investigated by Hiruma's group.<sup>99,100</sup> The most common method to evaluate doping in bulk semiconductors is through electrical characterization techniques like Hall measurement. But electrical characterization of nanostructures is very challenging compared to their bulk and planar counterparts. The small dimensions of nanostructures require dedicated device fabrication techniques and unique methodologies that are suitable for analysis at the nanoscale. Yi Cui *et al.*<sup>101</sup> from Lieber's group were the first to develop a method for evaluating the charge carrier concentration and mobility in Si nanowires using a back gated nanowire field effect

transistor (NW-FET). Ever since, a standard method for electrical characterization<sup>100</sup> of nanowires is to fabricate a NW-FET and perform transport measurements on them. Other methods for doping evaluation include but are not limited to four-point probe resistivity measurement, PL, secondary-ion mass spectrometry (SIMS),<sup>102</sup> atom probe tomography (APT)<sup>103</sup> and electron energy loss spectroscopy (EELS).<sup>94,100</sup>

In Aerotaxy, doping is carried out *in situ* by mixing dopant precursors like DEZn (for *p*-type) and TESn (for *n*-type) during nanowire growth. Adding dopant precursors during Aerotaxy growth might have complex effects on the growth and they are discussed in Chapter 4. In Paper II, NW-FETs (Figure 3.2 b) were fabricated from Sn doped GaAs nanowires in order to perform four-point probe measurements. The rationale behind fabricating a NW-FET and using it to perform four-probe measurement must be explained here. Field effect characterization measures properties very close to surface and relies on estimated gate capacitance instead of the measured capacitance.<sup>104</sup> FET measurements are also sensitive to the contact resistance. Due to these drawbacks, data from four-point probe measurement was used to measure the resistivity and carrier concentration was deduced from literature. It must be noted, that four-point probe method deduces the carrier concentration from literature instead of direct measurement and must be verified through supporting characterization methods like PL spectroscopy.

The Sn doped GaAs nanowires collected on a Si substrate were manually transferred to a pre-patterned, insulated (100 nm SiO<sub>2</sub> and 10 nm HfO<sub>2</sub>) Si substrate. The bottom of the Si substrate was coated with 10 nm of Ti and 90 nm of Au to form the back-gate contact. The nanowires were transferred by gently wiping a cleanroom tissue on the Si substrate which contains the nanowires and then repeating the same motion on the pre-patterned Si substrate. This process was repeated until a significant population of nanowires was transferred (successful nanowire transfer can be easily identified with a light microscope). After nanowire transfer, SEM maps of the substrate were constructed in order to select suitable nanowires for contacting. Figure 3.2 a is an SEM image that shows nanowire clusters with random orientations on the pre-patterned Si substrate. The metal contacts and alignment crosses seen in Figure 3.2 a were defined prior to nanowire transfer using UV lithography (UVL). The alignment crosses were later used during electron-beam lithography (EBL) for navigation on the substrate and high-fidelity pattern writing. The substrate was the spin coated with a PMMA 950 A6 lift-off layer. Metal contacts (20 nm Pd, 80 nm Ge, followed by 100 nm Au) were deposited after EBL by thermal evaporation, connecting the NW-FET to the UVL defined contacts. In order to improve ohmic behaviour, the contacts were then annealed at 280 °C for 30 s in a furnace. In order to measure the resistivity of the NW-FET in Figure 3.2 b, current was passed through terminals '1' and '4' while measuring the voltage drop at terminals '2' and '3'.

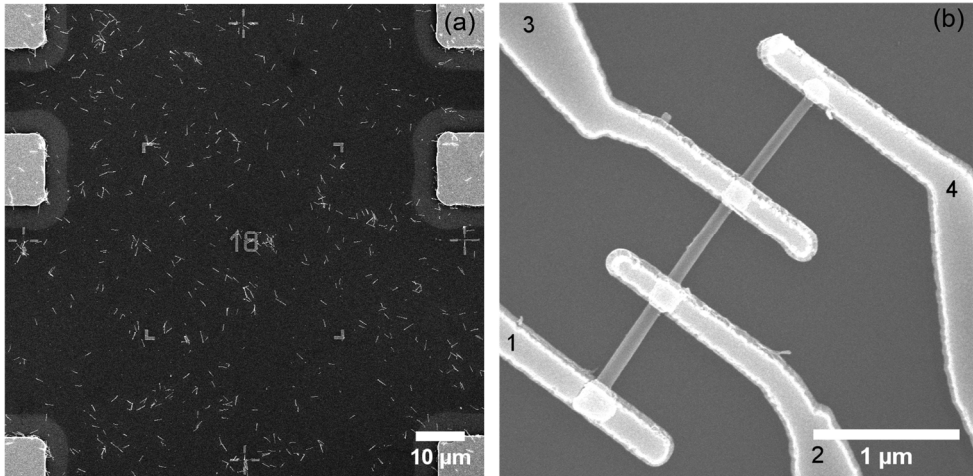


**Figure 3.2** (a) SEM image of randomly oriented Sn:GaAs nanowires on a pre-patterned Si substrate coated with 100 nm of insulating SiO<sub>2</sub> on top; the alignment crosses that are visible in the image were used for EBL lithography to define contacts to individual nanowires. (b) SEM image of a single NW-FET device that can be used for four-point probe measurements.

Once the resistivity was calculated and the corresponding charge carrier concentration was deduced from literature.<sup>105</sup> This method is only applicable for *n*- and *p*-doped GaAs and if reliable data is available for other material systems, then four-point probe measurement can be used to characterize doping concentration of those material systems. As mentioned earlier, this method of carrier concentration estimation must be supplemented with data from PL spectroscopy or other similar evaluation techniques. This is due to that fact that, the measured resistivity of a NW-FET is compared to data that was intended for bulk semiconductors. This is a very crude approximation and even a small error in resistivity measurement is compounded in the final estimation of carrier concentration.

In Paper IV, the carrier concentration of Zn doped GaAs nanowires was estimated through field effect (FE) measurements on NW-FETs fabricated using a process similar to the one mentioned above. The contacts to the nanowire were Ti/Au (10/180 nm) metal electrodes that was thermally evaporated after EBL patterning. To perform FE measurement on a NW-FET (Figure 3.2 b) a constant source (1)–drain (4) voltage was applied. The transfer characteristics of the NW-FET was studied by sweeping back-gate voltage from  $-5$  to  $5$  V and back in steps of  $0.5$  V. The mobility and the carrier concentration can be extracted from the transfer characteristics of the NW-FET. This method is more reliable than the one employed in Paper II, but was still supplemented with optical measurements in Paper IV.



# 4 Aerotaxy III-V nanowires

Direct, *in situ* observation of VLS growth of gold seeded Ge nanowires in 2001<sup>106</sup> using a high-temperature TEM, demonstrated the generality of particle-assisted growth and the potential for controlled synthesis of crystalline nanowires. Today, semiconductor nanowire research is a multi-disciplinary frontier, with ongoing efforts, directed both at understanding its fundamental limits and possible practical applications. The journey from fundamental understanding to practical application is often beset by factors like production capability, cost and safety. For example, the advent of titanium dioxide nanoparticles in a wide variety of consumer products like sunscreen, etc., is partly due to their industrialised production, apart from other relevant physical and chemical properties.

The motivation behind nanowire research is to create a platform similar to the existing planar device platform, while exploiting the novel properties offered by the nanowire architecture. As a result, the nanowire research community around the world primarily focusses on adapting planar semiconductor devices to the nanowire geometry and investigating their behaviour. Consequently, optimizing growth methods for smooth integration with existing platforms or incremental performance optimization<sup>107</sup> takes back seat. In order to establish the nanowire platform as an alternative to the planar platform, both fundamental research and efficient cost-reduction are indispensable. In this thesis, we attempt to bridge this gap by investigating Aerotaxy's capability to mass-produce crystalline III-V semiconductor nanowires at low-cost. Aerotaxy has piqued interest in the nanowire community due to its high growth rate and phenomenal production volume since the beginning.

This chapter deals with properties of Aerotaxy grown III-V semiconductor nanowires and is mainly based on Papers I–V, VII and other unpublished results.

## 4.1 Material system

A wide variety of materials including metals<sup>108</sup> and perovskites<sup>109</sup> can be fabricated controllably into nanowires.<sup>20,110,111</sup> III-V compound semiconductor nanowires are particularly important due to their excellent optical and electrical properties that are superior to their planar counterparts.<sup>112,113</sup> Most of them have a direct bandgap that

can be tuned over a wide range by manipulating their stoichiometry.<sup>114</sup> GaAs nanowires are reported to be excellent candidates for monolithic integration on Si multi-junction solar cells.<sup>115</sup> GaAs nanowire *pn*-junctions with excellent photo-response have been realized previously using a multi-stage Aerotaxy setup.<sup>116</sup> Ternary GaAsP nanowires are of great importance due to their bandgap tunability. Technically, GaAsP nanowires are alloys of two binary compound semiconductors (GaAs and GaP) and their bandgap and lattice spacing can be tuned between the two binary extremes by altering their stoichiometry. Bandgap tunability in semiconductor nanowires is relevant for full spectrum photovoltaics.<sup>114</sup> GaAs and GaAsP material systems were adopted to investigate the fundamentals of Aerotaxy growth. We designed studies to probe the effect of growth conditions on nanowire quality and evaluated the efficiency of *in situ* doping (*p*- and *n*-type doping) in Aerotaxy nanowires.

The following sections outline features common to GaAs and GaAsP nanowires fabricated in the third generation Aerotaxy setup at Lund Nano Lab (LNL).

## 4.2 Morphology

Nanowires represent a broad class of one-dimensional (1D) nanostructures defined mainly by their dimensional anisotropy. They can grow with a cylindrical, hexagonal, square or triangular cross-section while preserving the dimensional anisotropy.<sup>117–119</sup> Consequently, nanowires are reported to grow in a variety of morphologies through intentional manipulation of growth conditions<sup>120</sup> or in explorative studies. In substrate-based nanowire growth, morphology and growth direction of the nanowire are said to be governed by seed particle diameter and the properties of the substrate, i.e. crystallographic orientation, lattice spacing, etc.<sup>44</sup> III-V semiconductor nanowires in particular are reported to prefer the (111) B growth direction<sup>121</sup> irrespective of the growth mechanism. Aerotaxy experiments spanning various growth conditions and material systems demonstrated a complex inter-play of various growth parameters, exerting a collective influence on nanowire morphology. Although it is hard to quantify this interdependency among growth parameters and their influence on morphology in a system as complex as ours, parameters like catalytic particle size and growth temperature were found to consistently influence nanowire morphology. It is important to note that in an earlier version of our tool,<sup>8</sup> growth time (either by varying the dimensions of the reaction tube or by varying total gas flow) could also be tuned to modify nanowire morphology.

Variations in morphology can be invoked by change in catalytic particle diameter (Paper III), growth temperature and V/III ratio. Substrate-based VLS growth reports a direct dependence between the final nanowire diameter and the initial seed particle

size.<sup>65,122–124</sup> This is also the case for nanowires fabricated using Aerotaxy. To illustrate this, SEM images of GaAsP nanowires grown from two different initial particle diameters are shown in Figure 4.1. For same growth conditions, a smaller catalytic particle produced a thinner nanowire compared to a bigger particle as expected. The initial diameter of the catalyst particle determines the dimension of the growth interface and in turn the diameter of the emerging nanowire. Typically, the measured nanowire diameters are quite distributed with a standard deviation of 15–20% of the population average diameter. The standard deviation is presented as a range here because different experiments provide slightly different results for the measured deviation. This spread in nanowire diameter may be a consequence of spread in the initial seed particle diameter or the spatiotemporal variation in growth condition as explained in section 2.4.1.

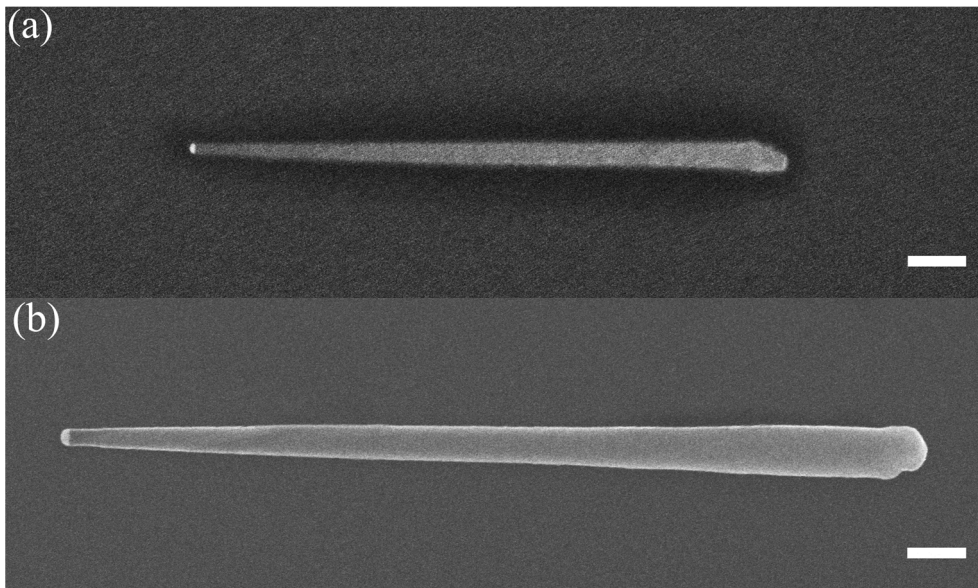


**Figure 4.1** SEM images of GaAsP nanowires grown from (a) 30 nm and (b) 50 nm Au particles. Scale bars: 200 nm



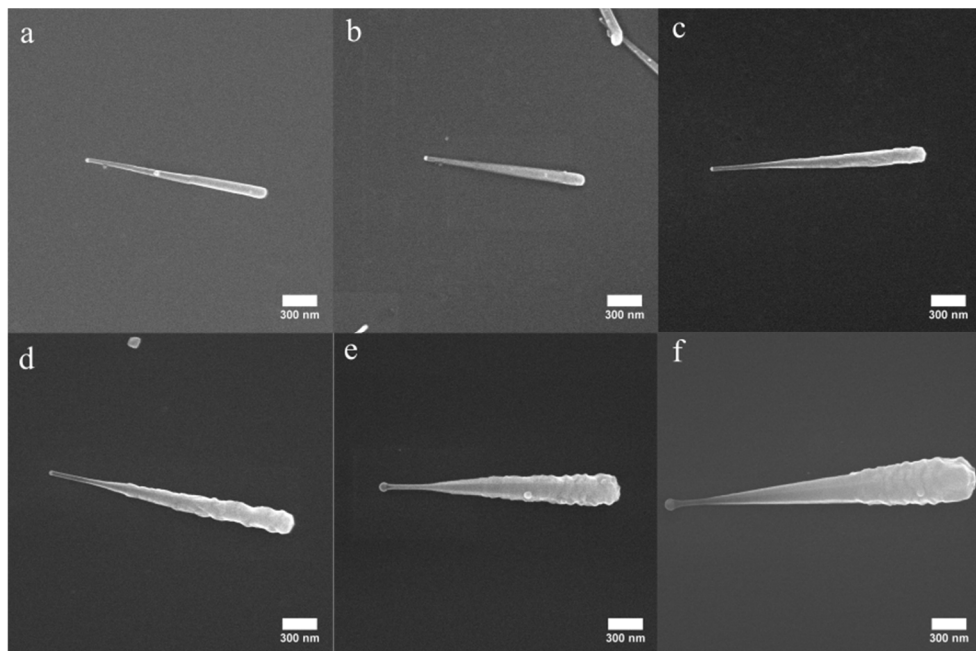


**Figure 4.2** SEM images of GaAs nanowires grown from 30 nm Au particles at reactor furnace set points of (a) 470 °C (b) 500 °C (c) 530 °C (d) 560 °C (e) 590 °C (f) 620 °C, and at a V/III ratio of 1.6. A version of this image can be found in Paper I.

In the study presented in Paper I, both the length and shape of the nanowires was observed to vary under different growth temperatures. A tapered nanowire geometry (i.e. a thicker base that progressively thins towards the tip), is commonly observed under most growth conditions, and tapering was observed to be enhanced by high growth temperature. This enhanced tendency for tapering can be explained by the enhancement of kinetic processes at elevated temperature. The axial growth rate of the nanowire is found to increase with increasing growth temperature. This observation is not consistent with the results from traditional substrate-based approaches,<sup>58,70</sup> where the axial growth rate is reduced at elevated growth temperature. Similar to nanowire diameter, we observe a spread in measured nanowire length that deviates 15–22% from the population average. Unintentional planar growth at the vapor–substrate interface starts to dominate substrate-based processes<sup>70</sup> in the high temperature regime, but a similar growth condition in Aerotaxy favors both axial and radial growth, leading to a long and tapered nanowire geometry. This is illustrated by Figure 4.2 (a–f), that shows SEM images of GaAs nanowires grown at different temperatures. High growth temperature also favors parasitic reactions between the III–V precursors, producing III–V nanoparticles in the gas phase (Paper II). These parasitic nanoparticles either get collected or become embedded in the nanowires (Figure 4.3). Alternatively, a tapered nanowire geometry can also arise from a gradually shrinking particle–nanowire interface. But

this is likely not the case for gold catalysed nanowires in Aerotaxy. However, when Ga is used to catalyse the growth of GaAs nanowires (Paper III), the Ga particle is consumed during growth, leading to a gradually shrinking particle–nanowire interface.

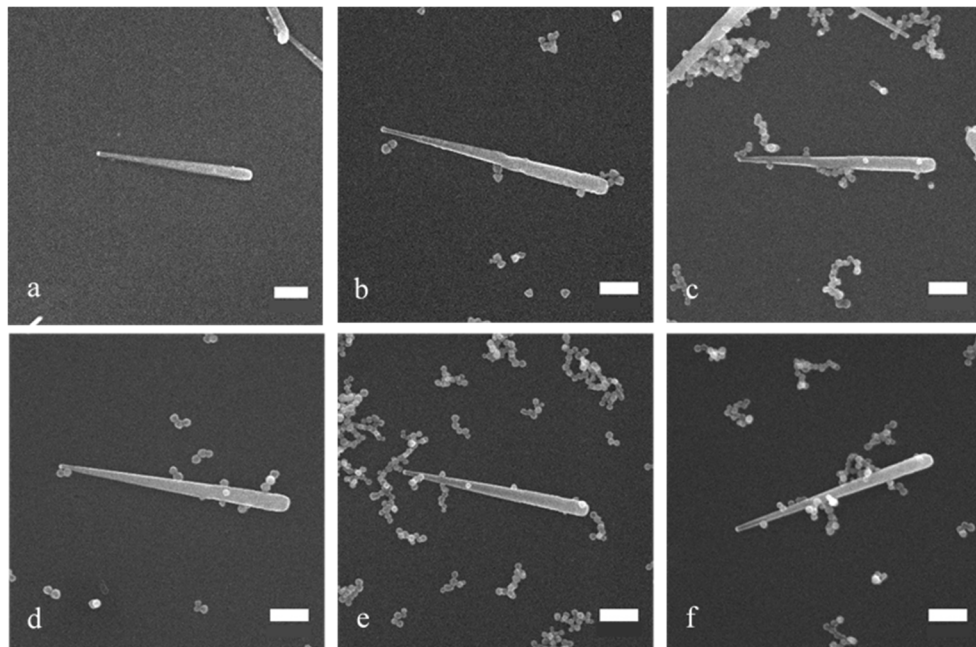


**Figure 4.3** SEM image of GaAs nanowires grown from 30 nm Au particles at V/III ratio of (a) 1.6 (b) 1.8 (c) 2.0 (d) 2.2 (e) 2.4 (f) 2.6 and at a reactor furnace set point of 530 °C. The parasitic particle density increases with increasing V/III ratio. Scale bars: 300 nm. (Image adapted from Paper I)

Morphology was found to be dependent on the gas-phase V/III ratio (Paper I), which is consistent with results from generic VLS nanowire growth reported in literature.<sup>58,85,125,126</sup> However, the effect of V/III ratio on nanowire morphology is quite complicated as a high V/III ratio can increase the probability of unintentional reactions between the precursors, thus promoting particle production. The study conducted in Paper I show that Aerotaxy nanowires have better morphology when grown at a low V/III ratio, and the axial growth rate is slightly increased at high V/III ratio along with unwanted particle production. At high V/III ratio, the axial growth rate of InAs nanowires is reported to drop as increasing the group V precursor flux reduces the diffusion length of group III adatoms,<sup>127</sup> this results in a reduced axial growth rate as the adatoms that impinge on the collection area cannot diffuse to the growth interface. However, in Aerotaxy, nanowire growth occurs at a very high precursor pressure, where particle supersaturation is attained with relative ease. As mentioned in section 2.4.2, for Aerotaxy growth, the axial growth rate is not limited by the diffusion of adatoms/molecules due to very high precursor pressures.

## 4.3 Crystal Structure

The bulk III-V semiconductors, except III-Nitrides (III-N), exist in the cubic zincblende (ZB) structure, while III-V nanowires typically exhibit a mixture of ZB and hexagonal wurtzite (WZ) phase along the  $\langle 111 \rangle$  growth direction.<sup>128–130</sup> Though nanowire polytypes in literature are often unintentional, polytypism can also be engineered by manipulating the growth conditions.<sup>52,59,128,129,131</sup>

The prominence of the WZ phase in III-V nanowires is often attributed to the formation of WZ nuclei at the triple phase line (site III in Figure 2.4) being energetically favored.<sup>129,132</sup> Control over crystal phase is usually achieved by tuning parameters like particle diameter,<sup>133,134</sup> dopant flow,<sup>135</sup> growth temperature<sup>136,137</sup> and V/III ratio.<sup>137</sup>

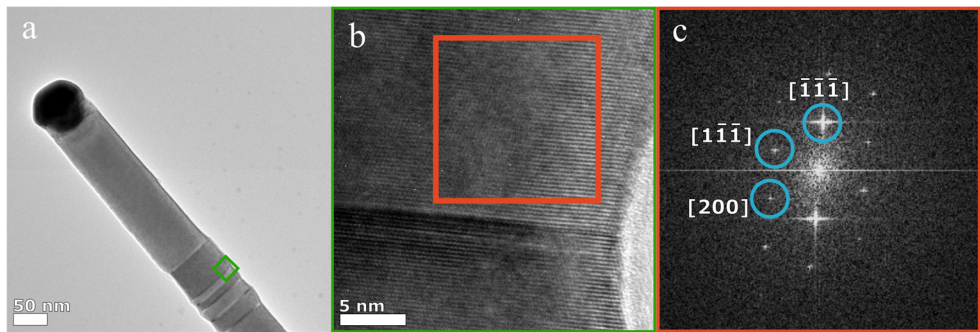


**Figure 4.4** (a) TEM image of GaAs nanowire. (b) High-resolution TEM image (HR-TEM) of the region highlighted by green square in (a) and (c) shows an FFT of the highlighted red square in (b) confirming that the nanowire has zincblende-structure. (Image adapted from Paper I)

Aerotaxy III-V nanowires behave similar to bulk semiconductors i.e. our nanowires prefer to grow with a predominantly ZB structure that is filled with multiple WZ sections in between. GaAs nanowires grown in the first generation Aerotaxy setup were found to exhibit growth temperature dependent mixing in crystal phase, leading to polytypic nanowire growth at high temperature.<sup>8</sup> In our current setup, studies involving various growth conditions and materials systems (Papers I, II, III, V and VII) show that the nanowires grow in a ZB (Figure 4.4) arrangement with highest concentration of dense stacking faults near the nanowire base. High density of stacking faults near the base might be due to the competitive, multi-crystallite nucleation (section 2.4.1) in Aerotaxy. We have yet to demonstrate intentional modulation of crystal phase by varying growth parameters. The ability to engineer the crystal phase using our synthetic Aerotaxy method may enable low-cost fabrication of nanowires with interesting electronic<sup>129</sup> and thermoelectric<sup>138</sup> properties.

## 4.5 Composition

The composition of the nanowires can be tuned by controlling the particle assisted VLS growth process and is essential for band-gap engineering.<sup>139,140</sup> *Ex situ* compositional analysis was performed either to confirm stoichiometric transfer of material to the crystal phase or to evaluate dopant incorporation. Intentional variation in composition is achieved by tuning growth parameters like V/III ratio, dopant flows, group III and V precursor fluxes, shape and diameter of the initial seed particle.<sup>140</sup>

In our Aerotaxy setup, the dopant and group III precursors mix with the catalytic particle in the alloying zone, which leads to the formation of a mixed alloy droplet. In Paper II, the composition of Sn doped GaAs nanowires was analysed to explore the mechanism of doping in Aerotaxy. We attempted to modulate the charge carrier concentration in the nanowires by directly altering the gas phase dopant injection ratio,  $X_{Sn} = [TESn]/[TMG]$ . TEM-XEDS analysis revealed a steadily increasing Sn concentration in the catalytic nanoparticle with increasing  $X_{Sn}$ . The amount of Sn present in the seed particle was also found to increase with increasing growth temperature for nanowires grown under the same  $X_{Sn}$ . This steady trend indicates that the dopant concentration in the catalytic particle drives dopant incorporation into the nanowire. Several studies show that the droplet-mediated dopant incorporation is the dominant doping pathway in VLS III-V nanowire growth.<sup>100,141</sup> Typical *n*-type dopants are reported to have low solubility of in the catalytic particle<sup>100</sup> and in our case this may lead to a rapid accumulation of Sn in the nanoparticle during the alloying stage of growth. The Sn concentration then gets depleted according to the axial growth rate of the nanowire. This cycle repeats and its effect was reflected in the axially non-uniform doping profile observed during XEDS characterization of the GaAs nanowires.

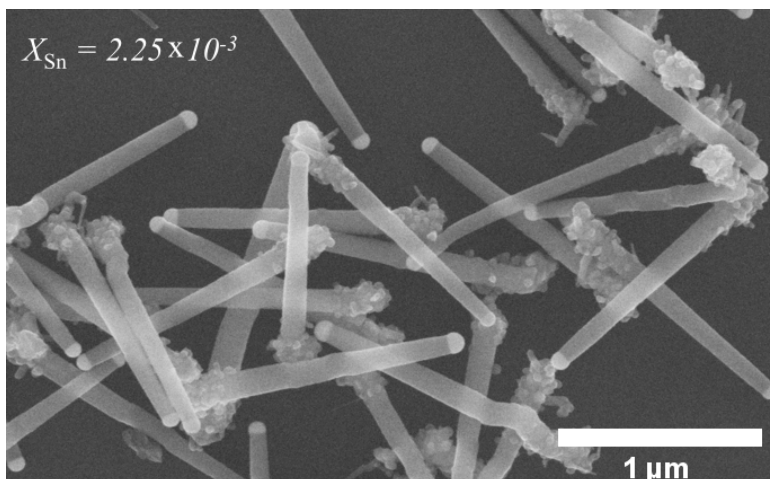


**Figure 4.5** SEM image of Sn doped GaAs nanowire ensemble. At high dopant injection ratio, the nanowires have a high density parasitic outgrowths/branches situated close the bottom.

*p*-type doping is notably more challenging in III-V semiconductor nanowires.<sup>100</sup> We attempted to dope GaAs nanowires with Zn at a constant growth temperature. XEDS analysis performed on a few selected Zn doped GaAs samples revealed that the catalytic particle was segregated into different elemental phases as shown in Figure 4.6. Similar to Sn doped GaAs nanowires, the dopant concentration in the seed particle increased with increasing  $X_{\text{Zn}}$ . However, Zn doped GaAs nanowires only showed evidence of Zn in the catalytic particle and not in the nanowire. The measured Zn composition in the seed particle could be adjusted by varying gas-phase  $X_{\text{Zn}}$ , indicating a linear dependence between the two. High solubility of Zn in Au and low partial pressure of DEZn is believed to trigger a delayed onset of Zn saturation in the catalytic particle compared to Ga.<sup>141,142</sup> This should ideally create an axial doping gradient along the nanowire, but no perceptible sign of such gradients was observed in the Zn doped GaAs nanowires.

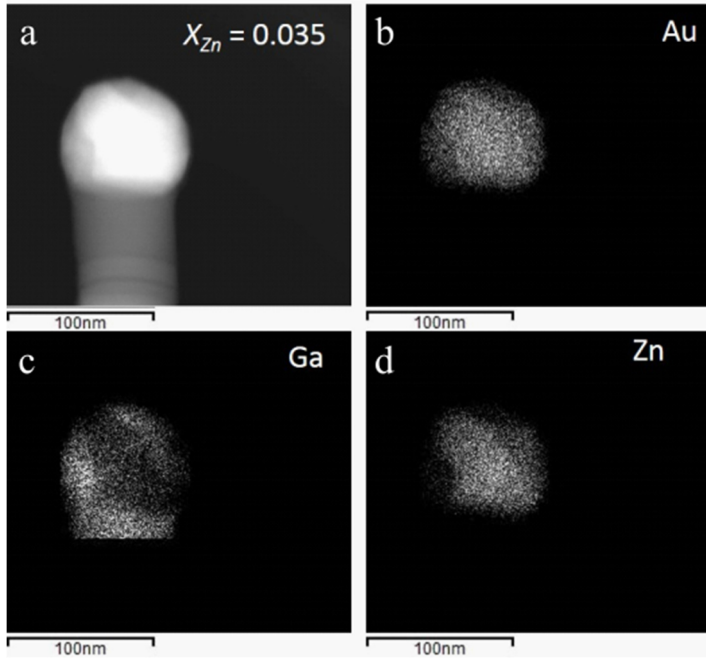


**Figure 4.7** (a) Overview TEM image of Zn doped GaAs nanowire grown at 530 °C. (b) XEDS elemental map of Au (c) Ga and (d) Zn.

Metaferia *et al*<sup>143</sup> demonstrated the growth of GaAsP nanowires with a tunable bandgap using Aerotaxy. Composition modulation in this study was achieved by varying the gas phase group V precursor fraction,  $X_g = \frac{[\text{PH}_3]}{[\text{PH}_3] + [\text{AsH}_3]}$ . However, no linear relationship between the gas phase  $X_g$  and nanowire composition was observed. This could be due to the difference in sticking co-efficient between the two group V precursors. Across multiple studies conducted using Aerotaxy, the nanowire composition roughly agrees with the gas-phase stoichiometry. However, further studies are required to provide more quantitative conclusions about the efficiency of compositional tuning in Aerotaxy nanowires.

## 4.6 Nanowire doping

Doping of nanowires is essential to functionalize the wires for novel and existing opto-electronic device applications. Traditional semiconductor doping is carried out by molecular diffusion or ion implantation, but very few studies adapt these techniques for doping nanowires.<sup>100</sup> Successful and controlled doping in III-V

nanowires was first achieved by introducing the dopant impurities along with group III and V precursors during VLS nanowire growth.<sup>99</sup>

III-V nanowire growth in Aerotaxy is inherently complex, even without considering the doping. *In situ* doping in Aerotaxy, similar to MOVPE is achieved by introducing the dopant precursors during growth. The effect of Zn doping on Aerotaxy GaAs nanowire growth rate and morphology reports<sup>141</sup> conflicting observations when compared to the Sn doping study reported in Paper II. This may be due to difference in the type of dopants and the growth setup used for these studies. For low to moderate levels of *p*-type doping using DEZn as a dopant precursor, no direct impact on morphology or growth rate was reported.<sup>141</sup> During *p*- and *n*-type doping studies conducted for this thesis, using DEZn (unpublished) and TESn (Paper II) respectively, for high dopant injection the nanowire morphology changed (illustrated in Figure 4.7) and the nanowires were shorter.

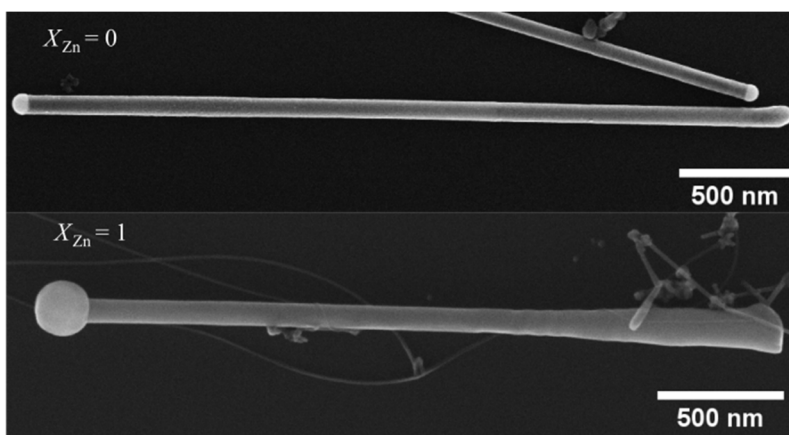


**Figure 4.7** SEM images of undoped and Zn doped GaAs nanowires. The images illustrate the change in nanowire morphology upon doping. Note the seed particle, which has expanded significantly due to the Zn concentration present in the seed particle. Zn doped nanowires from this study was also used for the results published in Paper IV.

#### 4.6.1 Doping evaluation

The dimension of a nanowire makes it challenging to implement standard doping evaluation techniques like Hall effect measurement.<sup>100</sup> We used optical, electrical and XEDS characterization for the quantitative evaluation of doping in Aerotaxy nanowires.

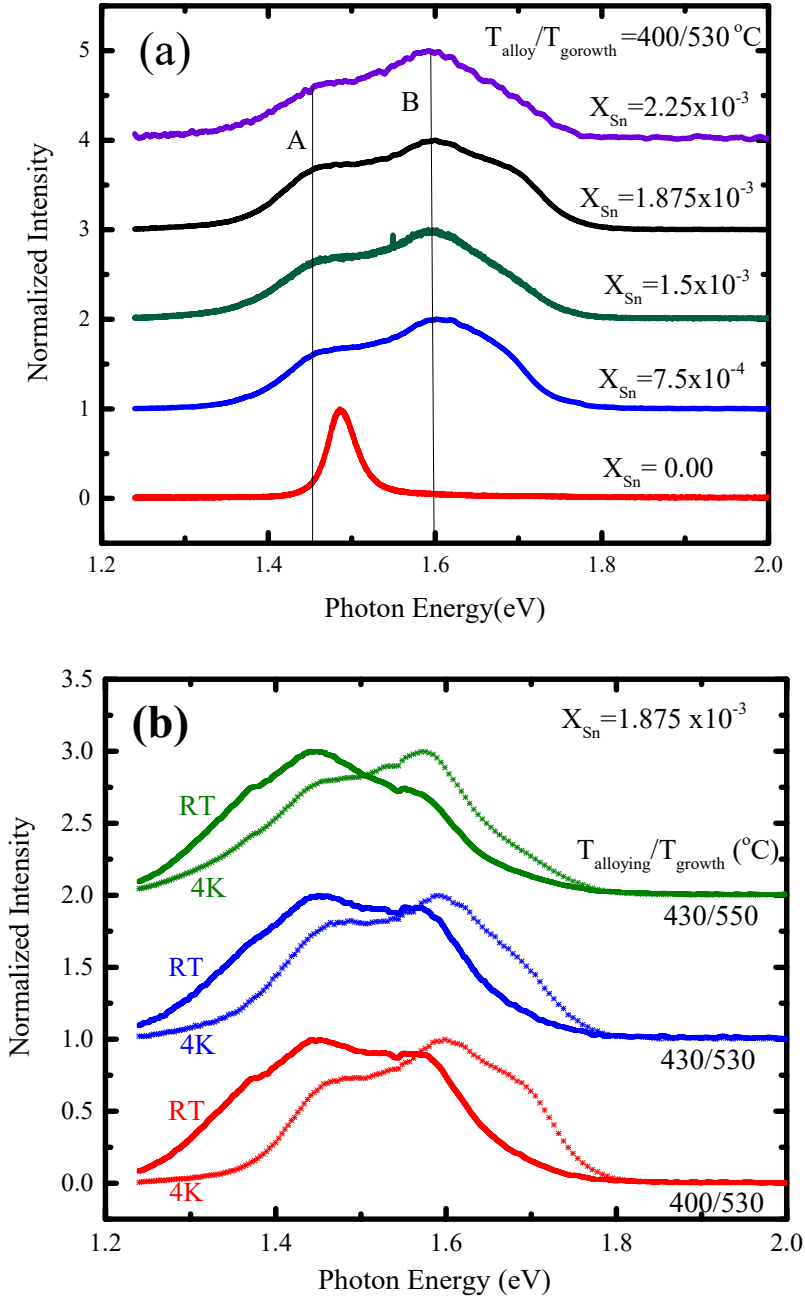


**Figure 4.8** (a) 7 K PL spectra of Sn doped GaAs nanowires grown at different  $X_{\text{Sn}}$  ( $0.00$ – $2.25 \times 10^{-3}$ ) and alloying and growth temperatures of  $400/530$  °C, and (b) room temperature (RT) and 4 K PL spectra of Sn doped GaAs nanowires grown at different alloying and growth temperatures but same  $X_{\text{Sn}}$  of  $1.875 \times 10^{-3}$ . (Plots adapted from Paper II)



The optical response of Sn doped GaAs nanowires in Paper II was studied using low-temperature  $\mu$ -PL spectroscopy. Corresponding PL spectra of doped nanowires in Figure 4.8 a, show two peaks with FWHM situated at 1.46 eV and 1.60 eV. The low energy peaks at 1.46 eV correspond to carbon acceptor levels, originating from by-products of precursor pyrolysis. The high energy peak at 1.60 eV corresponds to the Burstein–Moss shifted PL peak of heavily *n*-doped GaAs. Heavy *n*-type doping pushes the fermi energy level into the conduction band edge, leading to a significantly blue-shifted PL signal. Carrier concentration is extracted using the method explained in section 3.3.1. The extracted carrier concentration presented in Figure 4.9 a implies the same dopant concentration for all tested dopant injection ratios ( $X_{\text{Sn}}$ ). However, the PL measurements were performed on nanowire ensembles, and fermi-tail fitting provides information about the highest doping concentration within the ensemble. As mentioned in section 2.4.1, Aerotaxy system fosters a spatiotemporal variation in growth conditions, which leads to this spread in doping concentration within a given nanowire population. Four-point probe measurement technique explained in section 2.4 was used to acquire the carrier concentration in individual nanowires, plotted in Figure 4.9 b. It is clear from the plot that carrier concentration extracted from single nanowire measurements shows a spread, unlike the data from nanowire ensemble characterization.

For the studies presented in Paper IV, low-temperature  $\mu$ -PL measurements were performed on Zn doped GaAs nanowire ensembles and the optical response of a few selected samples are shown in Figure 4.10 a. In heavily *p*-doped GaAs, band–band optical transition is reported to occur both with and without *k*-conservation.<sup>141,144</sup> The Burstein–Moss shifted high energy shoulders appearing above 1.58 eV and 1.8 eV for Zn doped GaAs are caused by non-*k*-conserving transitions from conduction band to acceptor states close to fermi level. The low-energy peaks below 1.4 eV represent *k*-conserving direct band–band transitions.

Carrier concentrations estimated from PL spectra of Zn doped GaAs is given in Figure 4.10 b. The data shows small and steady incremental variation in carrier concentration for increasing  $X_{\text{Zn}}$ . Complementary electrical measurements of Zn doped nanowires revealed degenerate doping similar ( $\sim 10^{20} \text{ cm}^{-3}$ ) to the PL study. In Paper IV, the measured elemental concentrations of Au, Zn and Ga in the seed particle were used to calculate the hole concentration with a predictive model, which used defect formation energy in GaAs as proposed by Zhang and Northrup.<sup>145</sup> Both measured and calculated values for *p*-doping concentration are in good agreement, especially for low dopant injection ratios ( $X_{\text{Zn}}$ ). Both *n*- and *p*- doping studies indicate tangible difference in carrier concentration between undoped and doped nanowires. However, strong modulation of the carrier concentration by varying dopant injection ratio is yet to be achieved.

The key conclusion from these studies is that; it is possible to grow both *n*- and *p*-doped III-V semiconductor nanowires in Aerotaxy. However, it is not possible to achieve low to moderate levels of doping in Aerotaxy.

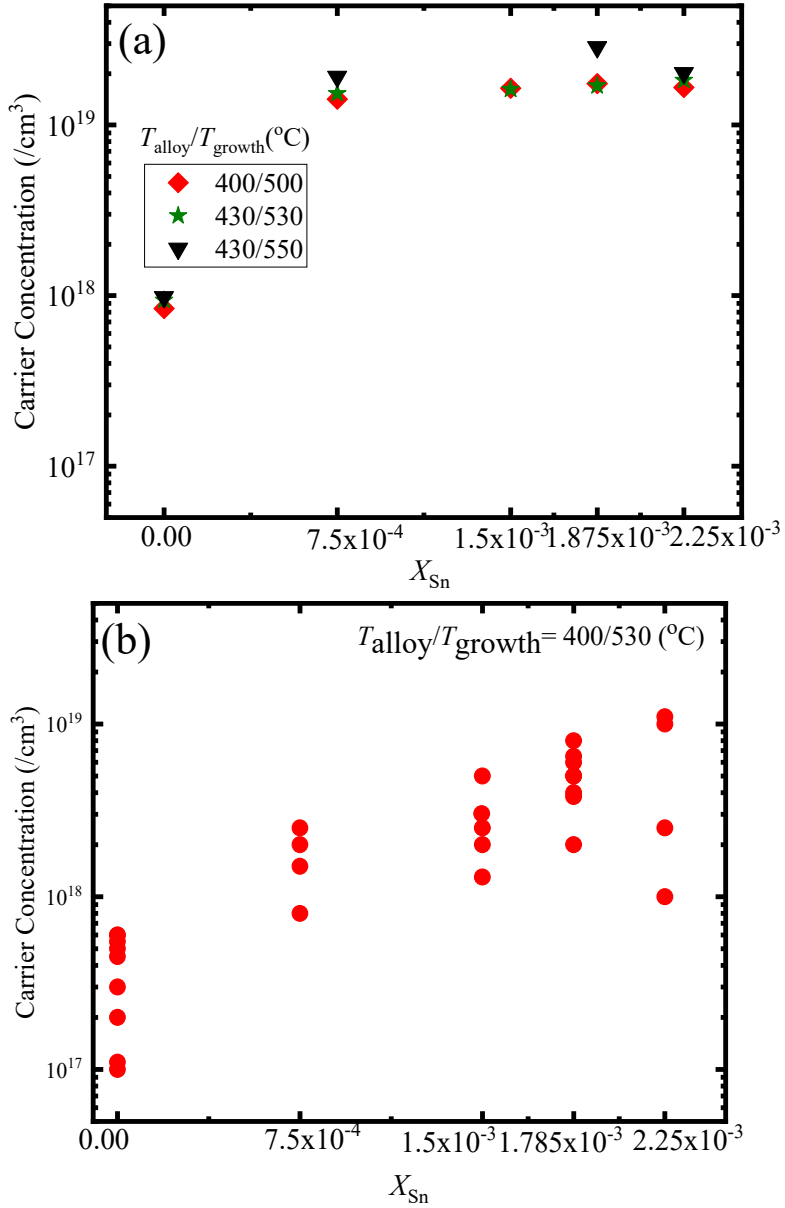


**Figure 4.9.** (a) Carrier concentration estimated from 7 K photoluminescence FWHM, for the undoped NWs and Fermi-tail method for  $n$ -doped GaAs NWs grown at varying alloying and growth temperatures and varying  $X_{\text{Sn}}$ . (b) Carrier concentration estimated from four probe resistivity measurement of GaAs NWs grown at alloying and growth temperature of 400 and 530 °C and with varying  $X_{\text{Sn}}$  ( $0.00$ – $2.25 \times 10^{-3}$ ). (Plots adapted from Paper II)

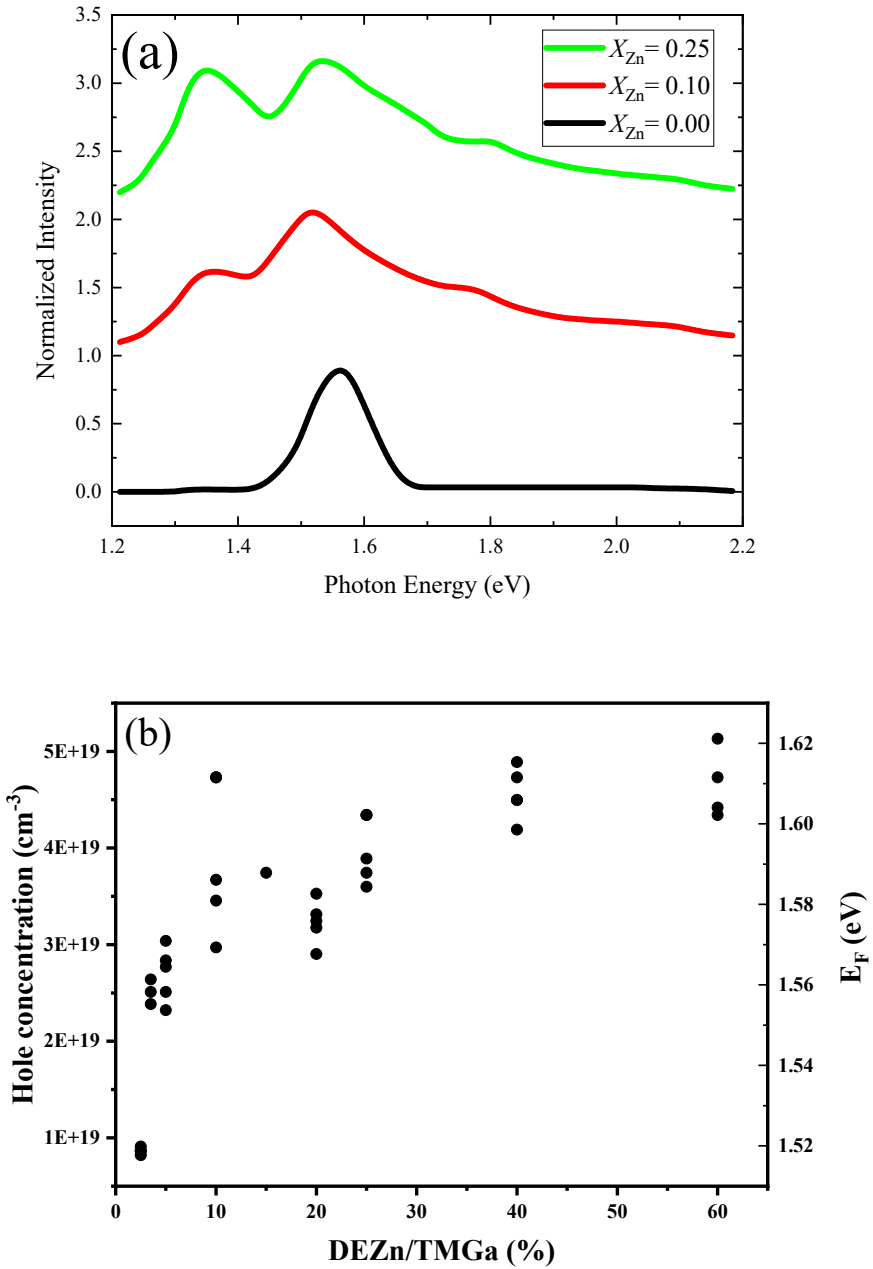


**Figure 4.10** (a) 4 K PL spectra of Zn doped GaAs nanowires grown at three different  $X_{Zn}$  (0.00,0.10,0.25) and alloying and growth temperatures of 400/550 °C. (b) Carrier concentration estimated from 4 K photoluminescence spectra using Fermi-tail method for p-type doped GaAs NWs grown at varying  $X_{Zn}$ .

## 4.7 Branched nanostructures

A typical catalyst-assisted branched nanostructure is produced by sequential deposition of a seed particle on to the primary nanowire surface.<sup>24,146</sup> In Paper III, we report the unintentional growth of branched GaAsP epitaxial nanostructures using a single step VLS process in Aerotaxy. In Figure 4.11 b, it can be seen that each of the branches has its own catalytic particle. This indicates that the branching events are driven by particle assisted VLS growth.

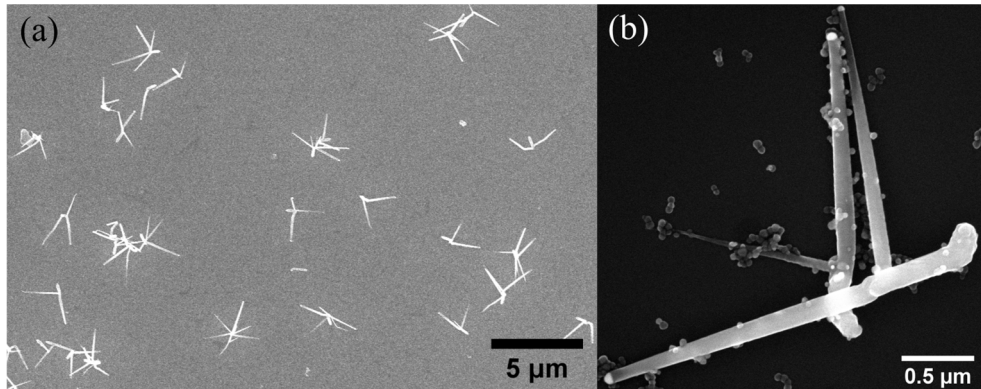


**Figure 4.11** (a) An overview SEM image showing branched GaAsP nanostructures on an Si substrate. (b) Magnified SEM image shows epitaxial branches originating from the primary GaAsP nanowire.

Additionally, some of these branches were found to elongate into an ultrafine tip with a tiny metal particle as illustrated by Figure 4.12 b. The length and diameter of these secondary branches varied widely. But one common observation is that a thicker primary nanowire produced many long branches, while a thinner nanowire produced few short branches. This points to the underlying diameter dependence of branching. To further probe this mechanism, the initial particle size was varied in steps of 10 nm from 20 to 80 nm and the resulting nanostructures were analysed. Single GaAsP nanowires with no branches or parasitic particles were observed for seed particle diameters up to 50 nm. For diameters above 50 nm, there is a gradual onset of branching with a drop in the density of single GaAsP nanowires. To illustrate this, SEM images of GaAsP nanostructures grown from various particle diameters are collectively presented in Figure 4.13.

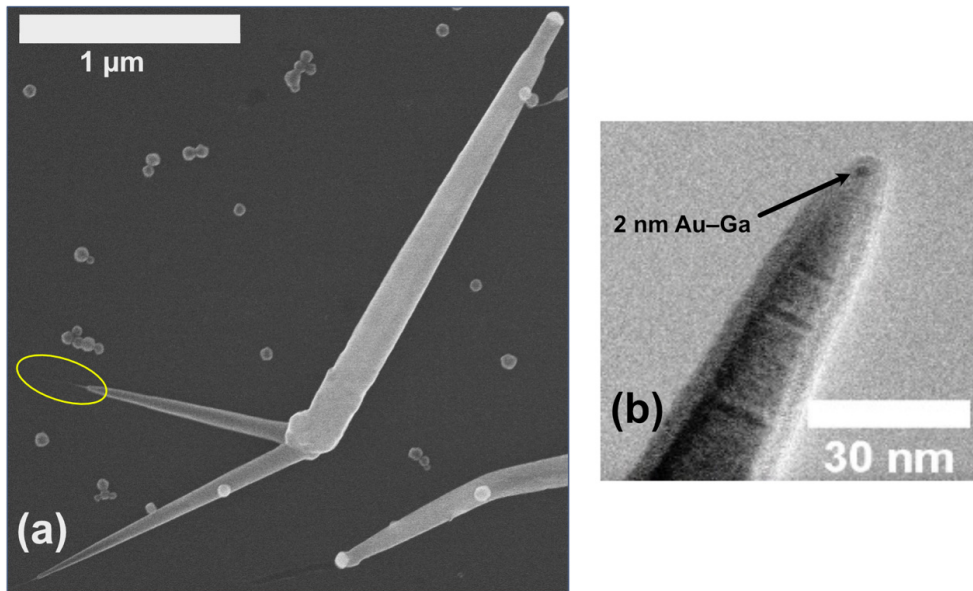


**Figure 4.12** (a) SEM image of a typical GaAsP nanowire cluster. The inset is a magnified SEM image of the tip. The branches seem to extend into a very tiny whisker as the Ga in the seed particle gets consumed during growth leaving a tiny whisker behind. (b) TEM image of a representative whisker with a 2 nm Au seed at its tip, EDX point analysis (not shown here) shows that the 2 nm particle is Au with <10% Ga. (Image adapted from Paper III)

TEM investigation on these branched structures show that they grow in a ZB arrangement and that the branches are in fact epitaxially connected to the primary nanowire. These highlights show that our synthetic approach can yield branched GaAsP nanostructures, and the diameter of the catalytic particle can be used to induce branching on the primary nanowire.

Conventional planar Si photovoltaics requires a thicker substrate to absorb ~90% of the incident sunlight (compared to III-V PV) and suffers in conversion efficiency due to short carrier lifetimes.<sup>147,148</sup> Lifetimes can be improved by fabricating high quality crystalline material, which ultimately increases the overall production cost. The key issue involves the use of same long pathways for light absorption and charge carrier collection. The obvious solution is to use long light absorption pathway, while photo-generated carriers are collected immediately upon generation. The nanowire geometry provides a suitable platform to overcome these challenges.<sup>7,149,150</sup> Such 3D nanostructures can have diverse applications in many key areas like photovoltaics, photocatalysis<sup>151</sup> and efficient energy storage.<sup>152</sup>

Based on our current understanding, size-dependent branching is attributed to (i) rupturing of the catalytic droplet into many smaller particles or and (ii) insolubility of P in Au.<sup>153</sup> The Aerotaxy reactor has a temperature gradient that rises and falls along its three different zones. This gradient might induce interfacial instability at

the droplet–nanowire interface and the dynamic temperature gradient may increase the volume of the liquid seed particle and wet the side facets of the primary nanowire which leads to kinking<sup>52,154–156</sup> of the primary nanowire.

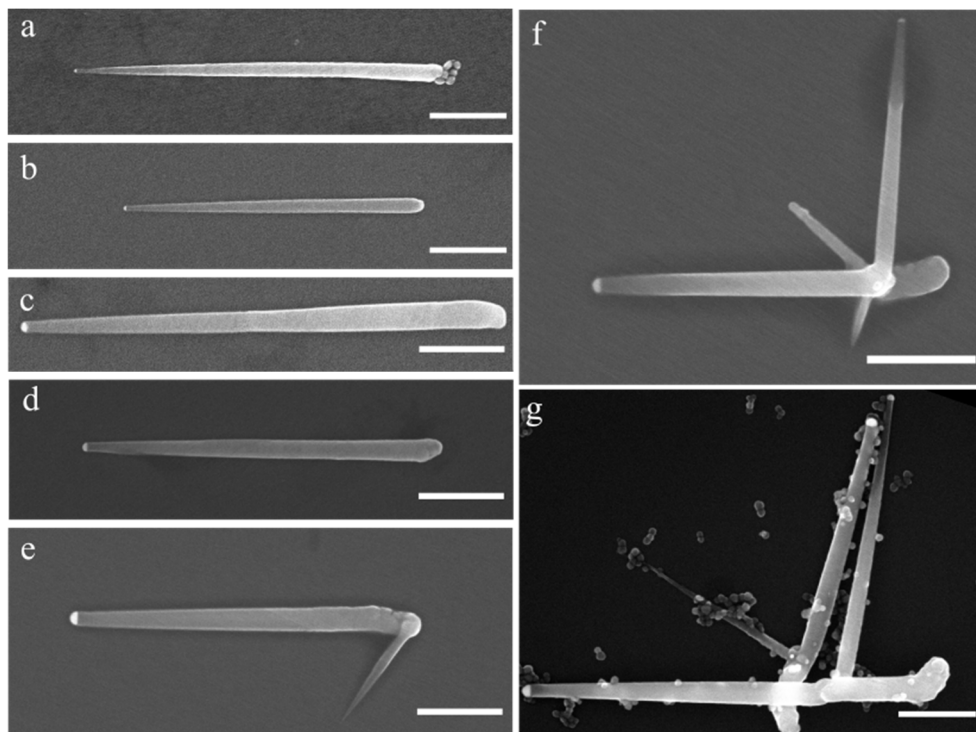


**Figure 4.13** SEM images of GaAsP nanowires grown from a) 20 nm b) 30 nm c) 40 nm d) 50 nm e) 60 nm f) 70 nm g) 80 nm Au particles at a V/III ratio of 0.5. The images show that the secondary branches start to appear for Au particle sizes 60 nm and above. Scale bars: 500 nm. (Image adapted from Paper III.)

Another contributing factor to this volumetric increase of the liquid droplet might be our continuous flow-through reactor design. The amount of material available in the gas-phase reduces continuously as precursor materials are being consumed to produce nanowires. The low solubility of group V precursors in the catalyst particle is well known for III-V nanowire growth. Additionally,  $\text{PH}_3$  does not decompose completely<sup>157</sup> at our growth temperature, but the decomposition is enhanced significantly in the presence of a growth surface. This will enhance the concentration of Ga in the primary Au droplet, which in turn may increase the volume of the liquid droplet. Increasing the Ga concentration in the liquid droplet lowers the surface tension<sup>158,159</sup> and may rupture the primary particle leaving small Au–Ga particles along the nanowire sidewalls.

XEDS study shows that the branches are compositionally similar to the primary GaAsP nanowire. As for the branching dependence of GaAsP on seed particle diameter, if growth initiates from a small seed particle (20–50 nm), the change in volume and surface tension may not be sufficient to rupture the primary particle.

Parasitic outgrowths/branches were also observed at high growth temperatures and high dopant precursor concentration for Sn doped GaAs as reported in Paper II. XEDS studies revealed that these juvenile branches exhibited a location dependent compositional variation i.e., branches close to the top of the primary nanowire were composed of Ga, while the branches at the bottom were composed of GaAs (illustrated in Figure 4.14). As mentioned earlier, group V precursors have low solubility in the catalytic particle, which may enhance the Ga concentration locally. C. Yan *et al.*<sup>160</sup> reports that for GaSb nanotrees fabricated using MBE, a locally enhanced supply of Ga induced spontaneous deposition of Ga nanoparticles on the side facets of the primary GaSb nanowire. Although MBE and Aerotaxy are two very different growth technologies, upon careful consideration, a locally increasing Ga concentration may spontaneously deposit Ga nanoparticles for Aerotaxy nanowires too. Hence, we assume that the branches near bottom started out as Ga nuclei and catalysed GaAs growth, while the branches closer to the top did not have enough time to form GaAs. This reinforces our hypotheses that a locally increasing Ga concentration can lead to spontaneous Ga nucleation on the primary nanowire. The common observation is that branching and other parasitic processes tend to dominate Aerotaxy III-V growth under extreme growth conditions.

For the GaAsP material system, this spontaneous branching can be controlled by tuning the size of the seed particle. To summarize, a large catalytic particle ruptures to form smaller catalytic particles that induce branching, while a small catalytic particle is found to be stable during growth and avoids branching.

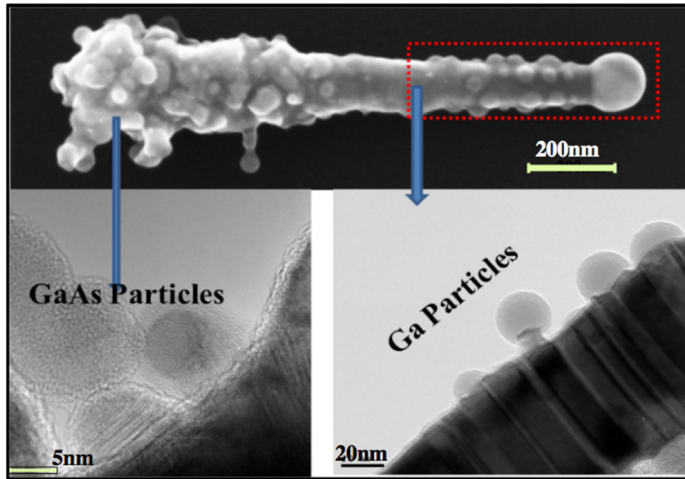


**Figure 4.14** High resolution TEM studies of the parasitic nanoparticles and branches of a GaAs nanowire grown at  $T_d/T_g = 430/450$  °C and  $X_{Sn} = 5 \times 10^{-3}$ . XEDS studies reveal that the particles/branches at the base of the nanowire are GaAs in composition whereas those in the upper half of the nanowire are Ga particles. (Image adapted from Paper II)

## 4.8 Alternative metal seed particles

Currently, gold nanoparticles are mostly used to catalyse VLS III-V nanowire growth.<sup>154,155</sup> The success of gold as a starting material is attributed to its ability to induce controllable nanowire growth over a wide range of growth conditions.<sup>155</sup> This provides a large parameter space over which the properties of the nanowires can be tuned. However, the nanowire community has voiced concerns regarding the detrimental effect of gold on Si and the consequent incompatibility of gold with Si technology.<sup>52,154,155</sup> Gold has very high diffusivity in semiconductors and negatively impacts the potential opto-electronic properties.<sup>26,161</sup> There is currently a huge vested interest in exploring gold-free III-V nanowire growth. Alternative catalytic particles made from Ni,<sup>162</sup> Fe,<sup>163</sup> Ag<sup>154</sup> and Pd<sup>52</sup> are already being used to catalyse III-V nanowire growth in addition to self-catalysed pathways.<sup>26</sup>

So far, the nanostructures discussed in this thesis were catalysed exclusively by size-selected gold nanoparticles. Aerotaxy can already offer significant cost-reduction over batch production methods, when it comes to high throughput synthesis of III-V nanomaterial. Reducing component costs even slightly can have a substantial impact on the production cost and make Aerotaxy an attractive large-scale production technology. So, there is an incentive for exploring cheaper alternatives that can serve as a catalytic particle in Aerotaxy.

We have investigated growth of GaAs nanowires initiated by 30 nm Au-Ag (50:50 at% alloy) and pure Ag catalytic particles generated in a Spark Discharge



Generator (SDG). The SDG used electrodes with corresponding stoichiometry to produce Au-Ag alloyed nanoparticles.

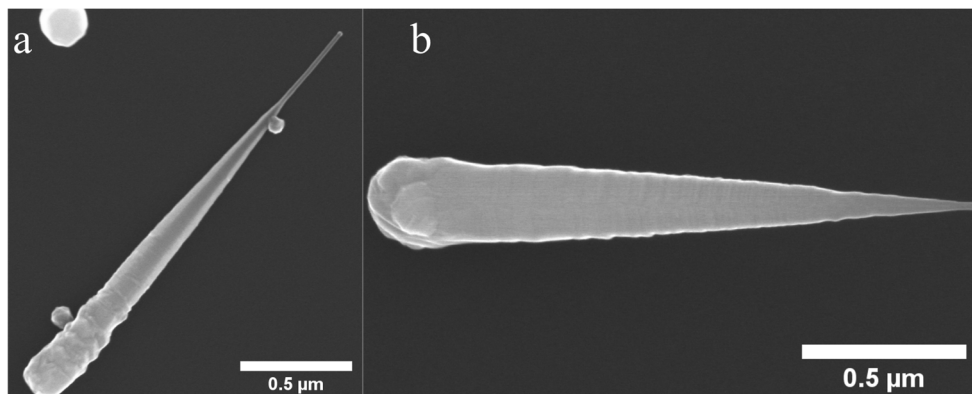


**Figure 4.15** (a) SEM image of GaAs nanowire grown from 30 nm Au-Ag particle at 520 °C. (b) SEM image of GaAs nanowire grown from 30 nm Au-Ag particle at 550 °C, a higher tendency for tapering was observed at 550 °C than at 520 °C.

Figure 4.15 shows GaAs nanowires grown from 30 nm Au-Ag seeds at two different growth temperatures (520 °C and 550 °C). The nanowires grown from Au-Ag shows considerable overlap in morphology with GaAs nanowires catalysed by Au. More importantly, this observation is consistent with the temperature dependent tapering/radial growth commonly observed for Au catalysed GaAs nanowires shown in Figure 4.2. GaAs nanowires grown from Au and Au-Ag seeds using substrate-based MOVPE are reported to exhibit similar trends in morphology under moderate to high growth temperature regime.<sup>164</sup> This is due to significant similarities in physical and electronic properties of both gold and silver.<sup>155,164</sup> However, the morphology of our GaAs nanowires deteriorated and nanowire growth failed at low temperatures, when pure Ag particles were used to catalyse Aerotaxy growth; another observation that is consistent with the available literature on MOVPE growth using Ag particles.<sup>164</sup>

Ga seeded GaAs nanowire growth can provide a clean growth environment free from incorporation of the foreign metal catalyst into the nanowire.<sup>155,165,166</sup> One main drawback of self-catalysed growth is that the catalytic particle can be consumed during growth inducing a tapered morphology; the growth conditions must be tailored to avoid consumption of the catalytic particle.<sup>155</sup> In Paper V, we report the fabrication of self-catalysed GaAs nanowires using Aerotaxy. Size-controlled metallic Ga nanoparticles were mixed with TMG and AsH<sub>3</sub> to initiate VLS growth. The growth parameters used for Au catalysed GaAs growth served as a good starting point for this explorative study.

Several authors<sup>161,166–170</sup> report an inverse tapered nanowire morphology (gradually increasing diameter toward the top) for self-catalysed nanowires grown under a low

V/III injection ratio. Conversely, the catalytic droplet is observed to be consumed at high V/III injection ratios. However, this is not true for Aerotaxy as the Ga droplet is observed to shrink from its initial diameter even at low V/III ratios. This indicates that the emerging nanowires perceive a locally enhanced V/III ratio. Similar to gold, Arsenic precursor species have a low solubility in the liquid Ga catalytic particle.<sup>171</sup> The Ga droplet serves as a reservoir and nanowire growth is initiated by the arrival of As species. The high partial pressures of precursors in Aerotaxy might lead to rapid consumption of the Ga droplet before it could be replenished from the vapor phase. Consequently, a gradually shrinking growth interface even at low V/III injection ratios might explain our observation of tapered nanowire morphology. The nanowires passing through the reactor will experience a gradual decrease in V/III ratio as they travel from the growth zone towards the exit of the reactor. Due to this spatiotemporal variation observed in Aerotaxy, the tapered morphology of Ga seeded GaAs nanowires is inevitable.

Self-catalysed growth of III-V nanowires in literature is usually a two-step process,<sup>161,167–169</sup> where nucleation and nanowire growth require different V/III injection ratios and the axial growth rate is limited by group V precursor flux.<sup>169</sup> Unfortunately, it is not possible to decouple nucleation and nanowire growth in Aerotaxy and both processes must occur under similar conditions. So, Ga seeded GaAs growth in Aerotaxy proceeds through a single-step process.

## 4.9 Pseudo-particle continuum model

The design of the Aerotaxy tool makes it difficult to incorporate *in situ* monitoring or sampling ports into the design without affecting nanowire growth. To better understand Aerotaxy growth and to explain the qualitative observations, we modelled Aerotaxy growth using computational flow dynamics (CFD) modelling in COMSOL based on a novel nanowire growth model as described by Johansson and Magnusson.<sup>86</sup>

Aerotaxy growth is modelled as chemical reaction between the Ga- and As-containing precursor gases forming GaAs, occurring only in the presence of a gold catalytic particle. The precursor gases as well as the catalytic particles and growing nanowires are described as continuous chemical species and the amount of GaAs at any given point is interpreted as the length of the nanowire, where the nanowire width and concentration in the gas are given by the catalytic particles. This type of pseudo-particle continuum modelling circumvents the complexity of modelling and monitoring individual particles in a gas-phase synthesis environment. The results from the simulation are compared to the experimental data and is presented in Paper I.

The underlying nanowire growth model is based on a surface diffusion model for substrate-based growth at high precursor pressures (which is the case for Aerotaxy). According to the model, the axial growth rate  $G$  is given as:

$$G = \Omega I \frac{J_3 \varphi}{J_3 \varphi \left(1 + \frac{k_d}{J_5}\right) + I}, \quad 4.1$$

where  $\Omega$  is the molar volume of a III-V pair in the solid phase,  $I(T)$  is a rate limiting incorporation factor,  $J_3$  and  $J_5$  are the impingement rates of group III and group V precursor species,  $k_d$  is the desorption rate of group V atoms, and  $\varphi$  is a seed particle radius dependent shape factor. At very high precursor pressures, the axial growth rate in eq-4.1 becomes independent of both the precursor flows and wire radius, which agrees with our qualitative observation presented under section 4.2. The incorporation rate is assumed to be an activated process with an Arrhenius dependence on growth temperature.

Wire growth is then simulated with steady state computational flow dynamics in a simplified Aerotaxy reactor (rotated 2D geometry), where the growth model eq-4.1 governs the simplified chemical reaction  $\text{Ga} + \text{As} \rightarrow \text{GaAs}$ . Since each catalytic particle (and thus growing nanowire) follows a unique time–temperature trajectory, the model provides not only an average but also a distribution of the wire length.

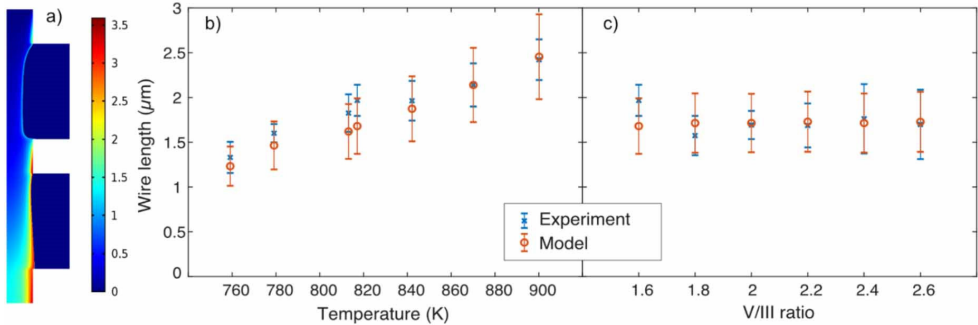


**Figure 4.15** (a) plot of the wire length during steady-state growth in the reactor, shown in radial cross section. (b) Wire length as a function of peak temperature for GaAs nanowires grown at a fixed V/III ratio of 1.6. (c) Length as a function of V/III ratio for nanowires grown at a peak temperature of 815 K (set point 530 °C). In both plots, the model is shown as red rings and the experiment as blue crosses, with the error bars indicating plus/minus one standard deviation. (plots and image adapted from Paper I)

Figure 4.15 shows results of the GaAs nanowire growth simulated with this method, together with experimental data used for parameter fitting. The only fitting parameters are the activation energy and scaling pre-factor the incorporation factor  $I$ . As mentioned earlier, GaAs nanowire growth only occurs in the presence of Au catalyst particles. The length of the GaAs wire is calculated by dividing the concentration of continuous GaAs species by the concentration of Au, and the length average and spread are calculated from the wires exiting at bottom of the reactor.

The model was tested under different growth temperatures (Figure 4.15 b) and V/III ratios (Figure 4.15 c). The results show good agreement between the experimental and simulated nanowire lengths under various growth conditions. The simulated wire length is independent of the initial seed particle diameter and shows only a weak dependence on the precursor flows, in agreement with observation. Currently, there is an ongoing effort to expand this model to better understand gas-phase production.



# 5 Aerotaxy instrumentation and Safety

The investigations of crystal growth reported within this thesis were conducted in a custom-built, third generation Aerotaxy system. At present, this Aerotaxy system is one of its kind and is not commercially available. This chapter deals with description of the Aerotaxy instrument and the challenges encountered during its operation. In addition, the importance of safety in a gas-phase nanomaterial production environment is highlighted here. (Papers I and VI.)

## 5.1 The Aerotaxy Instrument

The Aerotaxy instrument, at its core, is an Aerosol particle generator in combination with a gas-handling system, designed with inspiration from MOVPE. Both parts of the system supply nanowire building materials to a heated stainless-steel furnace where crystal growth occurs. A categorical description of the instrumentation is provided in the following sections i.e., nanoparticle generation and nanomaterial growth/collection (combined gas-handling and growth system).

### 5.1.1 Aerosol Particle Generator

The purpose of the Aerosol Particle Generator (APG) in our system is to supply the liquid droplet which assists the VLS growth process. In order to design complex experiments that involve different material systems, our APG must be (i) compatible with a range of different materials; (ii) have control over characteristics like nanoparticle size and its density in the aerosol; (iii) deliver nanoparticles in the vapor phase to the growth reactor.

At present, there is a variety of methods to produce metal and semiconductor nanoparticles and the manufacturing process can be tailored to meet specific requirements.<sup>172-174</sup> But, the most direct method to aerosolize a source material (Ga or Au) for our process is to vaporize the source material in an inert carrier gas.

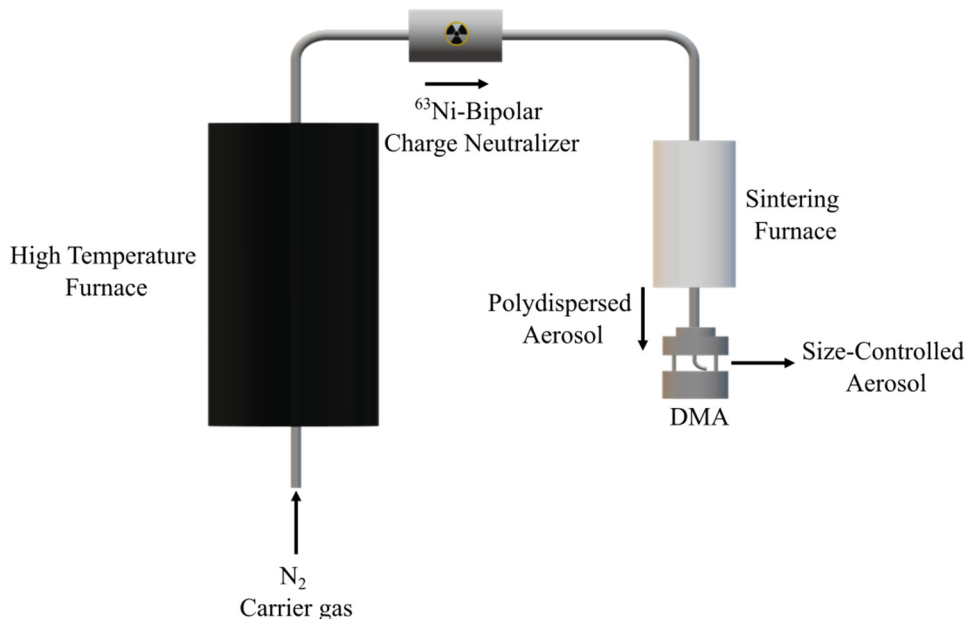


**Figure 5.1** Schematic of the Aerosol Particle Generator. The radioactive charge neutralizer induces a known charge distribution in the agglomerate population exiting the high temperature furnace. The charged agglomerates coalesce (sinter) in the sintering furnace to a roughly spherical shape and are size-selected in the DMA based on their mobility in an applied electric field.

Figure 5.1 shows a schematic of the APG used for controlled generation of catalytic particles in Aerotaxy. The high temperature furnace in Figure 5.1 is capable of reaching 2000 °C and is water cooled to prevent thermal degradation of the refractory lining. A graphite crucible inside the furnace holds the material to be vaporised into the carrier gas. The temperature of the furnace is ramped to a setpoint (based on the material), at which the vapor pressure of the material is high enough to attain an acceptable evaporation rate at a carrier gas pressure of ~1 bar. A mass flow controller (MFC) limits the flow of  $N_2$  carrier gas into the high temperature furnace at 1.5 l/min. Homogenous nucleation of the source material is initiated in the carrier gas and the rate at which the primary particles nucleate depends on the degree of supersaturation in the vapor phase. To promote Brownian coagulation of primary particles, they are transported away from the evaporating source material by the carrier gas flow. The tiny primary particles coagulate into agglomerates, and agglomeration depends on the number concentration of primary particles in the gas phase. The size of the final particles depends on the size of the initial agglomerates. The carrier gas transports the agglomerates into a radioactive charge neutralizer<sup>178</sup> that uses low-energy beta decay from  $^{63}\text{Ni}$  to create a bipolar ionic environment inside the neutralizer. Since the particles are produced using an evaporation–condensation process, they carry an unknown charge distribution, but is net negative due to thermionic emission in the high-temperature furnace.<sup>172</sup> The dimensions of

the bipolar charger are dictated by the residence time i.e., the time required to bring a known steady-state or Boltzmann equilibrium charge distribution. Using a diffusion bipolar charger, almost 80% of particles below 20 nm remain uncharged, giving a lower limit in particle production size for our APG. The agglomerates with a known charge distribution enter a sintering furnace downstream. The sintering furnace is maintained at a lower temperature ( $< 600\text{ }^{\circ}\text{C}$ ) and reshapes the agglomerates to a compact spherical shape. The temperature of the sintering furnace is selected to ensure coalescence of agglomerates and to avoid inducing multiple charges, as it exaggerates the measured particle concentration and impairs the size selection.<sup>172</sup> The sintered aerosol usually has a wide distribution in nanoparticle size due to the size variation within the initial agglomerates. To achieve a narrow size distribution, the sintered aerosol is passed through a Differential Mobility Analyser (DMA).<sup>175</sup> The DMA size selects the charged particles in the aerosol by subjecting them to an electric field. The mobility of a charged particle in an applied electric field is inversely proportional to its aerodynamic diameter.<sup>175,176</sup> So, the DMA effectively filters out unintended particle sizes by removing them from the primary aerosol flow. A part of the flow (0.1 l/min) is directed to an electrometer (not shown in the schematic) to continuously monitor the particle number concentration in the aerosol. The number concentration for a given size can be modulated either by varying the temperature setpoint of the high-temperature furnace or by adjusting the carrier gas flow. The size-controlled aerosol is then transported to the Aerotaxy reactor to assist nanowire growth.

### 5.1.2 Aerotaxy Reactor and Precursor Supply System

The Aerotaxy Reactor (AR) provides a closed reaction environment for the gaseous precursors and is made from stainless-steel tubes fastened together with high-temperature, ultra-high vacuum seals. The continuous AR tube ( $\sim 750\text{ mm}$  long) is mounted vertically inside a three-zone split clamshell furnace and the zones can be independently heated to a user-defined setpoint. Figure 5.2 is a simplified schematic that depicts the different components of the Aerotaxy system. The size-controlled aerosol containing the Au catalytic particles is fed to the alloying zone of the reactor, which is maintained at a temperature that is at least  $100\text{ }^{\circ}\text{C}$  below the growth zone temperature.

To supply the alloying zone with group III precursor, a dedicated MFC automatically controls the flow of ultrapure  $\text{N}_2$  carrier gas through a bubbler cylinder according to the user-defined setpoint. The bubbler cylinder contains MO group III precursor in a chiller bath, and the temperature of the bath can be adjusted to achieve a suitable precursor vapor pressure. The gold aerosol and gaseous group III precursor are mixed in the alloying zone. A fraction of the group III precursor undergoes thermal decomposition into reactive species and initiates the alloying process with gold to form the alloyed liquid droplet as explained in section 2.4.1.



The amount of group III precursor supplied to the alloying zone can be varied by either adjusting the temperature of the chiller bath or the carrier gas flow through the bubbler.

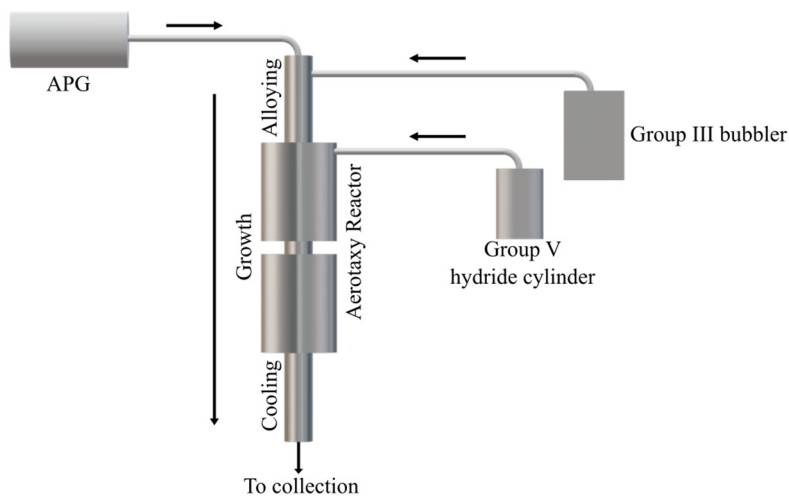


**Figure 5.2** Schematic of the Aerotaxy Instrument. The size controlled aerosol from the APG is mixed with group III and group V precursors and grow to nanowires in the Aerotaxy Reactor. The nanowires are then transported to an electrostatic precipitator where they are collected on a suitable substrate/medium.

The alloyed nanoparticles are transported further downstream into the growth zone, which is maintained at a higher temperature. The primary gas mixture (alloyed nanoparticles and Group III aerosol) enters a wider reaction space (~55 mm in diameter) in the growth zone. The primary gas mixture is confined to the centre of the reactor, shielded from the hot reactor wall by a sheath gas flow that enters and exits the growth zone via showerhead diffusers (Figure 5.3). The sheath gas flows both into and out of the growth zone is controlled by dedicated MFCs. The purpose of the showerhead diffuser is to ensure a laminar flow profile and to avoid turbulent mixing of gases in the growth zone. Gas flowing through a circular pipe has a parabolic velocity profile i.e., the velocity profile has a maximum at the centreline and minimum at the pipe walls. The sheath flow thereby also ensures a narrow effective gas velocity profile by functionally eliminating the slowest moving parts of the gas, close to the pipe wall. The group V precursors are usually hydrides with high enough vapor pressure and is mixed with the sheath gas which confines the primary flow. In this case, the precursor supply can be modulated with an MFC fitted to the supply line. Figure 5.3 is a detailed schematic of the Aerotaxy reactor as reported in Paper I. In the growth zone which is maintained at the growth temperature and at near atmospheric pressure, the alloyed particle is exposed to group V precursor flux which is mixed with the sheath gas. VLS growth occurs at a

rapid rate of  $\sim 1 \mu\text{m s}^{-1}$ , forming crystalline nanowires on the catalytic particles as explained in section 2.4.

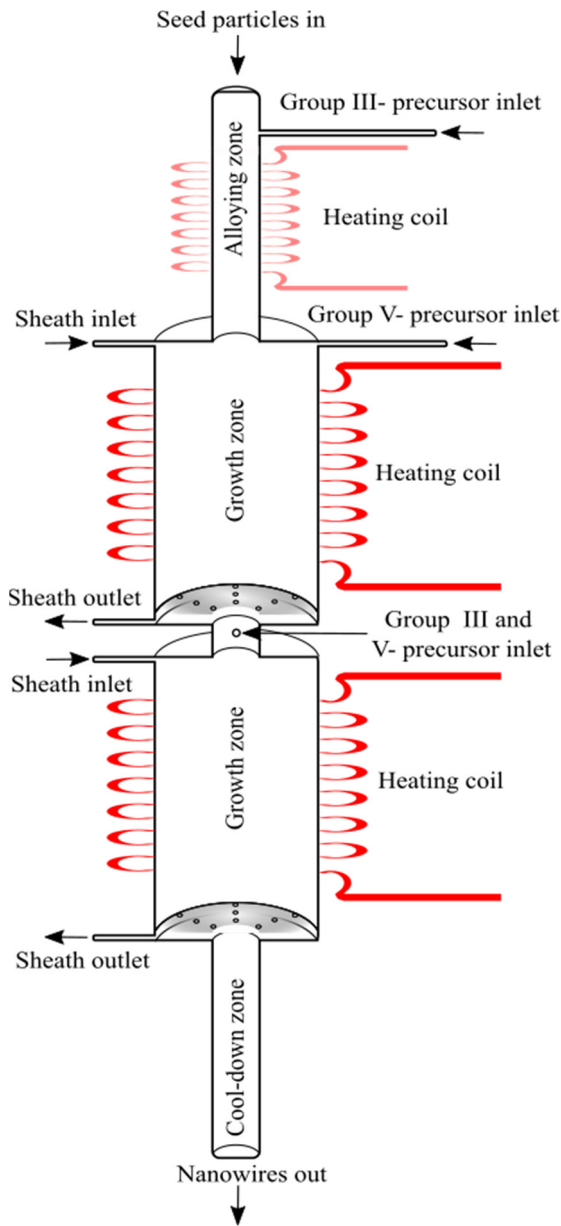


**Figure 5.3** Schematic of the Aerotaxy reactor, drawn approximately to scale; the heated zones have a total height of 750 mm. Au aerosol particles enter the reactor at the top through the alloying zone, travels down into the growth zone to mix with group III and V precursors, producing nanowires that exit from the cooling zone. Sheath gas enters and exits both growth zones through showerhead diffusers that ensure laminar flow. The gas transit time from top to bottom is around 6 s for standard flow and temperature settings. (Image adapted from Paper I)

Figure 5.3 shows an additional precursor inlet between two growth zones. This inlet enables supply of precursors for nanowire doping or for fabricating complex core-shell nanostructures. The nanowires along with the remainder of the undecomposed precursors flow out of the reactor through the cooling zone, which prevents turbulent mixing in the lower zone by gradually reducing the temperature of the aerosol. The outgoing flow from the AR, which now contains the nanowires and residual gases is also controlled by a dedicated MFC.

### *Nanowire Collection*

The outgoing flow cools rapidly as it exits the reactor and is directed to a Dixkens and Fissan type electrostatic precipitator (ESP)<sup>177,178</sup> placed inside a glove box for safety reasons. The charge carried by the size-selected gold aerosol is retained by the nanowires and as a result, the aerosol exiting the reactor also carries a known charge distribution. The ESP exploits this by efficiently capturing the nanowires based on their mobility in an applied electric field. The nanowires are usually deposited as a circular spot on the ESP. The nanowires are collected by placing a Si substrate covering the circular spot and it is not possible to collect all the wires with this method. The uncollected wires, along with residual gases are pumped out of the Aerotaxy instrument through a gas scrubber. Alternatively, to collect most of the wires, a filter with a pore size smaller than the nanowire's aerodynamic size can be fitted directly above the inlet of the ESP.

## 5.2 Aerotaxy Challenges

The main goal of this thesis is to demonstrate the capability of our synthetic approach to manufacture III-V nanowires on a large scale in a controlled manner. Over the past several decades, the potential of III-V nanowires for integration with planar Si technology is well established through several studies.<sup>44,179,180</sup> Despite the obvious potential, there is a substantial gap between the current nanowire research and functional devices that are available to the general public. Controlled nanowire doping and up-scalability of nanowire growth technology are reported to be the main drivers of this divide.<sup>181,182</sup> The challenges related to fundamental physics at the nanoscale and other device-related, application-specific obstacles must be overcome to make the nanowire platform a viable alternative to existing Si technology. Growth technology and tools like MOVPE and MBE have undergone numerous empirical design iterations since the early 1960s.<sup>183,184</sup> Research groups around the world are still studying those growth systems under various contexts. Aerotaxy is a young technology in comparison to those methods and is being actively pursued only at Lund, Sweden. Consequently, the Aerotaxy tool and technology poses some unique challenges to nanowire growth. They are summarized in the following sections.

### **5.2.1 Reactor Memory Effect**

Reactor memory effect is a common observation in non-optimized MOVPE processes, where growth materials are unintentionally deposited on the reactor walls.<sup>185,186</sup> Material deposited on the wall may desorb during growth and contaminate the growth environment. It is challenging to purge the Aerotaxy reactor of such memory effects. The III-V material diffusing away from the primary reactant flow inside the Aerotaxy reactor, gets deposited on the hot reactor wall. These wall-deposits serve as sites for further deposition of III-V material during subsequent growth experiments. When we attempted etching the wall deposits with HCl gas, it severely damaged the stainless-steel reactor. At present, post-growth cleaning is performed by blowing high-pressure nitrogen to blast away the wall-deposits and pump them out of the reactor. The reactor walls are inspected using an endoscope camera after the cleaning. The efficiency of this cleaning process drops with increasing reactor lifetime. The wall-deposits act as reservoirs of III-V material, discharging them back slowly when the reactor is heated again during the next growth cycle. This contaminates the growth environment and removing contaminants is challenging. In the study presented in Paper III, the As concentration measured in GaAsP nanowires is due to this reactor memory effect. Currently, the only effective alternative is to replace the contaminated parts until efficient cleaning methods are developed.

### **5.2.2 Reactor lifetime and conditioning**

A typical Aerotaxy reactor that is built to serve academic purposes has a lifespan of roughly one year. This estimate is based on limited practical experience with the Aerotaxy instrument. The life of a reactor can likely be extended by developing efficient cleaning protocols or by preventing wall deposition. A short lifetime of an instrument might be a limiting factor in an industrial production environment. But in an academic environment, this is challenging due to many possible differences in the growth environment that stems from the hardware. The growth environment is altered when a new reactor is installed and the growth parameter window may shift significantly. Each new installation requires a period of explorative conditioning to find the right parameters for nanowire growth. This is particularly challenging if there is a reactor-specific growth effect that is difficult to reproduce in different reactors.

Currently, it is hard to quantitatively estimate the reactor lifespan as it depends on the frequency and mode of operation. It is equally difficult to estimate the amount of conditioning required for a new installation. This poses obvious limitations in terms of reproducibility, and the reactors are not production-ready immediately after installation.

### 5.2.3 Software issues

It is unusual to consider software issues as a challenge for a nanowire growth technology. But the custom software used to control the current Aerotaxy hardware is a result of numerous design iterations. Unlike hardware products whose reliability is measured in terms of age and production quality, the software's reliability cannot be quantified from wear and tear. The software used is unreliable and led to extended maintenance periods during which the tool could not be used. This was personally challenging and delayed many experiments.

## 5.3 Nano Safety

Since the 1990's there has been a substantial interest to exploit nanomaterials for various consumer applications. It is possible that materials seemingly non-toxic in bulk form may exhibit very different properties at the nanoscale. As a result, there is an increasing concern expressed regarding the impact of nanomaterials on human health and the environment.<sup>187,188</sup> Nano safety deals with the evaluation of risks to human health and the environment from engineered nanomaterials.

According to the European regulation on the Registration, Evaluation, Authorisation and Restriction of Chemicals (REACH, EC No 1907/2006),<sup>189</sup> risk evaluation of nanomaterials should include investigation of the alleged (i) toxic effects (ii) possible level of exposure and (iii) risk classification. Despite the enormous efforts in risk evaluation, the health effects of nanomaterial exposure are still under debate and some studies report contradictory findings.<sup>190</sup> Studies show that the manufacturing method might influence the nanomaterial's toxicity, which means the biological response varies depending on the method of fabrication.<sup>191</sup> Apart from the method of fabrication, the morphological and physiochemical properties of the nanomaterial like size, agglomeration, surface chemistry, number and mass concentrations play a significant role in the toxicological response of the nanomaterial.<sup>191,192</sup> But, we still lack conclusive data establishing the toxicological effects of engineered nanomaterials.

In order to design appropriate exposure prevention strategies, it is important to understand the manufacturing process and possible routes of exposure. The advent of engineered nanomaterials in consumer products has increased the likelihood of human exposure throughout the life cycle of the product. Exposure in the workplace will be the primary point of contact between humans and engineered nanomaterials. In particular, a high-throughput nanomaterial production environment increases the probability of human exposure. For example, cleaning and other maintenance activities in Aerotaxy dramatically increases the likelihood of nanomaterial exposure. Given that the most likely route of nanomaterial of exposure is through

inhalation of airborne particles, the gas phase Aerotaxy method raises major concern in terms of safety.

### 5.3.1 Exposure in the workplace

At present, the best method to evaluate the exposure to engineered nanomaterials at a workplace is by using the nanoparticle emission assessment technique (NEAT).<sup>193</sup> NEAT assessment is based on detection of airborne nanomaterials using portable monitoring instruments containing filters which enable offline characterization of collected nanomaterial. Paper VI discusses the results of an intervention study conducted in an Aerotaxy production environment using the NEAT assessment method. The intervention study measured exposure during tasks like nanomaterial production, manual reactor cleaning, replacement of outflow particle filters and other related daily activities. The study was conducted before and after up-scaling the production capacity of an industrial version of the Aerotaxy instrument. Filter samples and time-resolved direct measurements of airborne nanomaterials were performed during several daily tasks to characterize workplace exposure. Collection on filters is carried out by pumping air through a filter with a known pore size. Both types of measurements were performed in four different measuring zones (*emission zone*, *personal breathing zone*, *background zone* and *general ventilation*) around a human subject. The *emission zone* is closest to a suspected emission source while the *personal breathing zone* is around the nose and mouth of a human subject. A handheld particle counter was used to measure the particle number concentration in the *personal breathing zone*. In addition to filter sampling, adhesive tapes were used to collect nanomaterials deposited on relevant surfaces. The tape and filter samples are analysed post-collection using SEM XEDS to evaluate the size, composition and distribution of the nanomaterial.

The study indicates that the probability for potential nanomaterial exposure is high during cleaning and maintenance procedures and not during the actual manufacturing process. The results agree with our expectations as Aerotaxy production occurs inside a leak tight environment and the leak rate of the tool is measured after each maintenance cycle. Following this study, in order to mitigate the risk of exposure during reactor cleaning, a blow-out kit was attached to our Aerotaxy setup as an engineering control. Activities like cleaning the DMA exhibit clear signs of particle emission both in the *emission* and *background zone*. This indicates that cleaning increases the potential risk of exposure to the user and others present in the vicinity. After collection, SEM-XEDS characterization of the filter and surface samples detected gold nanoparticles indicating that the emission originated from the cleaning task. This is particularly important because in our current Aerotaxy setup, the *emission* and *personal breathing zones* significantly overlap during cleaning tasks. Post-production activities like sonication and sample processing also increased the particle emission, indicating additional modes of

exposure. Surface contamination of III-V material was limited to the reactor enclosure, and the risk of exposure is therefore limited to the operator performing the cleaning tasks.

Though the toxicity of semiconductor nanowires is not well understood, it is important to practice caution and to install proper engineering controls to mitigate the exposure risk. The current academic version of the Aerotaxy instrument is operated by following strict safety protocols while using suitable personal protection equipment and portable monitoring devices. However, automating maintenance activities that require opening the instrument like cleaning the APG might reduce the risk of potential exposure.

## 6 Concluding remarks

Having spent the past five years trying to understand Aerotaxy growth, I would like to take a step back and share few thoughts about the technology and its potential.

I am hopeful about the prospects for III-V semiconductor nanowires as building blocks of future electronic and photonic systems. However, the nanowire platform faces a myriad of challenges that are either related to growth or specific to a particular application. Succumbing to these challenges will lead the nanowire platform into a technological cul-de-sac. Despite the many challenges, my optimism stems from the continuous progress in our fundamental understanding of semiconductor nanowires. Currently, there are many start-ups, both local and global, trying to commercialize some of the beneficial functionalities of nanowires. Sol Voltaics AB was one of the most promising start-ups of yesteryear, which attempted to commercialize Aerotaxy nanowire synthesis for solar cell applications. Aligned Bio, Glō, NordAmps and Hexagem are few other tech start-ups working in close collaboration with academia to bring nanowire-based devices to the market. The growing number of such tech start-ups or my optimism based on experience may be insufficient to argue the potential of semiconductor nanowires. Regardless of my belief, the nanowire research community is convinced that the beneficial properties found at the nanoscale are too exciting to be abandoned due to the many challenges or concerns over safety.

The experimental results in this thesis clearly demonstrate Aerotaxy as a suitable method for high-throughput nanowire fabrication in a controlled fashion. In any experimental work, the results obtained are typically non-self-explanatory. Often, a suitable theory from available literature is adopted to add reliability and context to the results. And it is very easy to accept a theory or model that agrees well with our experimental observation, circumventing the required critical consideration. As an example, the description of nanowire branching under Section 4.7 hypothesised that branching might be induced after the primary seed particle ruptures. While this description is grounded in literature, the similarity might be a coincidence. Since it is not possible to directly observe such phenomena in Aerotaxy, it is difficult to experimentally verify our hypothesis. Therefore, we settle for the best available description in literature as a plausible explanation.



One must also consider the statistical significance of the results in experimental research. Often, only a small set of samples is characterized either due to lack of resources or time in academia. Hence, there is always a chance of accepting generalized conclusions from a small set of data. In addition, microscopy characterization and single nanowire testing only probe a miniscule sample volume, and producing results of statistical significance with such techniques is almost a herculean task. An example would be doping evaluation of GaAs nanowires using electrical methods. The electrical measurements were performed on single nanowire devices fabricated carefully on Si chips. Drawing generalized conclusions just by testing a few nanowire devices is obviously undesirable. For this reason, the electrical characterization was supplemented with PL measurements performed on nanowire ensembles. Undoubtedly, Aerotaxy can produce vast quantities of semiconductor nanowires; I can safely assert that it is currently impossible to characterize each single nanowire.

Despite several reports about *in situ* nanowire doping in substrate-based growth, precise control and fundamental understanding of the doping mechanism is still a work in progress. The lack of simple and reliable measurement methods is a major reason for the slow progress in basic understanding of nanowire doping. The measured carrier concentration in doped Aerotaxy nanowires points us to the conclusion that the nanowires are degenerately doped even at low dopant injection. As a researcher, I am tempted to conclude that further studies are required to achieve controlled doping in Aerotaxy. But our observations clearly indicate that it is difficult to achieve low and intermediate doping levels for both dopant polarities. Aerotaxy nanowires may not be suitable for devices or applications that require low to moderate doping levels. Doping of the ternary GaAsP material system is more complicated and the evaluation results are inconclusive at best.

One key difference between the substrate-based growth and Aerotaxy is that the nanowires land randomly on to the collection surface. For device related applications, billions of such nanowires must be aligned so that they can be contacted electrically. Randomly oriented wires cannot be used for most device applications. The tech start-up Sol Voltaics, during its peak expansion, developed an efficient method to align the Aerotaxy grown nanowires so they can be incorporated into functional devices. This nanowire alignment technology is now used by Aligned Bio to align and fabricate nanowire devices for bio-sensing applications. I am convinced about the commercial viability of Aerotaxy synthesis, especially in combination with the alignment technology.

It is difficult to envision a future in which gold catalysed III-V nanowires emerge as ideal candidates for phasing out Si. Recent development in Aerotaxy demonstrates the possibility to achieve GaAs growth using Ga, Au-Ag and Ag catalytic particles. Since the particles generated by the APG are directly fed to the growth system, the probability of oxidation or cross-contamination is greatly

reduced compared to traditional systems, where the particles are usually exposed to the ambient atmosphere during transfer between the deposition and growth systems.

Preliminary results from CFD modelling of the Aerotaxy process agree well with some of the experimental observations. Continued efforts are necessary to improve the model and develop the fundamental understanding of the Aerotaxy process. Simulations are often based on highly idealized scenarios and consequently the results obtained may be far removed from reality. Simply, complex thermodynamic interactions in a physical system cannot be completely reflected in a model, and simplifications are important. So, one must be careful while designing and interpreting the results from a model.

Substrate-based growth techniques like MOVPE are undeniably advanced due to decades of world-wide research and development. The controllability and overall production quality of nanowires in Aerotaxy strongly indicate that Aerotaxy is still at an early stage of its developmental journey. Due to the fact that we are the only group that is involved in developing Aerotaxy, I expect the progress to be slow. Each nanowire that is fabricated in Aerotaxy is likely to experience slightly varying growth conditions as it traverses the growth system. As a result, there is substantial spread in measured nanowire properties. The continuous gas-phase design of the Aerotaxy instrument will likely hinder any attempts to reduce this spread.

Despite some obvious limitations, I believe that the Aerotaxy grown nanowires show tremendous potential, especially due to their low production cost. Skimming through vast amount of nanowire reports, I find a significant number of reports that claim novelty through a new method of fabrication or a novel functionality. But very few reports exist in device/application front due to possible engineering optimization issues. This indicates an obvious disconnect between the device front and fundamental nanowire research. Development of simple and robust characterization tools might expedite the progress of the semiconductor nanowires. Rapid, high-throughput characterization techniques may be monumental in commercializing nanowires. At this point, I think it is too early to assert the potential for commercial success of Aerotaxy technology.



# References

1. Bardeen, J. & Brattain, W. H. The transistor, a semi-conductor triode. *Physical Review* vol. 74 230–231 (1948).
2. *World Energy Outlook 2020*. (OECD, 2020).
3. Ahmad, T. & Zhang, D. A critical review of comparative global historical energy consumption and future demand: The story told so far. *Energy Reports* vol. 6 1973–1991 (2020).
4. Adib, R. *et al. Renewables 2020 Global Status Report*. <https://www.ren21.net/reports/global-status-report/> (2020).
5. Fischer, M., Woodhouse, M., Herritsch, S. & Trube, J. *International Technology Roadmap for Photovoltaics (ITPV)*. <http://itrpv.vdma.org/documents/27094228/29066965/Readiness0ITRPV02020/2a8588fd-3ac2-d21d-2f83-b8f96be03e51> (2020).
6. Von Behren, J., Van Buuren, T., Zacharias, M., Chimowitz, E. H. & Fauchet, P. M. Quantum confinement in nanoscale silicon: The correlation of size with bandgap and luminescence. *Solid State Commun.* **105**, 317–322 (1998).
7. Garnett, E. C., Brongersma, M. L., Cui, Y. & McGehee, M. D. Nanowire Solar Cells. *Annu. Rev. Mater. Res.* **41**, 269–295 (2011).
8. Heurlin, M. *et al.* Continuous gas-phase synthesis of nanowires with tunable properties. *Nature* **492**, 90–94 (2012).
9. Cui, Y. Functional Nanoscale Electronic Devices Assembled Using Silicon Nanowire Building Blocks. *Science* **291**, 851–853 (2002).
10. Wallentin, J. *et al.* InP Nanowire Array Solar Cells Achieving 13.8% Efficiency by Exceeding the Ray Optics Limit. *Science* **339**, 1057–1060 (2013).
11. Arnold, M. S., Avouris, P., Pan, Z. W. & Wang, Z. L. Field-effect transistors based on single semiconducting oxide nanobelts. *J. Phys. Chem. B* **107**, 659–663 (2003).
12. Huang, M. H. Room-Temperature Ultraviolet Nanowire Nanolasers. *Science* **292**, 1897–1899 (2001).

13. Wolfstetter, A. *et al.* Comparison of the top-down and bottom-up approach to fabricate nanowire-based Silicon/Germanium heterostructures. *Thin Solid Films* **518**, 2555–2561 (2010).
14. Hobbs, R. G., Petkov, N. & Holmes, J. D. Semiconductor nanowire fabrication by bottom-up and top-down paradigms. *Chem. Mater.* **24**, 1975–1991 (2012).
15. Hiruma, K. *et al.* Growth and optical properties of nanometer-scale GaAs and InAs whiskers. *J. Appl. Phys.* **77**, 447–462 (1995).
16. Thompson, A. G. MOCVD technology for semiconductors. *Mater. Lett.* **30**, 255–263 (1997).
17. Dauelsberg, M., Thrush, E. J., Schineller, B. & Kaeppler, J. *Technology of MOVPE Production Tools. Optoelectronic Devices: III Nitrides* (Elsevier B.V., 2005).
18. Pellegrino, S. & Tarricone, L. MOVPE growth and study of InP-based materials: opportunities and challenges. *Mater. Chem. Phys.* **66**, 189–196 (2000).
19. Samuelson, L., Magnusson, M. H., Deppert, K. & Heurlin, M. Gas-phase synthesis method for forming semiconductor nanowires. US PATENT 9447520B2. vol. 87 021001 (2016).
20. Wagner, R. S. & Ellis, W. C. Vapor-liquid-solid mechanism of single crystal growth. *Appl. Phys. Lett.* **4**, 89–90 (1964).
21. Memmert, U. & Yu, M. L. Pyrolysis of trimethylgallium on GaAs(100) surface as. *Appl. Phys. Lett* **56**, 1990 (1990).
22. Assali, S. *et al.* Exploring Crystal Phase Switching in GaP Nanowires. *Nano Lett.* **15**, 8062–8069 (2015).
23. Tornberg, M. *et al.* Kinetics of Au-Ga Droplet Mediated Decomposition of GaAs Nanowires. *Nano Lett.* **19**, 3498–3504 (2019).
24. Dick, K. A. *et al.* Synthesis of branched ‘nanotrees’ by controlled seeding of multiple branching events. *Nat. Mater.* **3**, 380–384 (2004).
25. Manna, L., Milliron, D. J., Meisel, A., Scher, E. C. & Alivisatos, A. P. Controlled growth of tetrapod-branched inorganic nanocrystals. *Nature Materials* vol. 2 382–385 (2003).
26. Zhang, Y. *et al.* Droplet manipulation and horizontal growth of high-quality self-catalysed GaAsP nanowires. *Nano Today* **34**, 100921 (2020).
27. Cheng, C. & Fan, H. J. *Branched nanowires: Synthesis and energy applications.* *Nano Today* vol. 7 327–343 (Elsevier, 2012).

28. Jun, K. & Jacobson, J. M. Programmable growth of branched silicon nanowires using a focused ion beam. *Nano Lett.* **10**, 2777–2782 (2010).
29. Andrews, D. H. The Collected Works of J. Willard Gibbs. Two volumes. *J. Chem. Educ.* **6**, 591 (1929).
30. Mayer, J. E. & Streeter, S. F. Phase transitions. *J. Chem. Phys.* **7**, 1019–1025 (1939).
31. Frenkel, J. Statistical theory of condensation phenomena [1]. *The Journal of Chemical Physics* vol. 7 200–201 (1939).
32. Job, G. & Herrmann, F. Chemical potential - A quantity in search of recognition. *Eur. J. Phys.* **27**, 353–371 (2006).
33. DeHoff, R. *Thermodynamics in Materials Science - 2nd Edition - Robert - R.* (CRC press, 2006).
34. Papon, P., Leblond, J. & Meijer, P. H. E. *The physics of phase transitions: Concepts and applications. The Physics of Phase Transitions: Concepts and Applications* (Springer Berlin Heidelberg, 2006).
35. Dubrovskii, V. G. Theory of VLS growth of compound semiconductors. in *Semiconductors and Semimetals* vol. 93 1–78 (Academic Press Inc., 2015).
36. Markov, I. V. *Crystal Growth for Beginners. Crystal Growth for Beginners* (WORLD SCIENTIFIC, 2003).
37. Nanev, C. N. Theory of Nucleation. in *Handbook of Crystal Growth: Second Edition* vol. 1 315–358 (Elsevier Inc., 2015).
38. Karthika, S., Radhakrishnan, T. K. & Kalaichelvi, P. A Review of Classical and Nonclassical Nucleation Theories. *Cryst. Growth Des.* **16**, 6663–6681 (2016).
39. Volmer, M. Kinetik der phasenbildung. (1939).
40. Vekilov, P. G. Nucleation. *Cryst. Growth Des.* **10**, 5007–5019 (2010).
41. Newman, N. & Vahidi, M. Kinetic Processes in Vapor Phase Epitaxy. in *Handbook of Crystal Growth: Thin Films and Epitaxy: Second Edition* vol. 3 835–868 (Elsevier Inc., 2015).
42. Rubbo, M. Basic concepts in crystal growth. *Cryst. Res. Technol.* **48**, 676–705 (2013).
43. Dayeh, S. A., Yu, E. T. & Wang, D. Surface diffusion and substrate-nanowire adatom exchange in inas nanowire growth. *Nano Lett.* **9**, 1967–1972 (2009).
44. Mårtensson, T. *et al.* Epitaxial III–V Nanowires on Silicon. *Nano Lett.* **4**,

1987–1990 (2004).

45. Noor Mohammad, S. For nanowire growth, vapor-solid-solid (vapor-solid) mechanism is actually vapor-quasisolid-solid (vapor-quasiliquid-solid) mechanism. *J. Chem. Phys.* **131**, (2009).
46. Thombare, S. V., Marshall, A. F. & McIntyre, P. C. Kinetics of germanium nanowire growth by the vapor-solid-solid mechanism with a Ni-based catalyst. *APL Mater.* **1**, 061101 (2013).
47. Ambrosini, S., Fanetti, M., Grillo, V., Franciosi, A. & Rubini, S. Vapor-liquid-solid and vapor-solid growth of self-catalyzed GaAs nanowires. *AIP Adv.* **1**, (2011).
48. Fukui, T., Ando, S., Tokura, Y. & Toriyama, T. GaAs tetrahedral quantum dot structures fabricated using selective area metalorganic chemical vapor deposition. *Appl. Phys. Lett.* **58**, 2018–2020 (1991).
49. Sato, T., Motohisa, J., Noborisaka, J., Hara, S. & Fukui, T. Growth of InGaAs nanowires by selective-area metalorganic vapor phase epitaxy. *J. Cryst. Growth* **310**, 2359–2364 (2008).
50. Tomioka, K. *et al.* Selective-area growth of III-V nanowires and their applications. *Journal of Materials Research* vol. 26 2127–2141 (2011).
51. Regolin, I. *et al.* GaAs whiskers grown by metal-organic vapor-phase epitaxy using Fe nanoparticles. *J. Appl. Phys.* **101**, 1–5 (2007).
52. Hallberg, R. T., Lehmann, S., Messing, M. E. & Dick, K. A. Palladium seeded GaAs nanowires. *J. Mater. Res.* **31**, 175–185 (2016).
53. Kodambaka, S., Tersoff, J., Reuter, M. C. & Ross, F. M. Germanium nanowire growth below the eutectic temperature. *Science* **316**, 729–732 (2007).
54. Pohl, U. W. *Methods of Epitaxy.* in 275–313 (Springer, Berlin, Heidelberg, 2013).
55. Dick, K. A. *et al.* Failure of the vapor-liquid-solid mechanism in au-assisted MOVPE growth of InAs nanowires. *Nano Lett.* **5**, 761–764 (2005).
56. Dubrovskii, V. G. Influence of the group v element on the chemical potential and crystal structure of Au-catalyzed III-V nanowires. *Appl. Phys. Lett.* **104**, (2014).
57. Otnes, G. *et al.* Strategies to obtain pattern fidelity in nanowire growth from large-area surfaces patterned using nanoimprint lithography. *Nano Res.* **9**, 2852–2861 (2016).
58. Paiman, S. *et al.* Growth temperature and V/III ratio effects on the

- morphology and crystal structure of InP nanowires. *J. Phys. D. Appl. Phys.* **43**, 445402 (2010).
59. Lehmann, S., Jacobsson, D. & Dick, K. A. Crystal phase control in GaAs nanowires: Opposing trends in the Ga- and As-limited growth regimes. *Nanotechnology* **26**, 301001 (2015).
  60. Wacaser, B. A. *et al.* Preferential Interface Nucleation: An Expansion of the VLS Growth Mechanism for Nanowires. *Adv. Mater.* **21**, 153–165 (2009).
  61. Dasgupta, N. P. *et al.* 25th Anniversary Article: Semiconductor Nanowires - Synthesis, Characterization, and Applications. *Adv. Mater.* **26**, 2137–2184 (2014).
  62. Wen, C. Y. *et al.* Periodically changing morphology of the growth interface in Si, Ge, and GaP nanowires. *Phys. Rev. Lett.* **107**, 025503 (2011).
  63. Jacobsson, D. *et al.* Interface dynamics and crystal phase switching in GaAs nanowires. *Nature* **531**, 317–322 (2016).
  64. Borgström, M. T., Immink, G., Ketelaars, B., Algra, R. & Bakkers, E. P. A. M. Synergetic nanowire growth. *Nat. Nanotechnol.* **2**, 541–544 (2007).
  65. Dubrovskii, V. Vapor–Liquid–Solid Growth of Nanowires. in 275–395 (Springer, Berlin, Heidelberg, 2014).
  66. Ramdani, M. R., Harmand, J. C., Glas, F., Patriarche, G. & Travers, L. Arsenic Pathways in Self-Catalyzed Growth of GaAs Nanowires. *Cryst. Growth Des.* **13**, 91–96 (2013).
  67. Dubrovskii, V. G. *et al.* Diffusion-induced growth of GaAs nanowhiskers during molecular beam epitaxy: Theory and experiment. *Phys. Rev. B - Condens. Matter Mater. Phys.* **71**, (2005).
  68. Jensen, L. E. *et al.* Role of surface diffusion in chemical beam epitaxy of InAs nanowires. *Nano Lett.* **4**, 1961–1964 (2004).
  69. Dubrovskii, V. G. *et al.* Gibbs-Thomson and diffusion-induced contributions to the growth rate of Si, InP, and GaAs nanowires. *Phys. Rev. B* **79**, 205316 (2009).
  70. Johansson, J., Svensson, C. P. T., Mårtensson, T., Samuelson, L. & Seifert, W. Mass Transport Model for Semiconductor Nanowire Growth. *J. Phys. Chem. B* **109**, 13567–13571 (2005).
  71. Dhaka, V. *et al.* High Quality GaAs Nanowires Grown on Glass Substrates. *Nano Lett* **12**, 2021 (2012).
  72. McAlpine, M. C. *et al.* High-Performance Nanowire Electronics and



- Photonics on Glass and Plastic Substrates. *Nano Lett.* **3**, 1531–1535 (2003).
73. McIntyre, P. C. & Fontcuberta i Morral, A. Semiconductor nanowires: to grow or not to grow? *Materials Today Nano* vol. 9 100058 (2020).
  74. Schwarz, K. W. & Tersoff, J. Multiplicity of steady modes of nanowire growth. *Nano Lett.* **12**, 1329–1332 (2012).
  75. Dao, K. A., Dao, D. K., Nguyen, T. D., Phan, A. T. & Do, H. M. The effects of Au surface diffusion to formation of Au droplets/clusters and nanowire growth on GaAs substrate using VLS method. *J. Mater. Sci. Mater. Electron.* **23**, 2065–2074 (2012).
  76. Deppert, K. & Samuelson, L. Self-limiting transformation of monodisperse Ga droplets into GaAs nanocrystals. *Appl. Phys. Lett.* **68**, 1409–1411 (1996).
  77. Borgström, M., Deppert, K., Samuelson, L. & Seifert, W. Size- and shape-controlled GaAs nano-whiskers grown by MOVPE: A growth study. *J. Cryst. Growth* **260**, 18–22 (2004).
  78. Hudson, J. G. Cloud condensation nuclei. *J. Appl. Meteorol.* **32**, 596–607 (1993).
  79. Whiticar, A. M., Mårtensson, E. K., Nygård, J., Dick, K. A. & Bolinsson, J. Annealing of Au, Ag and Au-Ag alloy nanoparticle arrays on GaAs (100) and (111)B. *Nanotechnology* **28**, 205702 (2017).
  80. Seinfeld, J. H. & Pandis, S. N. *Atmospheric chemistry and physics: from air pollution to climate change*. (John Wiley & Sons, Inc., 2006).
  81. Liao, H. G. *et al.* Facet development during platinum nanocube growth. *Science* **345**, 916–919 (2014).
  82. Tao, A. R., Habas, S. & Yang, P. Shape Control of Colloidal Metal Nanocrystals. *Small* **4**, 310–325 (2008).
  83. Xia, Y., Xiong, Y., Lim, B. & Skrabalak, S. E. Shape-controlled synthesis of metal nanocrystals: Simple chemistry meets complex physics? *Angewandte Chemie - International Edition* vol. 48 60–103 (2009).
  84. Tian, N., Zhou, Z. Y., Sun, S. G., Ding, Y. & Zhong, L. W. Synthesis of tetrahedral platinum nanocrystals with high-index facets and high electro-oxidation activity. *Science* **316**, 732–735 (2007).
  85. Givargizov, E. I. Fundamental aspects of VLS growth. *J. Cryst. Growth* **31**, 20–30 (1975).
  86. Johansson, J. & Magnusson, M. H. From diffusion limited to incorporation limited growth of nanowires. *J. Cryst. Growth* **525**, 125192 (2019).

87. Heurlin, M., Anttu, N., Camus, C., Samuelson, L. & Borgström, M. T. In situ characterization of nanowire dimensions and growth dynamics by optical reflectance. *Nano Lett.* **15**, 3597–3602 (2015).
88. Kumar, C. S. S. R. *In-situ Characterization Techniques for Nanomaterials*. (Springer-Verlag Berlin Heidelberg, 2018).
89. Kim, S. H., Mulholland, G. W. & Zachariah, M. R. Understanding ion-mobility and transport properties of aerosol nanowires. *J. Aerosol Sci.* **38**, 823–842 (2007).
90. Kim, S. H. & Zachariah, M. R. In-flight size classification of carbon nanotubes by gas phase electrophoresis. *Nanotechnology* **16**, 2149–2152 (2005).
91. Carlino, E. TEM for characterization of semiconductor nanomaterials. in *Transmission Electron Microscopy Characterization of Nanomaterials* 89–138 (Springer Berlin Heidelberg, 2014).
92. Ul-Hamid, A. *A Beginners' Guide to Scanning Electron Microscopy. A Beginners' Guide to Scanning Electron Microscopy* (Springer International Publishing, 2018).
93. Newbury, D. E. & Myklebust, R. L. Monte Carlo electron trajectory simulation of beam spreading in thin foil targets. *Ultramicroscopy* **3**, 391–395 (1978).
94. Williams, D. B. & Carter, C. B. *Transmission Electron Microscopy. Transmission Electron Microscopy: A Textbook for Materials Science* (Springer US, 2009).
95. Yu, P. Y. & Cardona, M. Optical Properties I. in *Fundamentals of Semiconductors - Physics and Materials Properties* 243–344 (Springer, 2010).
96. Grundmann, M. *The physics of semiconductors: An introduction including devices and nanophysics*. (Springer Berlin Heidelberg, 2006).
97. Bugajski, M. & Lewandowski, W. Concentration-dependent absorption and photoluminescence of n-type InP. *J. Appl. Phys.* **57**, 521–530 (1985).
98. Lindgren, D. *et al.* Study of carrier concentration in single InP nanowires by luminescence and Hall measurements. *Nanotechnology* **26**, 045705 (2015).
99. Haraguchi, K., Katsuyama, T., Hiruma, K. & Ogawa, K. GaAs p-n junction formed in quantum wire crystals. *Appl. Phys. Lett.* **60**, 745–747 (1992).
100. Wallentin, J. & Borgström, M. T. Doping of semiconductor nanowires. *J. Mater. Res.* **26**, 2142–2156 (2011).

101. Cui, Y., Duan, X., Hu, J. & Lieber, C. M. Doping and electrical transport in silicon nanowires. *J. Phys. Chem. B* **104**, 5215–5216 (2000).
102. Lew, K. K. *et al.* Structural and electrical properties of trimethylboron-doped silicon nanowires. *Appl. Phys. Lett.* **85**, 3101–3103 (2004).
103. Perea, D. E. *et al.* Direct measurement of dopant distribution in an individual vapour-liquid-solid nanowire. *Nat. Nanotechnol.* (2009).
104. Wunnicke, O. Gate capacitance of back-gated nanowire field-effect transistors. *Appl. Phys. Lett.* **89**, 083102 (2006).
105. Sze, S. M. & Irvin, J. C. Resistivity, mobility and impurity levels in GaAs, Ge, and Si at 300°K. *Solid State Electron.* **11**, 599–602 (1968).
106. Wu, Y. & Yang, P. Direct Observation of Vapor–Liquid–Solid Nanowire Growth. *J. Am. Chem. Soc.* **123**, 3165–3166 (2001).
107. Yang, P., Yan, R. & Fardy, M. Semiconductor nanowire: Whats Next? *Nano Lett.* **10**, 1529–1536 (2010).
108. Ye, S., Rathmell, A. R., Chen, Z., Stewart, I. E. & Wiley, B. J. Metal Nanowire Networks: The Next Generation of Transparent Conductors. *Adv. Mater.* **26**, 6670–6687 (2014).
109. Im, J. H. *et al.* Nanowire perovskite solar cell. *Nano Lett.* **15**, 2120–2126 (2015).
110. Björk, M. T. *et al.* One-dimensional heterostructures in semiconductor nanowhiskers. *Appl. Phys. Lett.* **80**, 1058–1060 (2002).
111. Wang, N., Cai, Y. & Zhang, R. Q. Growth of nanowires. *Materials Science and Engineering R: Reports* vol. 60 1–51 (2008).
112. Joyce, H. J. *et al.* III–V semiconductor nanowires for optoelectronic device applications. *Prog. Quantum Electron.* **35**, 23–75 (2011).
113. Li, J., Wang, D. & LaPierre, R. *Advances in III-V semiconductor nanowires and nanodevices.* (Bentham Science Publishers Ltd., 2011).
114. Fang, M. *et al.* III-V nanowires: Synthesis, property manipulations, and device applications. *Journal of Nanomaterials* vol. 2014 (2014).
115. Yao, M. *et al.* Tandem Solar Cells Using GaAs Nanowires on Si: Design, Fabrication, and Observation of Voltage Addition. *Nano Lett.* **15**, 7217–7224 (2015).
116. Barrigón, E. *et al.* GaAs Nanowire pn-Junctions Produced by Low-Cost and High-Throughput Aerotaxy. *Nano Lett.* **18**, 1088–1092 (2018).
117. Lieber, C. M. & Wang, Z. L. Nanowires As Building Blocks for Bottom-

- Up Nanotechnology Functional Nanowires. **32**, (2007).
118. Cui, Y., Duan, X., Huang, Y. & Lieber, C. M. Nanowires as Building Blocks for Nanoscale Science and Technology. in *Nanowires and Nanobelts* 3–68 (Springer US, 2003).
  119. Hu, J., Odom, T. W. & Lieber, C. M. Chemistry and physics in one dimension: Synthesis and properties of nanowires and nanotubes. *Accounts of Chemical Research* vol. 32 435–445 (1999).
  120. Dick, K. A., Deppert, K., Samuelson, L., Wallenberg, L. R. & Ross, F. M. Control of GaP and GaAs nanowire morphology through particle and substrate chemical modification. *Nano Lett.* **8**, 4087–4091 (2008).
  121. Güniat, L., Caroff, P. & Fontcuberta I Morral, A. *Vapor Phase Growth of Semiconductor Nanowires: Key Developments and Open Questions*. *Chemical Reviews* vol. 119 8958–8971 (American Chemical Society, 2019).
  122. Dick, K. A., Deppert, K., Samuelson, L. & Seifert, W. Optimization of Au-assisted InAs nanowires grown by MOVPE. *J. Cryst. Growth* **297**, 326–333 (2006).
  123. Seifert, W. *et al.* Growth of one-dimensional nanostructures in MOVPE. **272**, 211–220 (2004).
  124. Gudiksen, M. S., Wang, J. & Lieber, C. M. Synthetic control of the diameter and length of single crystal semiconductor nanowires. *J. Phys. Chem. B* **105**, 4062–4064 (2001).
  125. Plante, M. C. & Lapierre, R. R. Analytical description of the metal-assisted growth of III-V nanowires: Axial and radial growths. *J. Appl. Phys.* **105**, 114304 (2009).
  126. Dubrovskii, V. G. *et al.* Shape modification of III-V nanowires: The role of nucleation on sidewalls. *Phys. Rev. E - Stat. Nonlinear, Soft Matter Phys.* **77**, 031606 (2008).
  127. Persson, A. I., Fröberg, L. E., Jeppesen, S., Björk, M. T. & Samuelson, L. Surface diffusion effects on growth of nanowires by chemical beam epitaxy. *J. Appl. Phys.* **101**, 034313 (2007).
  128. Hiruma, K. *et al.* GaAs free-standing quantum-size wires. *J. Appl. Phys.* **74**, 3162 (1993).
  129. Dick, K. A. *et al.* Control of III-V nanowire crystal structure by growth parameter tuning. *Semicond. Sci. Technol.* **25**, (2010).
  130. Wacaser, B. A., Deppert, K., Karlsson, L. S., Samuelson, L. & Seifert, W. Growth and characterization of defect free GaAs nanowires. in *Journal of*

*Crystal Growth* vol. 287 504–508 (North-Holland, 2006).

131. Hallberg, R. T., Messing, M. E. & Dick, K. A. Nanowire morphology and particle phase control by tuning the in concentration of the foreign metal nanoparticle. *Nanotechnology* **30**, (2019).
132. Glas, F., Harmand, J. C. & Patriarche, G. Why does wurtzite form in nanowires of III-V zinc blende semiconductors? *Phys. Rev. Lett.* **99**, 146101 (2007).
133. Mårtensson, E. K., Lehmann, S., Dick, K. A. & Johansson, J. Effect of Radius on Crystal Structure Selection in III-V Nanowire Growth. *Cryst. Growth Des.* **20**, 5373–5379 (2020).
134. Shtrikman, H. *et al.* Method for suppression of stacking faults in wurtzite III-V nanowires. *Nano Lett.* **9**, 1506–1510 (2009).
135. Algra, R. E. *et al.* Twinning superlattices in indium phosphide nanowires. *Nature* **456**, 369–372 (2008).
136. Caroff, P. *et al.* Controlled polytypic and twin-plane superlattices in III-V nanowires. *Nat. Nanotechnol.* **4**, 50–55 (2009).
137. Joyce, H. J., Wong-Leung, J., Gao, Q., Hoe Tan, H. & Jagadish, C. Phase perfection in zinc blende and wurtzite III- V nanowires using basic growth parameters. *Nano Lett.* **10**, 908–915 (2010).
138. Moore, A. L., Saha, S. K., Prasher, R. S. & Shi, L. Phonon backscattering and thermal conductivity suppression in sawtooth nanowires. *Appl. Phys. Lett.* **93**, 083112 (2008).
139. Björk, M. T. *et al.* One-dimensional Steeplechase for Electrons Realized. *Nano Lett.* **2**, 87–89 (2002).
140. Ghasemi, M., Leshchenko, E. D. & Johansson, J. Assembling your nanowire: An overview of composition tuning in ternary III-V nanowires. *Nanotechnology* vol. 32 72001 (2021).
141. Yang, F. *et al.* Zn-doping of GaAs nanowires grown by Aerotaxy. *J. Cryst. Growth* **414**, 181–186 (2015).
142. Gutsche, C. *et al.* Controllable p -type doping of GaAs nanowires during vapor-liquid-solid growth. *J. Appl. Phys.* **105**, 024305 (2009).
143. Metaferia, W. *et al.* GaAsP Nanowires Grown by Aerotaxy. *Nano Lett.* **16**, 5701–5707 (2016).
144. Olego, D. & Cardona, M. Photoluminescence in heavily doped GaAs. I. Temperature and hole-concentration dependence. *Phys. Rev. B* **22**, 886–893 (1980).

145. Zhang, S. B. & Northrup, J. E. Chemical potential dependence of defect formation energies in GaAs: Application to Ga self-diffusion. *Phys. Rev. Lett.* **67**, 2339–2342 (1991).
146. Wang, D., Qian, F., Yang, C., Zhong, Z. & Lieber, C. M. Rational growth of branched and hyperbranched nanowire structures. *Nano Lett.* **4**, 871–874 (2004).
147. Bierman, M. J. & Jin, S. Potential applications of hierarchical branching nanowires in solar energy conversion. *Energy Environ. Sci.* **2**, 1050–1059 (2009).
148. Lewis, N. S. Toward cost-effective solar energy use. *Science* **315**, 798–801 (2007).
149. Kupec, J., Stoop, R. L. & Witzigmann, B. Light absorption and emission in nanowire array solar cells. *Opt. Express* **18**, 27589–27605 (2010).
150. Åberg, I. *et al.* A GaAs nanowire array solar cell with 15.3% efficiency at 1 sun. *IEEE J. Photovoltaics* **6**, 185–190 (2016).
151. Song, H. S. *et al.* Controllable fabrication of three-dimensional radial ZnO Nanowire/silicon microrod hybrid architectures. *Cryst. Growth Des.* **11**, 147–153 (2011).
152. Liu, J. *et al.* Co<sub>3</sub>O<sub>4</sub> Nanowire@MnO<sub>2</sub> Ultrathin Nanosheet Core/Shell Arrays: A New Class of High-Performance Pseudocapacitive Materials. *Adv. Mater.* **23**, 2076–2081 (2011).
153. Okamoto, H. & Massalski, T. B. The Au-P (Gold-phosphorus) system. *Bull. Alloy Phase Diagrams* **5**, 490–491 (1984).
154. Lindberg, C. *et al.* Silver as Seed-Particle Material for GaAs Nanowires - Dictating Crystal Phase and Growth Direction by Substrate Orientation. *Nano Lett.* **16**, 2181–2188 (2016).
155. Dick, K. A. & Caroff, P. Metal-seeded growth of III-V semiconductor nanowires: Towards gold-free synthesis. *Nanoscale* **6**, 3006–3021 (2014).
156. Schwarz, K. W. & Tersoff, J. From droplets to nanowires: Dynamics of vapor-liquid-solid growth. *Phys. Rev. Lett.* **102**, 206101 (2009).
157. Larsen, C. A. & Stringfellow, G. B. Decomposition kinetics of OMVPE precursors. *J. Cryst. Growth* **75**, 247–254 (1986).
158. Tornberg, M., Maliakkal, C. B., Jacobsson, D., Dick, K. A. & Johansson, J. Limits of III-V Nanowire Growth Based on Droplet Dynamics. *J. Phys. Chem. Lett.* **11**, 2949–2954 (2020).
159. Tornberg, M., Dick, K. A. & Lehmann, S. Thermodynamic stability of

- gold-assisted InAs nanowire growth. *J. Phys. Chem. C* **121**, 21678–21684 (2017).
160. Yan, C. *et al.* Heteroepitaxial growth of GaSb nanotrees with an ultra-low reflectivity in a broad spectral range. *Nano Lett.* **12**, 1799–1805 (2012).
  161. Colombo, C., Spirkoska, D., Frimmer, M., Abstreiter, G. & Fontcuberta I Morral, A. Ga-assisted catalyst-free growth mechanism of GaAs nanowires by molecular beam epitaxy. *Phys. Rev. B - Condens. Matter Mater. Phys.* **77**, 155326 (2008).
  162. Johnson, J. C. *et al.* Single gallium nitride nanowire lasers. *Nat. Mater.* **1**, 106–110 (2002).
  163. Kuykendall, T. *et al.* Metalorganic chemical vapor deposition route to GaN nanowires with triangular cross sections. *Nano Lett.* **3**, 1063–1066 (2003).
  164. Mårtensson, E. K. *et al.* Understanding GaAs Nanowire Growth in the Ag-Au Seed Materials System. *Cryst. Growth Des.* **18**, 6702–6712 (2018).
  165. Mandl, B. *et al.* Au-free epitaxial growth of InAs nanowires. *Nano Lett.* **6**, 1817–1821 (2006).
  166. Mandl, B. *et al.* Growth mechanism of self-catalyzed group III-V nanowires. *Nano Lett.* **10**, 4443–4449 (2010).
  167. Panciera, F. *et al.* Phase Selection in Self-catalyzed GaAs Nanowires. *Nano Lett.* **20**, 1669–1675 (2020).
  168. Küpers, H. *et al.* Diameter evolution of selective area grown Ga-assisted GaAs nanowires. *Nano Res.* **11**, 2885–2893 (2018).
  169. Kuyanov, P., Boulanger, J. & LaPierre, R. R. Control of GaP nanowire morphology by group V flux in gas source molecular beam epitaxy. *J. Cryst. Growth* **462**, 29–34 (2017).
  170. Fontcuberta I Morral, A., Colombo, C., Abstreiter, G., Arbiol, J. & Morante, J. R. Nucleation mechanism of gallium-assisted molecular beam epitaxy growth of gallium arsenide nanowires. *Appl. Phys. Lett.* **92**, 063112 (2008).
  171. Dubrovskii, V. G. *et al.* Self-Equilibration of the Diameter of Ga-Catalyzed GaAs Nanowires. *Nano Lett.* **15**, 5580–5584 (2015).
  172. Magnusson, M. H., Deppert, K., Malm, J. O., Bovin, J. O. & Samuelson, L. Gold nanoparticles: Production, reshaping, and thermal charging. *J. Nanoparticle Res.* **1**, 243–251 (1999).
  173. Meuller, B. O. *et al.* Review of Spark Discharge Generators for Production of Nanoparticle Aerosols. *Aerosol Sci. Technol.* **46**, 1256–1270 (2012).

174. Swihart, M. T. Vapor-phase synthesis of nanoparticles. *Curr. Opin. Colloid Interface Sci.* **8**, 127–133 (2003).
175. Knutson, E. O. & Whitby, K. T. Aerosol classification by electric mobility: apparatus, theory, and applications. *J. Aerosol Sci.* **6**, 443–451 (1975).
176. Zhang, S. H., Akutsu, Y., Russell, L. M., Flagan, R. C. & Seinfeld, J. H. Radial differential mobility analyzer. *Aerosol Sci. Technol.* **23**, 357–372 (1995).
177. Dixkens, J. & Fissan, H. Development of an electrostatic precipitator for off-line particle analysis. *Aerosol Sci. Technol.* **30**, 438–453 (1999).
178. Preger, C., Overgaard, N. C., Messing, M. E. & Magnusson, M. H. Predicting the deposition spot radius and the nanoparticle concentration distribution in an electrostatic precipitator. *Aerosol Sci. Technol.* **54**, 718–728 (2020).
179. Mauthe, S. *et al.* High-speed III-V nanowire photodetector monolithically integrated on Si. *Nat. Commun.* **11**, 1–7 (2020).
180. Barrigón, E., Heurlin, M., Bi, Z., Monemar, B. & Samuelson, L. Synthesis and Applications of III-V Nanowires. *Chem. Rev.* **119**, 9170–9220 (2019).
181. Thelander, C. *et al.* Nanowire-based one-dimensional electronics. *Mater. Today* **9**, 28–35 (2006).
182. Kim, W., Güniat, L., Fontcuberta I Morral, A. & Piazza, V. Doping challenges and pathways to industrial scalability of III-V nanowire arrays. *Appl. Phys. Rev.* **8**, 11304 (2021).
183. Foxon, T. History of MBE. in *Molecular Beam Epitaxy* 1–21 (John Wiley & Sons Ltd, 2019).
184. Wang, C. A. Early history of MOVPE reactor development. *J. Cryst. Growth* **506**, 190–200 (2019).
185. Welsch, E., Guter, W., Wekkeli, A. & Dimroth, F. Memory effect of Ge in III-V semiconductors. *J. Cryst. Growth* **310**, 4799–4802 (2008).
186. Xing, H. *et al.* Memory effect and redistribution of Mg into sequentially regrown GaN layer by metalorganic chemical vapor deposition. *Japanese J. Appl. Physics, Part 1 Regul. Pap. Short Notes Rev. Pap.* **42**, 50–53 (2003).
187. Zielinska, A. *et al.* Nanotoxicology and Nanosafety: Safety-by-Design and Testing at a Glance. *Int. J. Environ. Res. Public Heal.* **17**, 4657 (2020).
188. Wang, S. *et al.* Challenge in understanding size and shape dependent toxicity of gold nanomaterials in human skin keratinocytes. *Chem. Phys.*



- Lett.* **463**, 145–149 (2008).
189. Schwirn, K., Voelker, D., Galert, W., Quik, J. & Tietjen, L. Environmental Risk Assessment of Nanomaterials in the Light of New Obligations Under the REACH Regulation: Which Challenges Remain and How to Approach Them? *Integr. Environ. Assess. Manag.* **16**, 706–717 (2020).
  190. Krug, H. F. Nanosafety Research-Are We on the Right Track? *Angew. Chemie Int. Ed.* **53**, 12304–12319 (2014).
  191. Costa, P. M. & Fadeel, B. Emerging systems biology approaches in nanotoxicology: Towards a mechanism-based understanding of nanomaterial hazard and risk. *Toxicol. Appl. Pharmacol.* **299**, 101–111 (2016).
  192. Nel, A., Xia, T., Mädler, L. & Li, N. Toxic potential of materials at the nanolevel. *Science* **311**, 622–627 (2006).
  193. Nanoparticle Emission Assessment Technique (NEAT) for the Identification and Measurement of Potential Inhalation Exposure to Engineered Nanomaterials-Part A. (2009).



Lund University  
Faculty of Engineering  
Department of Physics

ISBN 978-91-7895-908-2

